INVESTIGATING CLIMATE AND LAND COVER DRIVEN CHANGES TO SURFACE AND GROUNDWATER RESOURCES ACROSS SCALES IN THE AMAZON BASIN

By

Brent Porter Heerspink

A THESIS

Submitted to
Michigan State University
in partial fulfillment of the requirements
for the degree of

Environmental Geosciences – Master of Science

2020

ABSTRACT

INVESTIGATING CLIMATE AND LAND COVER DRIVEN CHANGES TO SURFACE AND GROUNDWATER RESOURCES ACROSS SCALES IN THE AMAZON BASIN

By

Brent Porter Heerspink

The Amazon River and its associated tropical rainforest represent one of the words most important freshwater systems. The Amazon responsible for globally important water, nutrient and energy fluxes. Together the river and rainforest account for ~20% of global freshwater, 10% of global species diversity and store roughly 150Pg of carbon. Alterations to the Amazon's landscape including deforestation, agricultural expansion, infrastructure development, increased forest fire occurrence and changing precipitation patterns threaten the stability of the system. In this thesis, I work toward a better understanding how water resources are responding to changes in climate and land cover across the Amazon Basin.

In Chapter 1, I investigate how deforestation and climate change have altered the water balance in the Amazon Basin. Specifically, I used statistical analyses to quantify changes in streamflow, groundwater storage, and evapotranspiration, and link these the observed changes in land cover and precipitation. In Chapter 2, I focus on how groundwater dynamics are altered by deforestation and conversation to agriculture. To address these question, I developed a groundwater model for a site representative of the heavily defrosted southern headwaters of the Amazon Basin. Together, these efforts reveal how deforestation and climate change are effecting water resources in the Amazon. Better understanding these effects will be crucial to developing policy that balances resource development and environmental impact in this critically important region.

ACKNOWLEDGMENTS

This thesis represents three years of hard work and personal growth that would not have been possible without a great number of people including my family, friends, mentors, collaborators, students, advisors and lab mates. Completing my master's degree has been one of the most challenging and rewarding endeavors of my life thus far, and I am very thankful for the experiences I have had during this journey.

I would like to start by thanking my advisors, Dr. David Hyndman and Dr. Anthony Kendall for their mentorship, teaching and support throughout this degree. I would like to thank my primary advisor, Dr. David Hyndman for continuing to challenge, motivate and support me, both during my masters, and continuing on into my PhD. Dave has been a source of continual optimism, encouraging me to think beyond my self-imposed limits, and to stay positive in the face of the many challenges research provides. I would like to thank Dr. Anthony Kendall for conceptual, technical and personal support in developing and completing my research. Anthony pushed me to learn new skills and complete tasks I thought beyond my capability. I would also like to than Dr. Jay Zarnetske for serving on my thesis committee. Jay provided objective and critical feedback thought the development and completion of my thesis that undoubtedly pushed me to produce better science.

I would also like to thank my funding sources and collaborators, without whom this work would not have been possible. The National Science Foundation, MSU Graduate School, MSU College of Natural Science, and MSU Department of Earth and Environmental Science all provided funding for both my work, and to present this research at national conferences. I would like to thank the Rethinking Dams INFEWS team, especially Emilio Moran and Anthony Cak

for their support in developing and competing this project. I owe special thanks to the Woods Hole Research Center, and the Amazon Environmental Research Institute, especially Christopher Neill and Michael Coe. Without these individuals, my research, trip to Brazil, thesis, presentations and publications would not have been possible.

I would like to thank the members of the Hydrolab for their support both at work, and though the friendships I have developed with you all. I felt welcomed in this lab the moment I arriced, and your continued support has been invaluable. This starts with the leadership of the lab, Drs. David Hyndman, Anthony Kendall and Sherry Martian, who have built the basis for this supportive and successful work environment. I am lucky to have developed lifelong friendships with many fellow lab mates, and I would like to provide some special thanks to: Chanse Ford, Jake Roush, Baily Hannah and Ally Brady, for their dear friendship, especially during the most challenging periods of my master's work. Luwen Wan, for her eternal care, optimism and encouragement. Alex Kuhl and Quercus Hamlin for becoming my daily working companions and close friends, for keeping me accountable, and for their continued company, support and encouragement while remotely finishing my degree. Erin Haacker and Leanne Hancock, for their selfless advice and encouragement, especially in the decision to pursue my PhD. I would also like to thank the other members of the lab (past and present) including: Autumn Parish, Behnaz Mirzendehdel, Ben McCarthy, Jeremy Rapp, Jill Deines, and Ryan Vanier.

In addition to the Hydrolab, I would like to thank the other members of the Earth and Environmental Sciences department who have enriched my time here. I owe a special thanks Dr. Dalton Hardisty, with whom I taught Environmental Geochemistry, for training me to be an educator and for his mentorship, friendship and advice. I additionally thank my students, who

have inspired me to continue in science education and mentorship. I would also like to thank the EES staff who, including Ami McMurphy, Pam Robinson, Brittany Walter, Elizabeth McElroy, and Judi Smelser, who make the work and education within our department possible.

There are also a number of people outside of the university whom I should acknowledge. I would like to thank my previous mentors, including Dr. Tim Lincoln form Albion College, and Drs. Hakim Boukhalfa, Paul Dixon, and Florie Caporuscio from Los Alamos National Laboratory. I have learned an immense about myself and about science from each of you, and your continued friendship and advice has been invaluable. I wouldn't have pursued this master's degree if it wasn't for you. I would also like to thank my close personal friends, including Justin Pollard, Trent Pitko, Tori Malus, Kate Norskog and Sara Sams. Your friendship and support is a continual source of happiness in my life.

Finally, I would like to thank my family, in particular my parents Brent Heerspink and Julie Porter. Though time spent hunting, fishing, camping, horseback riding, gardening and countless other activities they instilled in me curiosity and love for nature. This jumpstarted what has been a career dedicated to better understanding and protecting our natural resources. My parents also provided a wonderful example of hard work and dedication, through lifelong devotion to their pottery. Above all, they have provided endless love and support though every challenge and success during this journey. In addition to my parents, I would like to thank my extended family for the love, support and lessons they have provided throughout my life.

Thank you all, I would not have made it through this degree without you.

TABLE OF CONTENTS

LIST OF TABLES

LIST OF FIGURES

KEY TO ABBREVIATIONS

CHIRPS	Climate Hazards group InfraRed Precipitation with Stations
ESA	European Space Agency
GRACE	Gravity Recovery and Climate Experiment
GW	Groundwater
K	Hydraulic Conductivity
LWE	Liquid Water Equivalent
MODIS	Moderate Resolution Imaging Spectroradiometer
RMSE	Root Mean Square Error
SW	Surface Water
TDR	Time Domain Reflectometry
TRMM	Tropical Rainfall Measuring Mission
TWS	Total Water Storage
USGS	U.S. Geological Survey
WBR	Water Balance Residual

CHAPTER 1: TRENDS IN STREAMFLOW, EVAPOTRANSPIRATION, AND GROUNDWATER STORAGE ACROSS THE AMAZON BASIN LINKED TO CHANGING PRECIPITATION AND LAND COVER

Abstract:

In the face of changing climate, land cover, and infrastructure development, it is critical that we understand how, where, and why surface water resources are changing in the Amazon Basin. Specifically, we must consider holistic changes to the water cycle to understand how water resources are affected by climate change and landscape alterations. In this study, we investigate changes to all major components of the water balance across the entire Amazon Basin. We seek to understand: 1) how changes to land cover and precipitation affect streamflow, 2) how these factors affect evapotranspiration and groundwater storage water balance components, and 3) how changes to the water balance partitioning may in turn alter streamflows. We find significant changes to streamflow of ± 9.5mm/yr on average across the Amazon Basin. Streamflow alterations show a spatially variable pattern, with increasing discharge in the northern and western portions of the basin, and decreasing discharge in the southern and eastern basin. We also observe significant changes in evapotranspiration of ± 29 mm/yr and groundwater storage increases of 7.1 mm/yr. Together, these results indicate that studies of streamflow change in the Amazon should consider changes to all parts of the water budget, including understudied aspects of groundwater storage across the Basin.

1. Introduction:

Changes in climate and land cover, including infrastructure development, have been shown to alter the quality and availability of freshwater resources around the world at multiple scales (Vörösmarty et al., 2000, Pekel et al., 2016). Rivers are a critical component of many human and natural systems, and river discharge patterns are changing globally (Hyndman et al., 2017, Hyndman 2014). The Amazon River and its associated rainforest is one of the world's largest and most important freshwater ecosystems; water fluxes to the ocean and atmosphere from this system affect the global water cycle (Coe et al., 2016). River discharge is determined by the balance among precipitation, surface and groundwater storage, and evapotranspiration (ET). To understand how Amazon River discharge is changing, we must understand each component that governs the water balance.

Previous work has investigated changes in streamflow dynamics across the Amazon Basin, with some studies finding opposing trends across regions (e.g., Espinoza et al., 2009a, Gloor et al., 2013, Hayhoe et al., 2011, Dias et al., 2015, Timpe and Kaplan, 2017, Levy et al., 2018, and Richey et al., 1989). Analysis of historical streamflow patters at the confluence of the Amazon River and Rio Negro at Manaus by Richey et al. (1989), showed no significant change in long-term discharge between 1903 and 1985. The discharge record analyzed in the study, however, predates a significant amount of the Amazon Basin deforestation, and much of the observable changes in climate. Analysis of more recent discharge records have shown significant changes in Amazonian streamflows. For example, Gloor et al. (2013) showed increases in streamflow and a shift toward more severe flows on the Amazon's main stem at Obidos from 1990-2010. They attributed this change to observed increases in precipitation, which were attributed to increased sea surface temperatures and delivery of water vapor to the basin.

Espinoza et al. (2009a) investigated the regional (sub-basin scale) changes in streamflow in the Amazon Basin, focusing primarily on the Andean region. They demonstrated increased streamflow in the northwestern basin, and decreased streamflow in the western and southern basin, with these observed changes attributed to changing precipitation. Patterns of streamflow change also vary in different locations and elevations across the basin. Molina-Carpio et al. (2017) observed decreasing baseflows in lowland tributaries of the Madeira River, although such changes in baseflow were not observed in the Andean tributaries of the Madeira. They also demonstrated that the Andean region is influenced by changes in Pacific Ocean sea surface temperatures (SST's), while the lowland tributaries are affected by alterations to changes in the North Atlantic Ocean SST's.

The Amazon River Basin water balance is primarily driven by precipitation, but is also affected by complex interactions between land cover, land use, soils, temperature, humidity, precipitation, and other landscape characteristics (Espinoza et al., 2009a, Coe et al., 2016, Coe et al., 2017, Maeda et al, 2017). There are also significant feedbacks from changes in such landscape characteristics. For example, deforestation decreases evapotranspiration and increases land surface temperature and streamflow (Costa et al., 2003, Dias et al., 2015, Coe et al., 2017). Interactions between these systems are especially complex in the Amazon, where the rainforest plays an important role in regulating regional and global climate and hydrologic cycles. There, intense evapotranspiration in excess of 1000 mm/yr provides considerable atmospheric moisture, much of which is recycled within the system, affecting precipitation and streamflow across the basin (Salati et al., 1979, Madea et al., 2017).

Regional-scale modeling efforts coupled with satellite and ground-based data have examined streamflow, precipitation, evapotranspiration and groundwater storage to assess the

changing water balance in the Amazon Basin Costa and Foley (1999) expanded the study of changing Amazon hydrology to investigate changes in evapotranspiration and atmospheric water vapor transport between 1979 and 1996. Their work demonstrated a significant decrease in water vapor transport both into and out of the Amazon basin, which was compensated by an increase in precipitation recycling within the basin. While they observed no significant change in runoff, the authors did note that future deforestation or climate change may disrupt evapotranspiration and precipitation recycling, altering the other water balance components. Costa et al. (2003) and Coe et al. (2011) showed that deforestation, by decreasing evapotranspiration, has contributed to an about 20% increase in the discharge of the Tocantins/Araguaia River system in southeastern Amazon. Panday et al. (2015) quantified the opposing effects of deforestation (+6%) and climate change (-14%) on streamflow, which led to an overall modest reduction in streamflow in the Xingu Basin. This demonstrated how the streamflow effects of deforestation can be masked by those of climate change in the opposite direction. These confounding responses are due to the complex interactions between land cover, precipitation and streamflow. While decreased ET from deforestation can directly increase streamflows, it can also decrease rainfall, indirectly decreasing streamflow (Stickler et al., 2013). Levy et al. (2018) analyzed observed streamflow, land cover and climate data using advanced statistical modeling approaches to isolate the effects of change in individual components on observed streamflow in the southern Amazon and Tocantins Basins. They found that climate changes have reduced the deforestation driven changes in streamflows by 42%. Smaller site-scale studies in the Upper Xingu basin have demonstrated through observational data (Hayhoe et al., 2010) and models (Dias et al., 2015) that conversion to soy agriculture decreased ET and increased catchment outflow. These studies

estimated the contribution of baseflow to river discharge but did not quantify changes in groundwater storage.

Large, basin-scale modeling efforts have also been undertaken in the Amazon region to study hydrologic function and understand changing hydrologic conditions. Work by Miguez-Macho and Fan (2012a, 2012b) investigated the role of groundwater in the Amazon hydrologic cycle, showing groundwater to be an important component in regulating both streamflows and evapotranspiration rates in the Amazon. The contribution of groundwater to total water storage has also been investigated. Work by de Pavia et al. (2013) modeled the hydrologic and hydrodynamics of the Amazon Basin using the MGB-IPH model to investigate which hydrologic processes control total water storage (TWS) change in the Amazon. Their results demonstrate that surface water accounts for 56% of total water storage change, while soil water accounts for 27% and groundwater 8%. Conversely, a similar study by Pokhrel et al. (2013) using the LEAF-Hydro-Flood (LHF) model found that ground and soil water account for 71% of TWS change, while flood waters accounted for 24% and rivers 5%. The difference in the estimated contribution of ground and soil waters between these two studies is like due to the explicit simulation of deep groundwater in LHF. This disagreement between the two simulation methods highlights the need to consider groundwater in studies of Amazon hydrology. While the importance of groundwater in the Amazon Basin has been considered in these studies, the long term effects of land cover and climate change on groundwater storage is less well understood. Guimberteau et al. 2017 used an ensemble of land surface models at the Amazon Basin scale to investigate the confounding effects of changing precipitation and land cover on streamflow in the region. They modeled changes in streamflow and ET using a range of deforestation scenarios.

Their results corroborate those of Panday et al. (2015) indicating that deforestation offsets the climate change driven impacts on ET and streamflow.

Changes to streamflow patterns are also predicted to continue under projected changes to global climate and precipitation patters. Sorribas et al. (2016) used the same MGB-IPH model to investigate changes in streamflow under the IPCC's Fifth Assessment Report (CMIP5) projected climate changes. They found significant alteration to streamflow and inundation extent from the Andean rivers to the lower Amazon River.

Changing streamflows driven by climate and landscape alterations also threaten other resources, such as energy development. Stickler et al. (2013) used land surface and climate models to demonstrate that when the land-atmosphere interactions of deforestation are considered, predicted energy generation at the Belo Monte hydropower dam on the Xingu River will be drastically reduced. By including the effects of deforestation on precipitation recycling, they found that projected deforestation of 40% of the Xingu basin would lower Belo Monte's energy generation capacity to 60% of the power industry's projections. This failure to consider the effects of changing water resources on energy production is widespread within Brazil. In the Tapajos Basin, with accounts for almost 50% of the planned potential hydropower development, climate and land cover change could result in decreased energy generation (up to -7.4%) and increased interannual variability in power generation capacity (up to 69%).

The studies outlined above have generally focused on changes in streamflow and precipitation driven by changes in land cover, climate, and sea surface temperature (Gloor et al., 2013, Espinoza et al., 2009a). Few studies have investigated changes in the other major water balance comports of evapotranspiration and groundwater storage. While changes in evapotranspiration have been included in some investigations of changing water resources,

alterations to the groundwater system have been the most understudied. Studies that have considered these factors used models and data at large watershed or catchment scales. In particular, Panday et al. (2015), using GRACE data and the IBIS land surface model, showed that changes in the groundwater storage associated with drought events significantly impacts interannual discharge variability in the 510,000 km2 Xingu River basin. Niu et al. (2017), using a process-based hydrological model, found that surface runoff variations in an upland Amazon catchment were largely controlled by interannual precipitation variability, evapotranspiration variability had less impact. There is a need to further study the integrated changes in water resources through all major components of the water balance across the full Amazon Basin, and to consider a broad range of factors affecting these changes. This need is driven by the rapid alteration to the landscape across the Amazon Basin (including deforestation and hydropower development). To better protect the water resources of the Amazon Basin in the face of such changes along with a changing climate, a more holistic understanding of how the landscape responds to such alteration is needed. This includes considering changes to the groundwater storage and evapotranspiration components of the water balance. Because streamflow is physically linked to the rest of the water balance, and any change in the amount of precipitation routed to groundwater storage or evapotranspiration is likely to affect streamflows.

Here, we seek to identify how and where streamflow characteristics change across the entire Amazon Basin in relation to changes in precipitation, land cover, groundwater storage, and evapotranspiration across scales, using a data-driven approach. We hypothesize that changes to the climate and landscape have altered all major components of the water balance, and that this shift of water balance partitioning affects streamflows. We first analyze over 35 years of streamflow data across the entire Brazilian Amazon and the neighboring Tocantins/Araguaia

Basin, and quantify changes in the magnitude and timing of discharge at seasonal and annual scales. These discharge data are from a set of 126 gauged river basins ranging in drainage area from 12,396km2 to 4,668,984 km2, with an average of 243,810 km2. We explore changes in streamflow patterns, which manifest as changes in the magnitude, timing, and number of events based on summary streamflow metrics (e.g., minimum and maximum flows). We expect that the magnitude and direction of these changes will vary across the basin, as has been demonstrated at coarser (Amazon Basin and large sub-basin) scales (Gloor et al., 2013). We then investigate changes in the other major components of the water balance by quantifying catchment-scale precipitation, groundwater storage, and evapotranspiration across the Basin. To fully investigate changes in the storage and ET components, as well as their relationship to discharge dynamics, we calculate the residual water budget within each streamflow basin and identify trends in these two components. We then compare our calculated residual water budget to independent, remotely sensed quantifications of groundwater storage and ET. While the data record for these products are not as long as those for our discharge and precipitation data, they provide valuable insights into recent changes to groundwater and ET, and aid in our interpretation of the residual water budget. We then discuss how changes in precipitation and land cover may be controlling the observed changes in streamflow, ET and groundwater storage. This research furthers our understanding of how the water balance in the Amazon Basin is changing and highlights the important and understudied role of changes in groundwater storage and ET across the basin.

2. Methods:

2.1 Site Description:

The Amazon River Basin (Figure 1.1) spans ~6.3 million km2 from the Andes Mountains in the west to the Atlantic Ocean in the east, accounting for ~17% of the world's total freshwater

discharge and hosting a majority of the Amazon rainforest. In total, about half of the world's remaining tropical forest lies within the Amazon Basin (Gloor et al., 2013). The Amazon Rainforest ecosystem encompasses ~5.4 million km2, providing 15% of global terrestrial photosynthesis, ~10% of global species diversity, and storing ~150 Pg of carbon (Malhi et al., 2008, Lewinsohn and Pardo 2005). Annual average rainfall is between ~1000 and ~3000 mm across most of the basin, with peak values of ~4000 mm in the northwestern basin, and minimum values of ~100mm in the Andes along the southwestern rim of the basin (Haghtalab et al., 2020, Maeda et al., 2017). The timing of rainfall also varies from early arrival in the southwestern basin (December to February) and later arrival in the northern basin (March to May). The far north and northwestern regions of the basin remain wet throughout most months of the year (Espinoza et al., 2009b). The rainforest also provides a massive water flux to the atmosphere, with annual average ET ranging from ~1000 to ~1500 mm/yr (Maeda et al., 2017). The water flux between the Amazon and the atmosphere is so large that the ecosystem partially regulates its own climate through precipitation recycling. As such the Amazon region affects atmospheric circulation and energy fluxes and on the global scale (Gloor et al., 2013, Coe et al., 2016, Costa and Foley 2000).

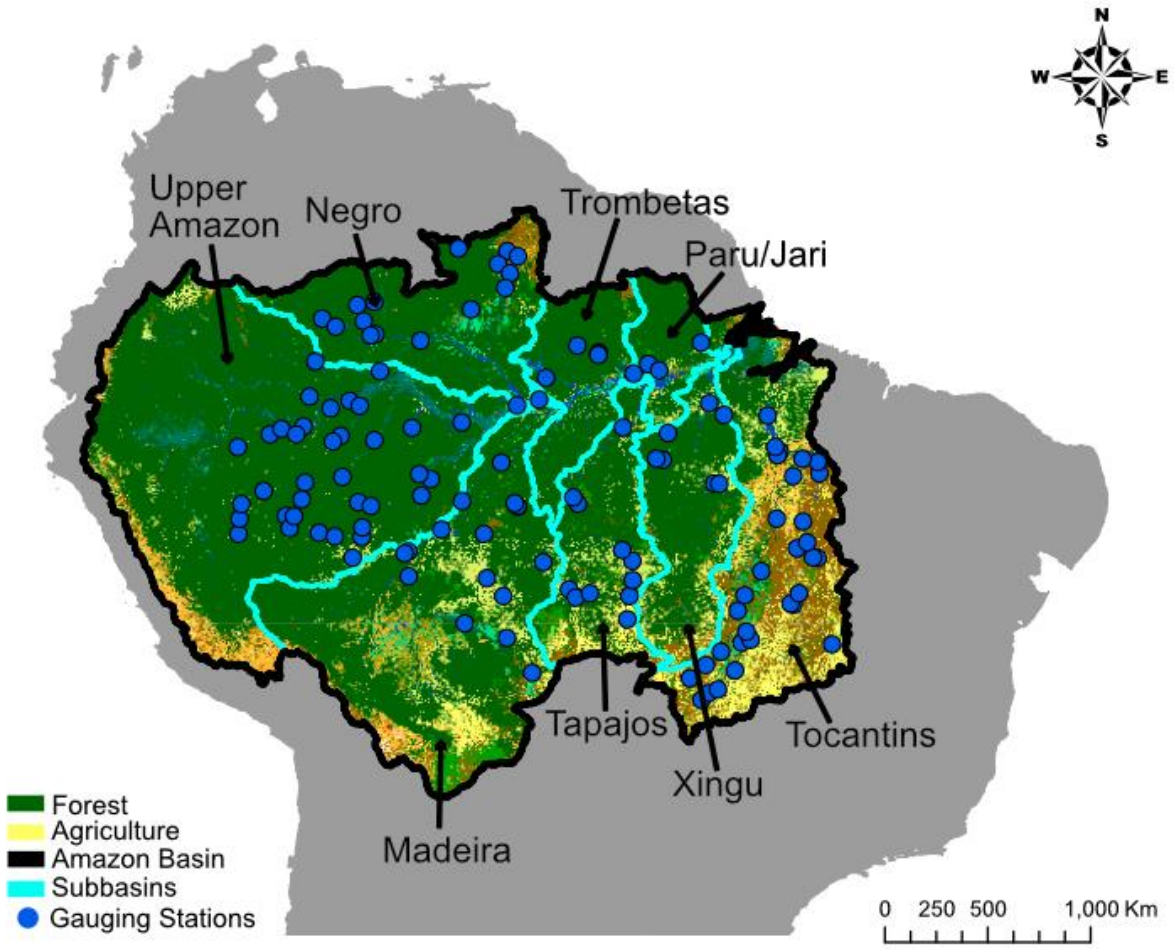

Figure 1.1 Study Region. Locations of the stream gauging stations and the major sub-basins of the Amazon, on top of 2015 remotely sensed land cover estimates from the European Space Agency (ESA, 2017).

2.2 Data:

Here, we used five major data sources to quantify changes in streamflow, precipitation, land cover, groundwater storage, and evapotranspiration. We used daily discharge data from stream gauging stations operated by Agência Nacional de Águas (ANA), Brazil's National Water Agency. The length of record for stations varies, but discharge data are generally available from the 1980's to 2014. These streamflow stations are only within the Brazilian Amazon, as we did not have access to streamflow data for any Amazon streamflow stations in Bolivia, Columbia, Ecuador and Peru, or more recent data from Brazil. Streamflow records are affected by all hydrologic processes upstream of the sampling point, so these data are affected by changing

climate and land cover conditions outside the Brazilian Amazon. As such, we compare changing streamflow at these stations to climate and land cover change data across the entire Amazon Basin. We obtained precipitation data from the Climate Hazards group InfraRed Precipitation with Stations (CHIRPS) gridded daily precipitation product, with 0.05 degree resolution from 1981-present (Funk, 2014). Haghtalab et al. (2020) validated this data against the ANA climate stations, and found that the CHIRPS data was more accurate than the Tropical Rainfall Measuring Mission (TRMM) product across our study region. For our land cover data, we used the European Space Agency (ESA) Climate Change Initiative (CCI) Land Cover Climate Research Data, which is available annually from 1992 to 2014 with 300m resolution (ESA, 2009). We derived groundwater storage changes over the study area from Gravity Recovery and Climate Experiment (GRACE) monthly Land Mass Grids from 2002 to 2014 with ~1 degree resolution (Swenson, 2012; Landerer and Swenson 2012; Swenson and Wahr 2006). To quantify evapotranspiration, we used the Moderate Resolution Imaging Spectroradiometer (MODIS) MOD16A2 gridded 8-day net evapotranspiration product available from 2000 to 2018 with 500m resolution (Running and Mu, 2015, Mu et al., 2007).

Before data processing and analysis, we formatted and quality-checked the discharge data using Python. Data for each station were cleaned to remove non-numeric, missing, or duplicate values. We then filtered the data by station to retain only years with greater than 95% of values present, and only stations with at least 10 years of available data. We further restricted this data to remove stations with drainage basins smaller than 12,321 km2, which is the approximate spatial resolution of our coarsest gridded dataset, the GRACE total water storage estimates. This resulted in a data set with 126 stations where the discharge records passed the quality assurance

steps. Remotely sensed data were spatially and temporally resampled over the gauge basins as described below.

2.3 Analysis:

For our analysis, we defined the water year as extending from December 1 to November 30 of the following year. This allowed us to capture a full hydrograph cycle starting and ending at relatively low-flows for most stations in each annual period. We defined the wet and dry seasons as December 1 to April 30 and May 1 to November 30, respectively, which provided a uniform seasonal definition across the basin based on previously established research in this region. Espinoza et al. (2009a) state that the wet season is December, January, and February in the south and March, April, and May in the north, although peak precipitation may fall outside these bounds in the far northwestern parts of the Amazon Basin. Our use of December through April is thus logical for the scale of our analyses. A different definition of the wet and dry seasons could alter results of seasonal metrics at some stations, however this should not significantly alter long-term trends in annual streamflow indices. All data sets with monthly or finer resolution were assigned a time index identifying both the water year and a wet season/dry season flag.

To understand how and where hydrology is changing within the study region, we developed a set of hydrologic indices to quantify changes in volumetric and temporal components of the hydrograph (Table S1). The indices generally correspond to characteristics in the magnitude, timing, and patterns of hydrograph events. Specifically, they describe average, high and low flows, flood and low flow occurrence, hydrologic reversals, and rates of water mass gain and loss in each subbasin. These indices were selected as they summarize the major components of the hydrograph, including important hydrologic conditions such as flood and

baseflow. We quantified these indices at monthly, seasonal, and annual timescales. In addition to describing the hydrograph, each defined streamflow index is also relevant to both ecological and ecosystem responses. For example, the timing, number, and magnitude of high flow events can alter habitat for fish species, affecting their spawning, migratory cycles, and abundance (e.g., Tomasella et al. 2013, Castello et al. 2015, 2019, Timpe and Kaplan, 2018). While a detailed discussion of the ecological impacts is beyond the scope of this study, the results of change in these indices may be useful to ecological investigations in this region (Melack and Coe, in review). To facilitate comparison with gauge basin-averaged driver variables (precipitation and land cover), the selected indices were computed using basin yield (BY), calculated as $BY = D/A$, where D is discharge and A is the basin area. We quantified all of the indices using statistical tools available in Python or in the NumPy (Oliphant, 2006), SciPy (Virtanen et al., 2020) and StatsModels (Seabold and Perktold, 2010) packages.

Discharge data are available at many stations prior to 1980, however we chose to limit the temporal scope of our analysis based on the number of stations available in each year, and the availability of precipitation data. Many of the discharge records before 1980 were incomplete, as assessed by our quality control process described above.

To link spatially-distributed drivers (i.e., land cover, precipitation, evapotranspiration, and groundwater storage) to gauged discharge, we delineated watersheds upstream of each river gauging station. For this, we generated D8 flow direction (Greenlee, 1987) and resultant flow accumulation rasters from the HydroSHEDS 3-arc second conditioned DEM (Lehner et al., 2006) using the ArcMap 10.2 Spatial Analyst Toolbox. Gauge stations were located according to their latitude/longitude coordinates and then snapped to the raster cell with the highest flow accumulation within 1500m. The location of each gauge station was checked manually, with 56

stations moved to overlie the appropriate cell (identified from the flow accumulation raster). Once proper placement of the gauge stations was confirmed, watersheds were generated from the flow direction raster using the watershed delineation routine within ArcMap.

To understand how the spatial and temporal pattern of precipitation and land cover compare to those of the water balance components in our gauge basins, we quantified changes in land cover and precipitation within each basin. The area and relative proportion of each land cover class were calculated for each basin in all available years. We combined all of the ESA land cover classes for different natural vegetative types into summary land cover classes of ‘‘natural vegetation” and different agricultural classes as “agriculture”. The “natural vegetation” summary class includes all naturally occurring terrestrial land cover types of the Rainforest and Cerrado Biomes. Both contain significant tree cover, and are the dominant biomes in the deforested regions of the Amazon Basin. We then developed time series of forest and agriculture proportions in each basin. To quantify daily gridded precipitation data, we first spatially averaged over each gauge basin then temporally resampled to summarize mean-annual and total-annual precipitation

We applied the Mann-Kendall (MK) test (Mann 1945, Kendall 1975) to detect significant changes in our time-series records for discharge and the associated driver variables, implemented through a Python script (Schramm, 2016). We interpreted the results of this test using the z-score metric, where the sign indicates the direction and magnitude in the trend. The Mann-Kendall test was applied to annually averaged discharge, precipitation, and land cover change data, as well as annual summaries of the discharge indices. In the Results section below, we report results for gauges and basins that were shown to have significant change using a p-value threshold of 0.1.

For basins with a significant trend as identified by the MK test, we used the Theil-Sen slope estimator (Theil 1950, Sen 1968) to calculate the slope of change. This method, which computes the median slopes of lines fit though pairs of points in the dataset, is much less sensitive to outliers than simple linear regression methods (Lavagnini et al., 2011). It has been used to identify trend magnitudes in hydrology and climate data records, and is often used with the MK test (Li et al., 2014). As with the Mann-Kendall test, the Theil-Sen Slope was applied to annual summaries of all data for which a trend was calculated. The Theil-Sen regression was implemented thought the SciPy-stats package in Python (Oliphant, 2006).

To understand changes in observed discharge in the context of the complete hydrologic cycle, we calculated the water balance for each gauge basin from 1983-2014. The standard water balance is shown in Equation 1, where the change in total basin storage (ΔS, mm/yr), is calculated by subtracting annual total basin yield (BY, mm/yr), and annual evapotranspiration (ET, mm/yr) from annual precipitation (P, mm/yr).

[1] $$\Delta S = P - ET - BY$$

Because we do not have evapotranspiration data for the entire period of the precipitation data, we calculated the water balance residual (WBR). We define the WBR as the difference between basin-averaged annual precipitation (P, mm/yr) and annual total basin yield (BY, mm/yr) for each gauge, which equals the sum of the basin-averaged annual evapotranspiration (ET, mm/yr) and change in total basin storage (ΔS, mm/yr), as shown in Equation 2.

[2] $$WBR = \Delta S + ET = P - BY$$

To reduce the effects of outliers, we computed a three-year moving average of our calculated WBR value. We assessed linear trends in this annual rolling-average metric over the

entire record length, and over shorter periods for comparison to other products as discussed below.

We used the GRACE Tellus Monthly Mass Grids to separate the ET and soil water storage values lumped within the WBR. While the GRACE data do not cover our full discharge period, they can help constrain changes to the individual components of the WBR from 2001 to 2014. We spatially averaged the GRACE data over each gauge basin using Google Earth Engine (Gorelick et al., 2017) to create time series data. These data are reported in units of Liquid Water Equivalent (LWE), which is the mass anomaly recorded by GRACE reported in terms of water depth. LWE values represent the monthly total water storage (TWS) on the landscape relative to the 2004-2010 average. We calculated the mean of the three monthly TWS products (calculated independently by NASA JPL, University of Texas Center for Space Research, and GFZ Potsdam) to use for further analyses. We then computed two annual quantities from monthly TWS: 1) annual (water year) average total water storage, and 2) annual change in storage (ΔS, originally cm/yr) for each basin by subtracting the LWE value in December of the next water year from the December value at the beginning of the current water year. Taking the difference in TWS values at the end of the dry season (December of the water year, November of the calendar year) minimized the effect of surface water on the signal, as this is the most hydrologically stable time of year. As such, the change between December TWS values is assumed to be due to changes in groundwater storage. We used data from 2003-2014 and interpolated the monthly mass values to fill in missing December values for 2011. An example of the time series data and trends for total water storage, groundwater storage, and delta S are shown in Figure A1.1 for selected basins. We then computed WBR-estimated ET for each basin as shown in Equation 3.

[3] $$ET = WBR - \Delta S$$

To estimate changes in groundwater storage, we also analyzed the linear trends in the December TWS values. As with our analysis of ΔS, we used the December TWS values in this analysis to minimize the effect of surface water changes on the signal. To further validate this approach, we quantified trends in the December streamflow values over the same period, as an indication of changes to the end of dry season surface water storage.

To constrain our estimated changes in ET, we compared our ET estimates with the MODIS Evapotranspiration 8-Day gridded product. We prepared the MOIDS grids for comparison with our estimated ET value by spatial and temporal resampling in Python. First, we spatially-averaged the MODIS ET composites over each gauge basin. To minimize the effect of missing pixel values, we then calculated the monthly average MODIS ET value for each basin. Because ET values are relatively stable day to day in this region, monthly averages provide a robust estimate of ET variation across the year. Here we do not assess the seasonality of missing composites or pixels, which might impart biases into our calculated average MODIS ET values. Analysis of the seasonality of missing MODIS data, or its overall accuracy, is beyond the scope of this study, but should be investigated in subsequent research. We then used monthly ET values to create annual averages of ET for each basin. Finally, we compared trends and average values of these annual ET estimates to our WBR-estimated ET calculations. Both the GRACE TWS data and MODIS ET data streams have much shorter records than precipitation and discharge in our region and as such, the length of record for the WBR estimated ET records were considerably shorter (see Figure A1.2). A graphical representation of our workflow for this study is presented in Figure A1.3.

Due to different temporal spans of the data sources used in this analysis, we were not able to independently quantify each water balance component for our full record from the early 1980's to 2014 for which precipitation and discharge records. Instead, we quantify the remotely sensed land cover, ET and groundwater storage estimates for their available records of: 1992-2014 for ESA land cover, 2002-2014 for GRACE total water storage and 2006-2014 for MODIS ET. We then use these data sources to contextualize our results, and validate our numerical water balance estimates of ET. A summary of the length of record for each dataset is presented in Figure A1.2. Additionally, the long term average of basin yield, CHIRPS precipitation, MODIS ET, and GRACE TWS are shown in Supplemental Figures A1.4 and A1.5.

3. Results

All of the hydrologic indices of the magnitude and timing of hydrograph events showed significant changes between 1980 and 2014 across most of the Amazon Basin. Here, we focus on five indices to describe changes in streamflow across the available data record: 1) annual average, 2) wet and 3) dry season averages (Figure 1.2), as well as 4) 10th and 5) 90th percentile discharge (Figure 1.3). These indices have a similar spatial pattern in trend direction, with the northern and western basin showing increasing discharge, and the southern and eastern basin showing decreasing discharge. Some of the smaller gauge basins show greater trend magnitudes or opposite trends as their surrounding larger regions, indicating heterogeneous hydrologic trends across the basin.

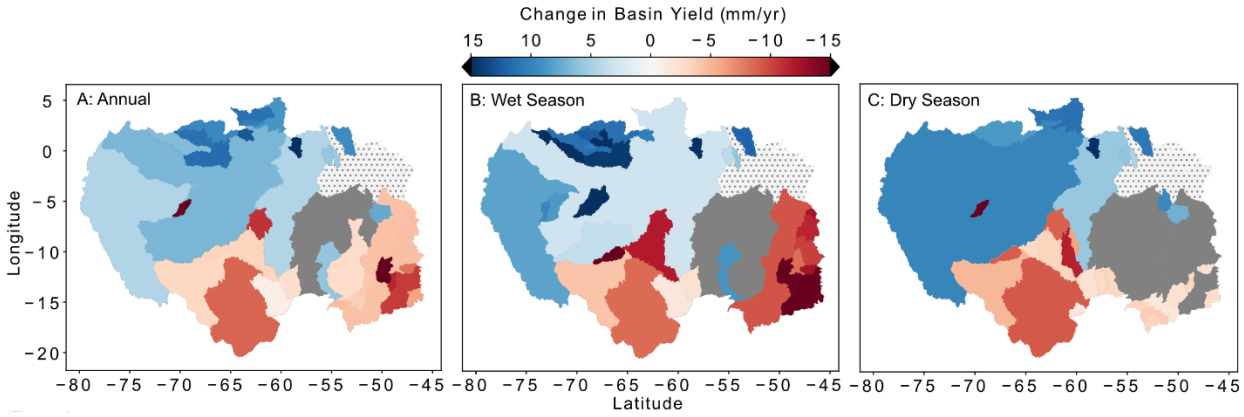

Figure 1.2 Change in Annual, Wet and Dry Season Streamflow. Slope of change in water-year basin yield (mm/yr) for: A) annual, B) wet season, and C) dry season periods between 1980 and 2014. The basins are drawn in descending size (largest first) to ensure all basins with significant changes are shown. Changes in average daily streamflow exist at both annual and seasonal intervals, with spatially distinct trends of decreased streamflow in the south and east, and increased streamflow in the north and west. Catchment areas in solid grey have no significant trend at the p=0.1 level, while the stipple patterned areas fall outside of gauged catchments.

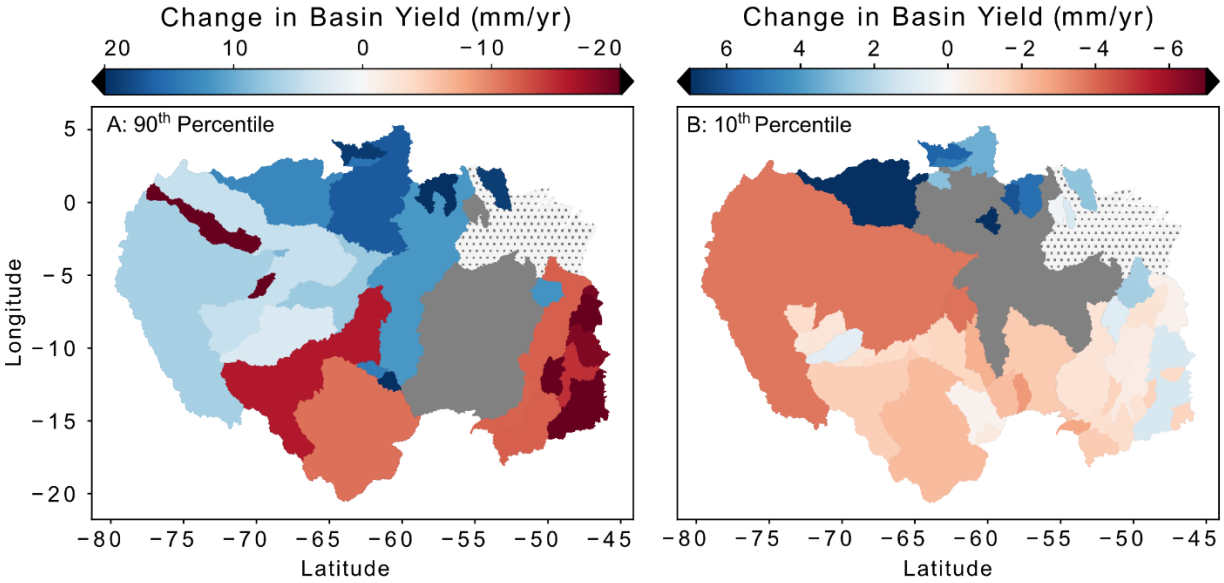

Figure 1.3 Change in 90th and 10th Percentile Discharge. Slope of change in 90th (A) and 90th (B) percentile discharge for between 1980 and 2014. Similar to the average discharge trends, both metrics show spatial variance in magnitude and trend direction. 10th percentile discharge is decreasing over most portions of the basin, though at a slower rate than change in annual averages. 90th percentile discharge shows similar patterns to the averages, but with larger magnitudes of change. Areas in solid grey represent no significant trend, while the patterned grey areas have no data.

Changes in annual, wet, and dry season basin yield are on average ± 9.5 mm/yr, but range up to ± 30 mm/yr. (Figure 1.2). The strongest trends of increasing flows in the north and decreasing flows in the south and ease are intensified during the wet season (72 basins with significant trends), especially in the northern Rio Negro and southeastern Tocantins basins (see location in Figure 1.1). Here, intensification (or intensified) refers to an increase in the absolute magnitude of the trend or value for a given streamflow index. Trends in dry season streamflow are similar to annual average changes in both number of stations (79 for annual average, 81 for dry season) and magnitude of changes. The 90th percentile of flow (Figure 1.3A) had similar trends across 69 stations, however for this index the dichotomy between north and south is intensified. Changes in peak discharge and flood pulses, represented by the 90th percentile of flow, range from -60 to +100 mm/yr. In contrast, the 10th percentile flow (Figure 1.3B, indicator of baseflow) had a different spatial pattern of change (107 stations). Baseflow, which we calculated as the 10th percentile of discharge, values are decreasing across most of the southern, eastern and western portions of the basin. The only areas experiencing increasing baseflow are in the far northern basin and select regions in the Tocantins. The magnitude of change in baseflow is also much smaller, as might be expected given their lower absolute magnitude, with a general range of ± 10 mm/yr, however increases as high as +40 mm/yr were observed in the upper Rio Negro river basin.

In addition to changes in streamflow volume, other hydrologic characteristics are changing across the Amazon Basin, including: the number of high/low flow events (Figure A1.6); the rates of water entering and leaving the basin (Figure A1.8), and the amplitude and period of the hydrograph (Figure A1.10). As with metrics of streamflow volume, changes in the number and timing of events are also spatially variable. For example, the northern and western

basins are experiencing an increase in the number of flood events, while the southern and southeastern basin are experiencing fewer flood events annually. Together, these metrics indicated intensification of the hydrologic cycle across the northern basin, with an increase in the number of flood events (Figure A1.6A), the rate of water gain and loss from the basin (Figure A1.8), and the amplitude and period of the annual hydrograph (Figure A1.9). Conversely, the annual hydrograph of the southern and eastern basin has dampened, with decreases in the number of flood events, a shorter hydrograph period, and a smaller hydrograph amplitude. The timing of hydrologic events is also changing; most notably a shift to later minimum flows in the western basin and earlier center of mass of flows in the northern and southern basin.

There have been significant increases in annual precipitation over most of the central and western basin (Figure 1.4). Areas of significant decrease in annual precipitation occurred in a small number of watersheds in the southern basin. Wet season precipitation shows a wider extent of increased precipitation across the basin (Figure 1.4B). Dry season precipitation shows much fewer areas of significant change, with increasing amounts in the western basin, and decreasing amounts in the upper Madeira Basin (Figure 1.4C).

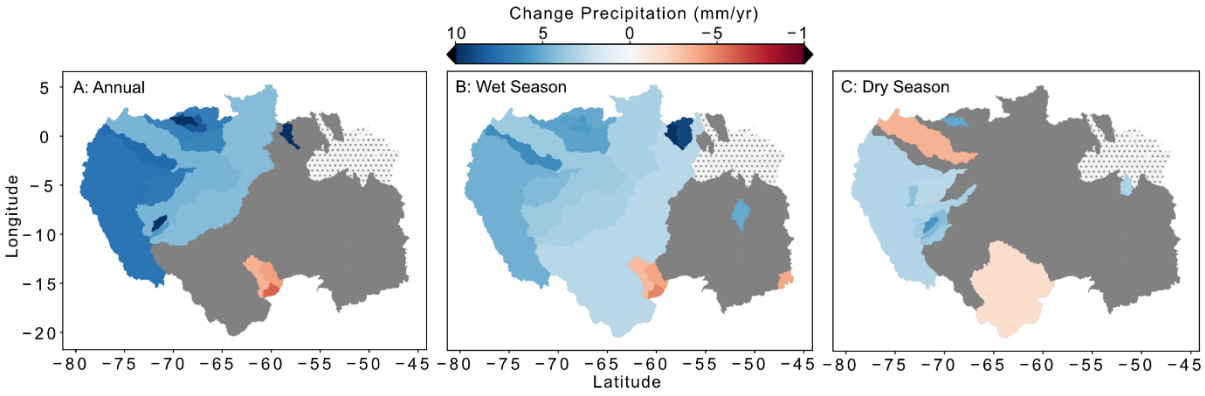

Figure 1.4 Annual, Wet and Dry Season Precipitation. Slope of change (mm/yr) in cumulative precipitation over the Amazon for A) annual, B) wet season and C) dry season between 1983 and 2014. Patterns are generally similar in the annual and wet season trends, with increasing precipitation in the northern and western portions of the basin, and isolated areas of the southern basin experiencing decreased precipitation. Areas in solid grey have no significant trend, while the patterned grey areas have no data.

Most of the forest loss in the basin from 1992 to 2015 occurred in the southern region, also known as the "Arc-of-Deforestation", which encompasses the upper Xingu, Tapajos and Madeira Basins (Figure 1.5, A1.11 and A1.12). At the basin scale, the amount of forest lost is directly proportional to the increase of agricultural land in the same basin. The Tocantins basin had already experienced significant clearing of the natural Cerrado vegetation, and conversion to agriculture prior to the start of our land cover record in 1992. Typical forest loss rates in the central and southern portions of the Amazon range from 0.5 to 1.5% of the basin area per year. Much of the western and northern Basin has experienced relatively little deforestation since 1992.

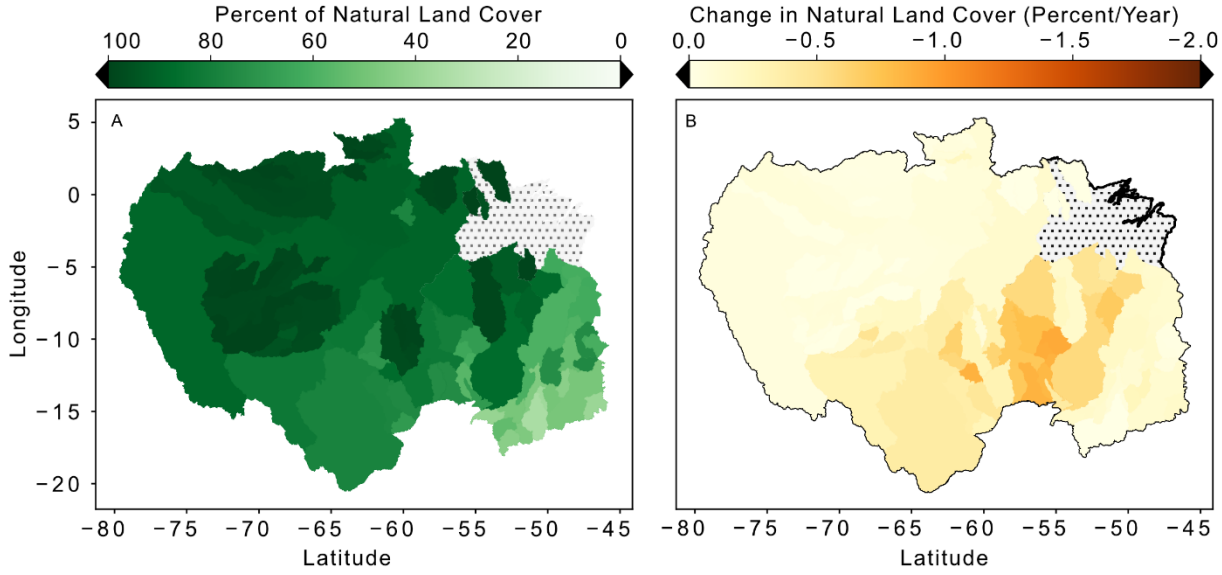

Figure 1.5 Change in Natural Land Cover. Slope of change (mm/yr) in cumulative precipitation over the Amazon for A) annual, B) wet season and C) dry season between 1983 and 2014. Patterns are generally similar in the annual and wet season trends, with increasing precipitation in the northern and western portions of the basin, and isolated areas of the southern basin experiencing decreased precipitation. Areas in solid grey have no significant trend, while the patterned grey areas have no data.

Analysis of the water balance residual for each gauge basin (Equation 1) shows significant changes in the sum of evapotranspiration and storage across the region (Figure 1.6C).

Previously discussed trends in basin yield (Figure 1.6A) and precipitation (Figure 1.6B) are mapped for the corresponding time period, 1983 – 2014 (limited by precipitation and GRACE data availability). Trends in the three-year moving average of this residual showed increases in the water balance residual over much of central and western portions of the region at the large gauge basin scale. Smaller basins throughout the region, and most of the Tapajos basin showed decreases in the water balance residual. The Tocantins showed a split pattern with increases in the WBR in the north and east, and decreases in the southwest portion of the basin. Most basins have changes between ±10 mm/yr, but they range from -20 to +39 mm/yr. No significant trend was detected for the Xingu basin or the northwestern Tocantins.

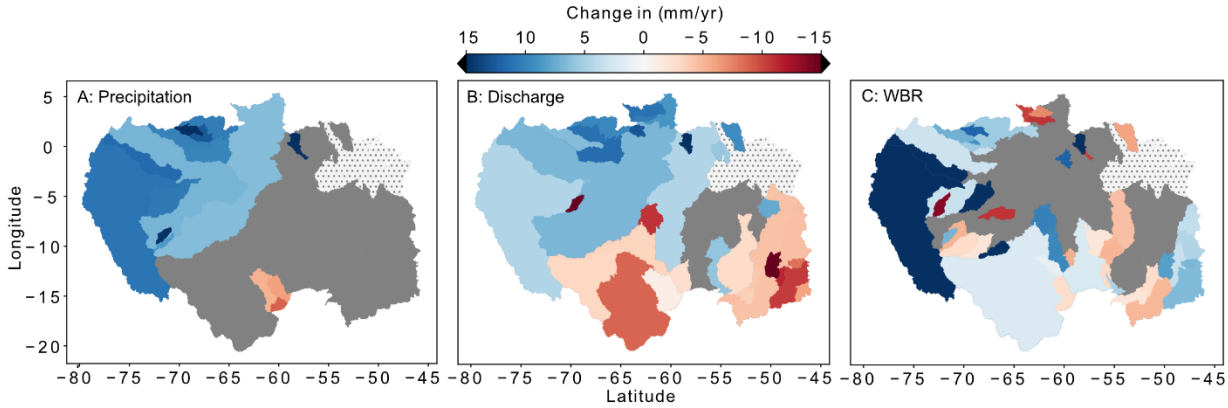

Figure 1.6 Change in the Water Balance Residual. Slope of change in water year basin-average: A) precipitation, B) basin yield, and C) water balance residual (Equation 2) calculated from discharge and precipitation data for 1983 – 2014. There are significant changes in the sum of ET and ΔS, representing shift in water partitioning within the landscape over this period. Areas in solid grey have no significant trend, while the patterned grey areas have no data.

Trends in the December TWS values from GRACE (Figure 1.7A) indicate significantly increased groundwater storage in the Xingu, Tapajos, and upper Madeira basins in the south, as well as in the upper Trombetas basin in the north. Average increases in groundwater storage across these basins were +7.1 mm/yr, with a maximum increase of 10.5 mm/yr; no significant decreases in groundwater storage were observed. During this same period (2002-2014), the end of dry season discharge, shown in Figure A1.14, has not significantly changed in the Xingu,

Madeira or Trombetas river basins. We do not have sufficient data to assess change in the Tapajos basin over this period, however analysis for the full discharge record show end of dry season discharge increases in the Trombetas, and decreases in the Tapajos basin. The GRACE gravity anomaly data also showed significant increases in annual total water storage over most of the Amazon Basin, but decreasing TWS in the Tocantins (Figure A1.12). The highest rates of TWS increase are observed in basins along the main stem of the Amazon River, and in the northern Trombetas Basin.

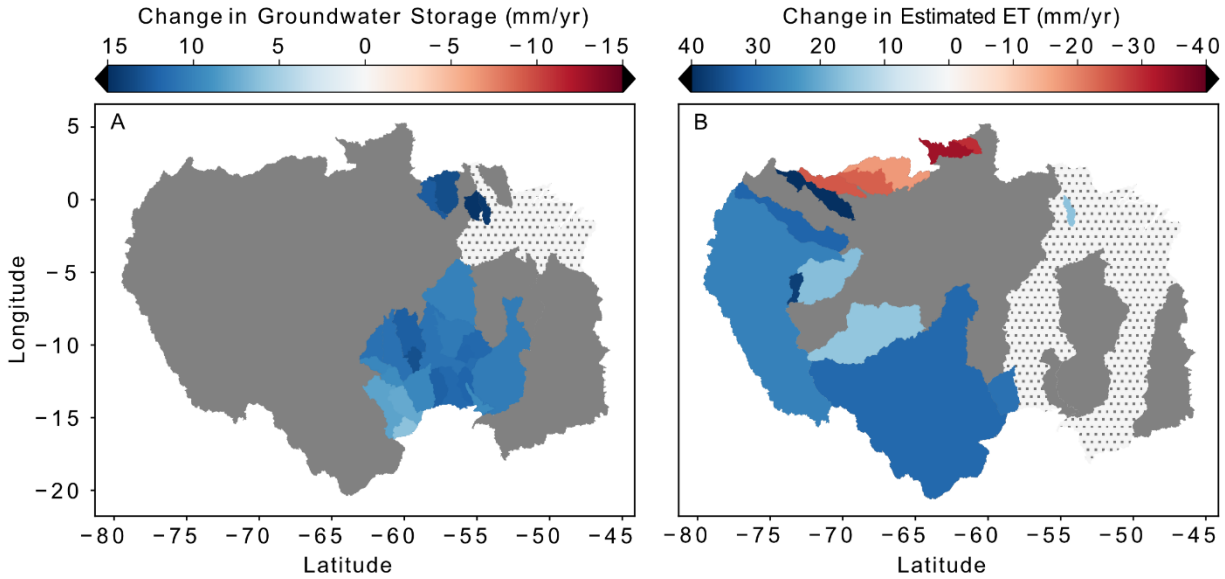

Figure 1.7 Changes in GRACE Groundwater Storage and Estimated ET. A) Changes in GRACE derived groundwater storage values, assessed as the trend in December TWS values between 2002 and 2014. Groundwater storage is shown to be increasing in the areas affected by deforestation and significant increases in precipitation. The GRACE-derived ΔS data were also used to estimate ET from the WBR. B) Trends in the resulting estimated ET between 2002 and 2014 show increasing ET in the south and west, and decreasing ET in the north. Areas in solid grey have no significant trend, while the patterned grey areas have no data.

Basins with significant changes in estimated ET (Equation 3) are shown in Figure 1.7B. The results of this analysis show increasing ET in the western and south-central Amazon, and decreasing ET in the far northern region of the Basin. The trends in ET are strong relative to the

other water balance components, with increases of 30 or more mm/yr and decreases of a similar magnitude.

Analysis of the MODIS ET data (available from 2006 to 2014) shows changes in annual average ET (Figure A1.13) with slopes from ±20 mm/yr. Specifically, the western, and northern basins are showing decreases in ET, while a portion of the upper madeira and Tocantins regions show increases in ET. Trends in our estimated ET (Figure 1.7B) over this period the magnitudes are different in the MODIS ET data for the far southern (Madeira) and northern portions of the basin, but contrast markedly in the Andean western part of the Basin. In addition, the significant increases in ET in the Tocantins shown in the MODIS data are not observed in our estimated ET. The magnitude of the significant trends in both datasets were similar. In addition to quantifying trends in both datasets, we also compared the values for annual average ET between the two datasets (Figure 1.8C).

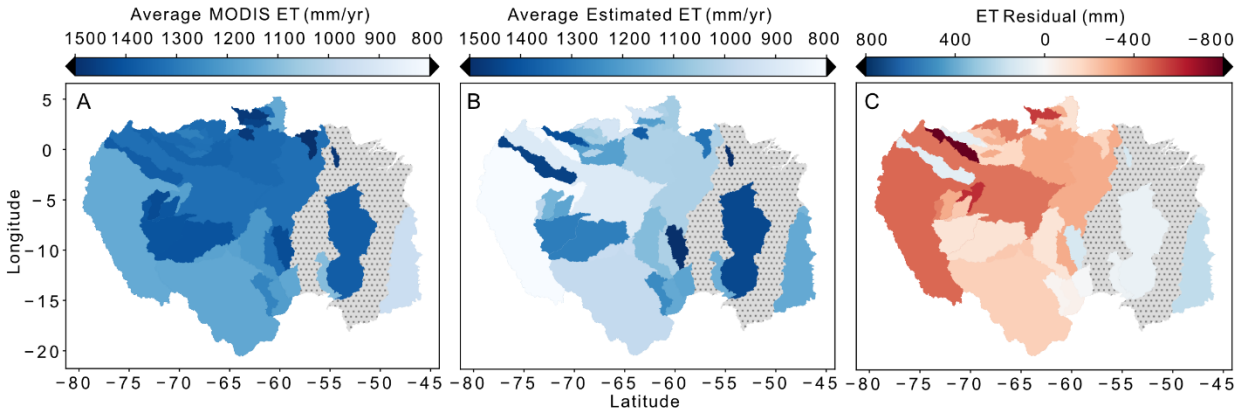

Figure 1.8 MODIS and Estimated ET Comparison. Annual average ET from: A) MODIS ET estimates (2006-2014) and B) estimated ET values corrected with GRACE data (2002-2014). Estimated ET values are higher in the Tocantins and lower in the western basin than those from the MODIS estimates. The residual of the two ET quantifications (C) shows that over most of the basin the WBR calculation provides lower ET estimates than MODIS. Areas in solid grey have no significant trend, while the patterned grey areas have no data. MODIS ET data are only quantified in basins for which we have sufficient data to estimate ET.

4. Discussion:

Within the water balance, streamflow is the most accurately measured quantity and commonly has the longest record (Figure A1.2). Streamflow is an integrator of landscape water dynamics because it is affected by changes in all parts of the water balance. As such, changes in streamflow provide an important record of changes in water resources in basins like the Amazon. A number of previous studies demonstrate significant streamflow changes in specific regions, or over restricted time spans, and have generally focused on one driving factor to help explain these changes (Costa et al., 2003, Espinoza et al., 2009a, Gloor et al., 2009, Coe et al., 2011, Hayhoe et al., 2011, Timpe and Kaplan 2017 and Levy et al., 2018). Our results demonstrate long-term changes in streamflow across the entire Amazon Basin at multiple scales and show that these changes are influenced by a complex interaction between climate and landscape factors. In addition to changing streamflow patterns, our work also demonstrates a significant and spatially variable change in precipitation patterns across the Amazon Basin. Haghtalab et al. (2020), analyzed changing precipitation patterns, including changes to the number of dry days and extreme events across the Amazon Basin. Their work showed a similar spatially explicit pattern of change in precipitation, with increasing rainfall in the northern basin, and decreasing rainfall in the southern basin.

Furthermore, our results indicate that changes in streamflow are also spatially variable, with increasing flows in the western and northern basin, and decreasing flows in the southern and eastern basin, as shown in Figure 1.2. These results support those of Espinosa et al. (2009) and are consistent with an analysis of satellite and ground-based data showing a shift in the climate of the southeastern Amazon to warmer and drier conditions since the 1970s (Rattis et al. in review). Work by Duffy et al. (2015) and Sorribas et al. (2016) indicates that this pattern of

change in precipitation and discharge will continue with changing climate. The Duffy et al. (2015) analysis of the output of 35 climate models taking part in the Coupled Model Intercomparison Project (CMIP), as summarized in the Intergovernmental Panel on Climate Change 5th Assessment Report (IPCC AR5), indicates that decreased rainfall and more frequent drought will occur in the south and eastern Amazon, while increased rainfall will occur in the north and west in the coming century. Hydrologic model discharge estimates from 2070 to 2099 by Sorribas et al. (2016), driven by the IPCC's Fifth Assessment Report CMIP5 indicate that the predicted changes in climate will continue to cause decreased streamflow in the eastern basin, and increased flows in the western basin.

In addition to changes in streamflows, we also observe significant changes in water balance residual (WBR, Equation 2) shown in Figure 1.6, which indicates that evapotranspiration and groundwater storage are also changing significantly across the Basin. This conclusion is supported by a first-principles understanding of the water balance. All of the precipitation reaching the land surface must be routed to streamflow, surface water bodies, subsurface storage, or evapotranspiration. Given the relatively limited surface water storage in the basin, any discrepancy in water mass between precipitation and discharge must either be stored in the subsurface or returned to the atmosphere via ET. Together, changes in streamflow data and the calculated WBR indicate that alterations to the landscape have likely affected all major components of the water balance in the Amazon Basin. Furthermore, processes exerting control on ET and groundwater storage including changes in climate, land cover, sea surface temperature and precipitation patterns have changed significantly since the 1980s (Malhi et al., 2008 Haghtalab et al., 2020, Espinoza et al., 2009a).

The observation that all parts of the water balance, including understudied groundwater storage processes (Gleeson et al., 2019) are changing, is further supported by our analysis of MODIS ET estimates and GRACE mass anomaly data. These independent quantifications of ET and groundwater storage show significant change in both parameters across the Basin. It is important to note that there are increasing trends in groundwater storage (Figure 1.7A) in areas of deforestation (Figure 1.5B, specifically in the Xingu, Madeira and Tapajos basins) and significant precipitation increases (Figure 1.4, in the northern Trombetas basin). A comparison of GRACE data to the LEAF-HydroFlood model indicated that changes in TWS in the southeastern Amazon are dominated by subsurface groundwater storage (Pokhrel et al, 2013), which supports our results indicating groundwater storage increased in the Madeira and Tapajos basins. The Trombetas basin also shows some of the highest increases in groundwater storage, while the Xingu, Tapajos, and Madeira show lower rates of storage increase. This further indicates that the processes driving groundwater storage increase are likely associated with precipitation increase in the northern basin, and deforestation in the southern basin. Our approach to estimating change in groundwater storage is further supported by the analysis of changing streamflow at the end of the dry season (December of the water year) shown in Figure A1.14. Changes in streamflow are representative of those in surface water storage. If changes in the end of dry season total water storage values were a result of changing surface water storage, we would expect to observe increasing streamflows. We however, observe no increases in end of wet season streamflows in the Xingu, Madeira or Trombetas basins between 2002-2014. This further indicated that changes in end of dry season total water storage in these regions are a result of increased groundwater storage. While we do not have a sufficient discharge record to assess, trends in end of dry season

discharge for the Tapajos basin during the GRACE record (2002-2014), trends calculated over the full discharge record show no significant increase in December discharge in the Tocantins.

Because the ability to estimate water balance fluxes remotely across large areas is a recent advance due to satellite data, the record lengths for the remotely sensed groundwater storage and ET datasets are relativity short. As such, validation of our WBR calculation across its whole streamflow record is not possible. Observed changes in the GRACE groundwater storage and MOIDS ET data are however of similar magnitude to those of the WBR and estimated ET. Although we cannot disentangle either groundwater storage or ET from the WBR over its full record length, this calculation suggests that changing climate and land cover have resulted in long-term changes in groundwater storage and/or ET in the Amazon Basin.

Site- and regional-scale studies of water dynamics in the Amazon also support our conclusion of changing water balance dynamics. Transitions from forest to pasture or cropland results in shallow rooted land cover, which cannot access deep soil moisture or groundwater (Coe et al., 2016, von Randow et al., 2000), and thus decreasing ET and affect groundwater storage in the system (Neill et al., 2013). For example, research in the upper Xingu and Tocantins Basins shows that deforestation can increase both runoff to stream channels and soil moisture, and decrease ET (Coe et al., 2011, Hayhoe et al., 2011, Neill et al., 2013, Silverio et al., 2015, Arantes et al., 2016, Spera et al., 2016, Coe et al., 2017). However, extensive deforestation can result in reduced precipitation recycling, leading to decreased streamflows (Stickler et al., 2013). As agriculture continues to expand, with changing climate patterns, Brazilian agricultural systems may shift from being rainfed to the use of irrigation, such as changes that are already occurring in the Tocantins region. A recent paper by Laturbesse et al. (2019) suggests that expansion of both agriculture and the use of irrigation could result in

decreasing water storage and streamflows across the Tocantins. Hydrologic modeling investigations have suggested groundwater plays an import role in the hydrology of the Amazon Basin. Miguez-Macho and Fan (2012a) used the LEAF-Hydro-Flood model to investigate the importance of groundwater in streamflow and surface hydrology across the Amazon. Their results indicate that groundwater buffers surface water resources during the dry season and drought conditions. These results also indicate that groundwater has varying contribution to streamflow, exerting the most control in headwater catchments. Further work by Miguez-Macho and Fan (2012b) indicates that groundwater can also affect ET capacity in the Amazon. The presence of groundwater below about 10 m depth can increase root water uptake, allowing for continued evapotranspiration across the dry season and drought periods.

There are uncertainties in the data sets used to quantify changes in the water balance. For example, the ET product is affected by cloud cover and land surface classifications, and the CHIRPS precipitation data product may underestimate rainfall in the western Amazon basin in a similar manner as has been shown for the Climatic Research Unit (CRU) data (Coe et al., 2009). This likely causes an underestimate of the water balance residual in this region, which may explain some of the discrepancy between our estimated ET and the MODIS data product. Second, MODIS ET underestimates ET from 2000 to 2005 in the Pantanal wetland of Brazil and Xingu (Penatti et al., 2015; Silverio et al., 2015), and a similar bias was observed for the Amazon Basin in this study. We thus restricted our MODIS data analysis to 2006-2014. While data availability for MODIS is limited in time, it does provide a robust estimation of ET across the entire Amazon. Previous estimates of ET have relied on mathematical estimation (from incoming solar radiation or precipitation and rainfall data) or the use of global climate models. Direct measurements of ET exist from field campaigns such as the Large-Scale Biosphere Atmosphere

(LBA), but have limited spatial coverage (Werth and Avissar, 2003). To better understand both natural variations in ET and its responses to climate and land cover changes however, we will need to expand our quantifications of ET across the basin. These methods have been used to demonstrate the seasonality of ET (Maeda et al. 2017) and the change in ET due to deforestation Silvério et al. (2015) but have not been used to assess long term trends in ET across the Amazon Basin. In addition, limited understanding of certain physical process dynamics in the Amazon also limits our analysis. For example, widespread measurements of depth to water or aquifer properties are not currently available in the Amazon. As such, we do not have good constraints on the extent of storage change in these systems. These processes affect the degree to which land cover and total storage change affect streamflow in a given region.

5. Conclusions:

The combined data records for discharge, precipitation, evapotranspiration and groundwater storage suggest spatially-variable changes in all components of the water balance across the Amazon Basin. Alterations to the water balance include average changes of ± 9.5mm/yr to discharge, ±7.7 mm/yr to precipitation, ± 29 mm/yr to ET and +7.1 mm/yr to groundwater storage. These observed changes are occurring in a spatially heterogeneous pattern, with the northern and eastern basins showing different hydrologic responses than the southern and eastern basin. Previous research has attributed changing streamflows to: 1) altered precipitation driven by natural climate variability and long-term climate changes, 2) increased runoff and deceased ET due to land cover change, 3) reduced precipitation due to reduced ET and water vapor recycling in deforested regions. Our results support these previous findings, and show that changing climate and land cover alter the major components of the water balance.

Furthermore, we suggest that that streamflows are also altered by changes to the water balance partitioning, specifically due to altered groundwater storage in response to deforestation.

While our work demonstrates significant changes to the Amazon Basin's water balance, we do not currently have enough data to separate changes in groundwater storage and ET over the full discharge record. Such an analysis would require a model based investigation of alterations to the region's water balance. Using process-based landscape hydrology and groundwater models would provide better understanding of the complex water cycle dynamics across the Amazon Basin. Such models could be used to explicitly simulate the historic effects of deforestation on groundwater storage and ET rates, and project changes in the Amazon water balance in response to climate change scenarios though the end of this century. In particular, it will be important to explicitly model the role of changing groundwater storage in the basin's hydrology, including how this storage is affected by landscape changes. Developing our understanding of this complex system, through both field and modeling investigations is critical to better project the state of surface water resources within the Amazon in the face of changes to both the climate and landscape.

Changes in climate, land cover and the hydrologic cycle are likely to continue in the Amazon, as population growth and increased resource demand continues. The resulting alterations to streamflow, precipitation, groundwater storage and ET can affect hydropower production, agricultural yield, fisheries, nutrient cycling and carbon sequestration. Better understanding how the water balance changes in response to an altered climate and landscape will be important to preserve the water, food, energy and ecologic resources of the Amazon Basin.

Acknowledgments:

This chapter was coauthored by Anthony D. Kendall, Michael T. Coe and David W. Hyndman. This work was primarily funded by the NSF though the following grants: INFEWS/T3 Grant No. 1639115 “Rethinking Dams: Innovative hydropower solutions to achieve sustainable food and energy production, and sustainable communities” and INFEWS/T1 Grant No. 1739724 “Intensification in the world's largest agricultural frontier: Integrating food production, water use, energy demand, and environmental integrity in a changing climate”. Additional funding was provided by the Department of Earth and Environmental Sciences at Michigan State University. We thank Emilio Moran and Anthony Cak for their contribution to the development of this work. Nathan Moore and Nafiseh Haghtalab for helping to process and interpret the CHIRPS precipitation data. Any opinions, findings, and conclusions or recommendations expressed in this material are those of the authors and do not necessarily reflect the views of the National Science Foundation.

APPENDIX

Table A1.1 Summary of Hydrologic Indices. Summary of the hydrologic indices developed to quantify changes in magnitude and timing of hydrologic events

Index	**Definition**	**Figure**
Average Discharge	Mean of daily discharge values across the water year, wet and dry seasons	Figure 1.2
Minimum/Maximum Discharge Date	The water year date at which the minimum/maximum flow occurred	Figure A1.7
90^{th} Percentile Discharge	The annual average of discharge values above the 90^{th} percentile for a given year	Figure A1.3
10^{th} Percentile Discharge	The annual average of discharge values below the 10^{th} percentile for a given year	Figure A1.3
Flood Count	The number of events in each year above the long term mean of 90^{th} percentile discharge	Figure A1.6
Low Flow Count	The number of events in each year below the long term mean of 10^{th} percentile discharge	Figure A1.6
Cumulative Flow Arrival	The date of arrival of 50% of cumulative discharge for each year	Figure A1.7
Rise and Fall Rates	The average rate at which the river gains or loses water, taken as the average of positive and negative values form running difference in daily discharge values	Figure A1.8
Standard Deviation	The standard deviation of daily discharge values in each year	Figure A1.9
Hydrograph Amplitude	The distance between the minimum and maximum discharge for each year	Figure A1.9
Hydrograph Period	The distance between the date of the minimum and maximum discharge for each year	Figure A1.9

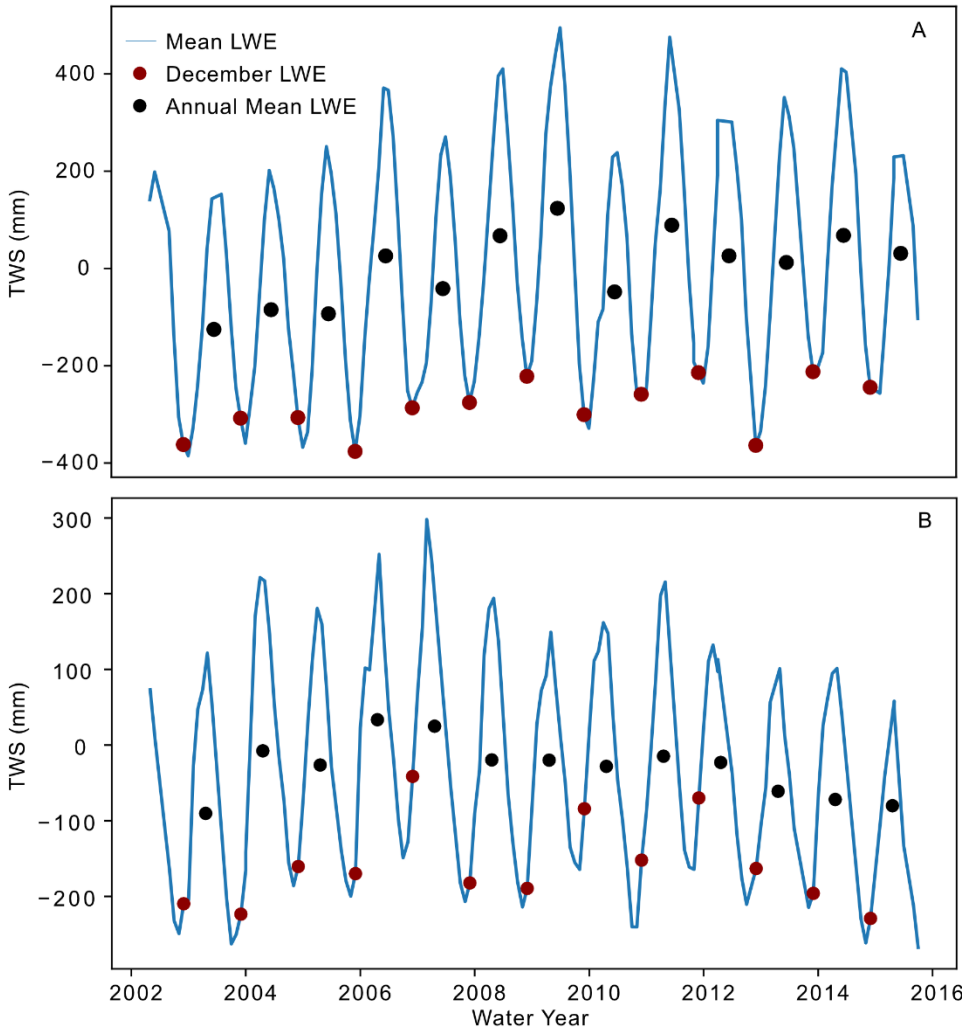

Figure A1.1 GRACE Data Example. Monthly total water storage (blue lines), December TWS values (red) and annual average TWS values (black) for a representative basin showing increasing (A) and decreasing (B) total water storage. Linear regression in the average TWS values are used to evaluate TWS trends, while December TWS values are regressed to assess groundwater storage trends. It should be noted that we observe no significant decreases in groundwater (December TWS values).

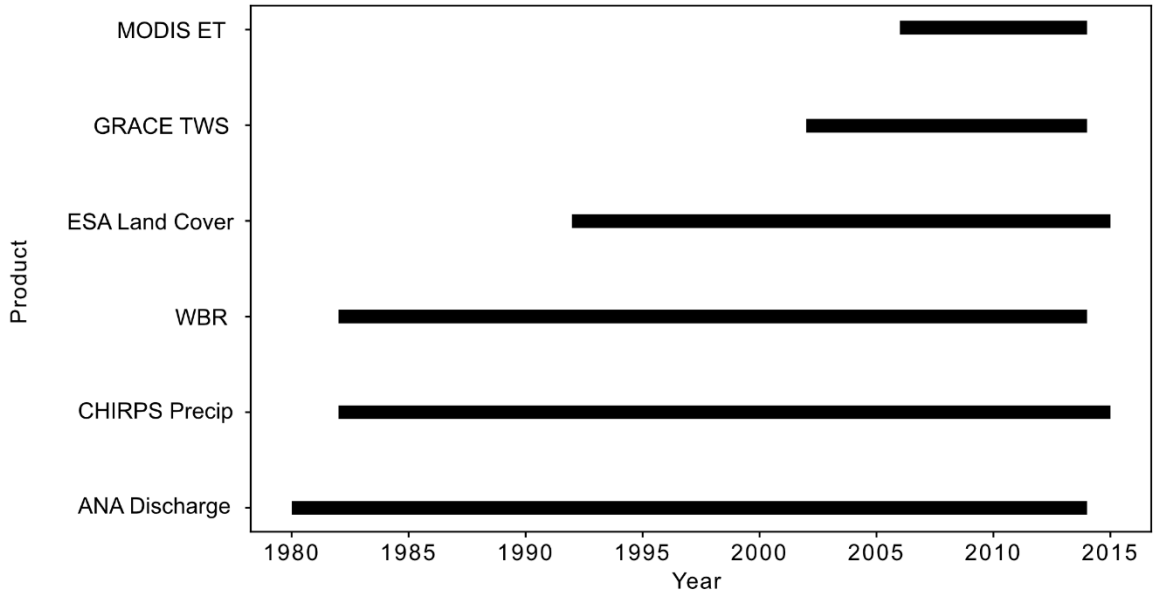

Figure A1.2 Summary of Data Product Temporal Coverage. Temporal coverages of the major data products used in this analysis

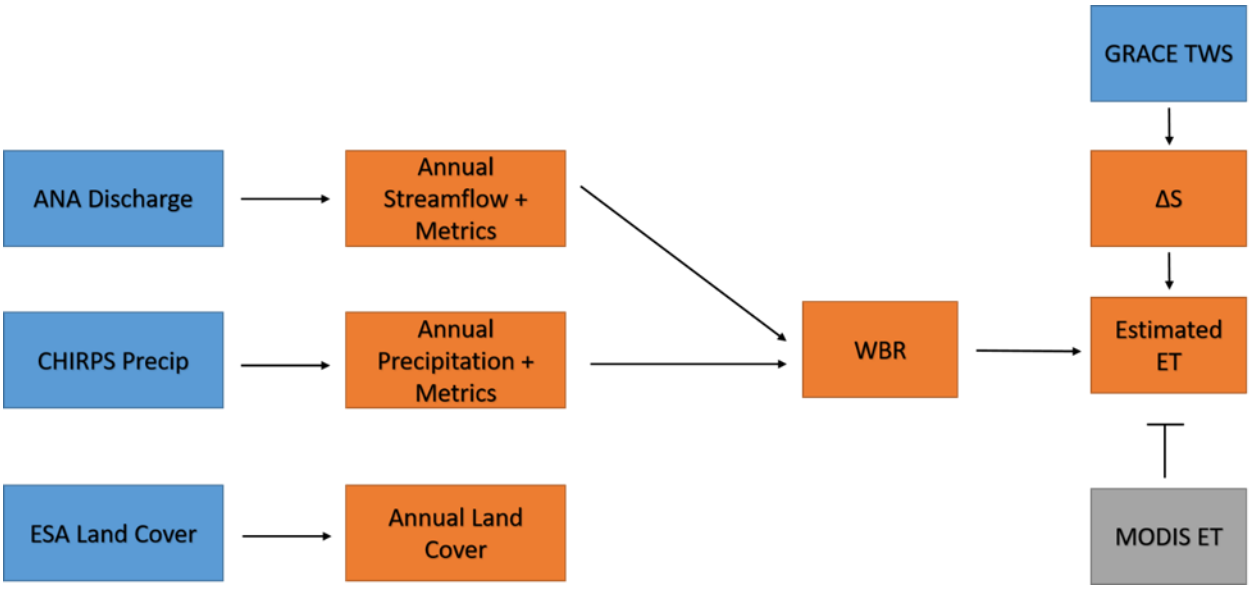

Figure A1.3 Conceptual Diagram of Statistical Workflow. Conceptual figure showing the methods workflow for this study. Blue boxes represent data sources, orange boxes represent derived outcomes from the work for which we calculated trends and grey boxes represent validation data. WBR; Water Balance Residual. ET; Evapotranspiration. TWS; Total Water Storage.

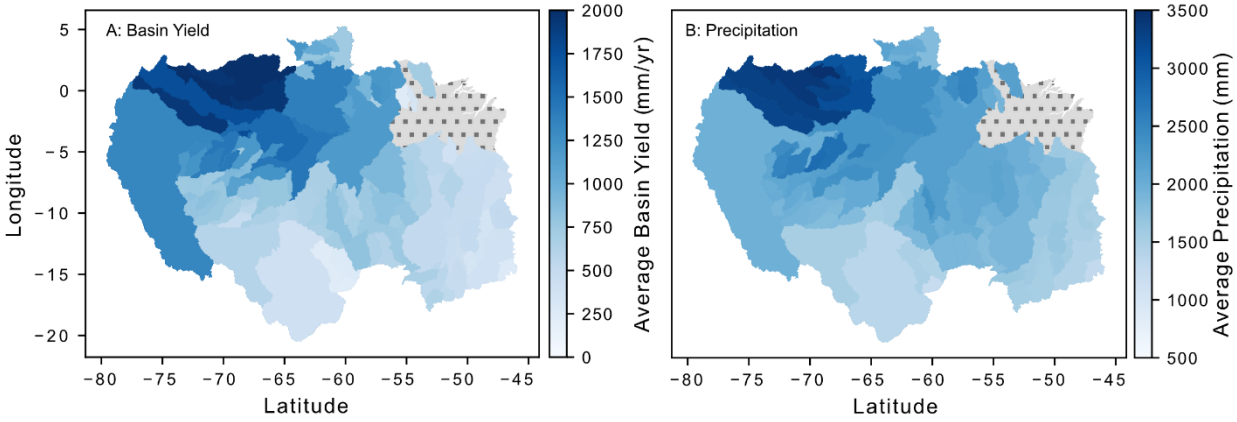

Figure A1.4 Long Term Average of Discharge and Precipitation. Long term average A) basin yield and B) CHIRPS precipitation. Areas in patterned grey lie outside of stream gauge catchments used in this study.

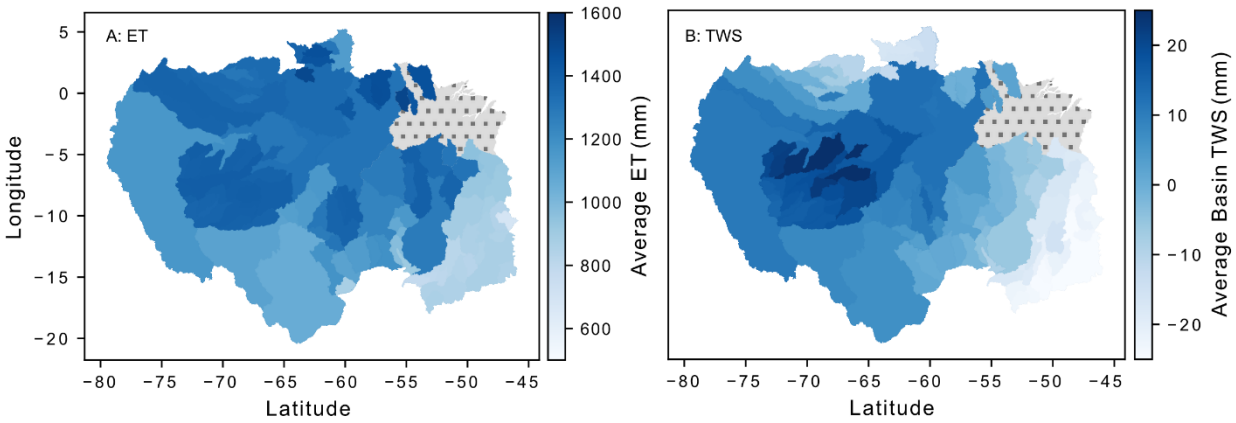

Figure A1.5 Long Term Average of ET and Total Water Storage. Long term average: A) evapotranspiration (MODIS), and B) total water storage (GRACE). Areas in patterned grey lie outside of stream gauge catchments used in this study.

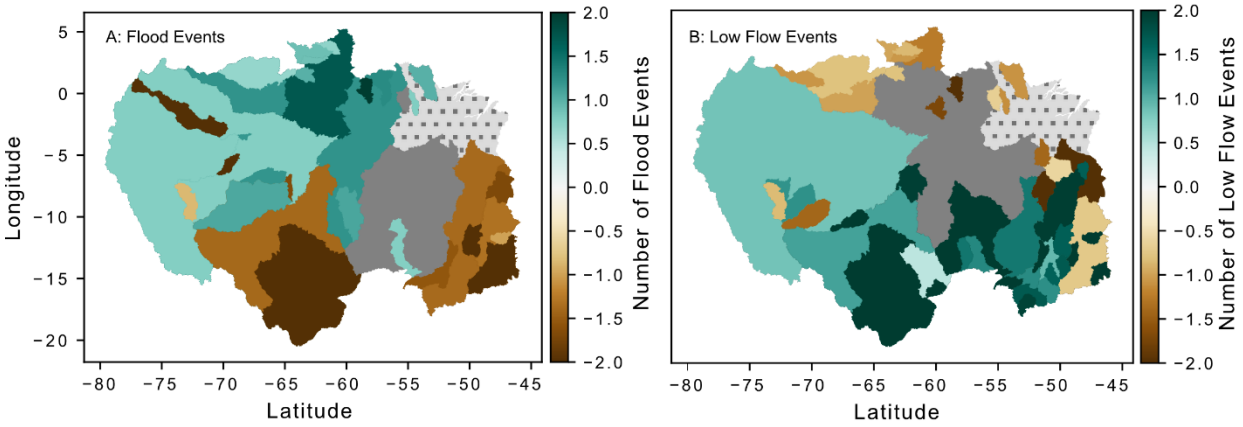

Figure A1.6 Change in the Number of Flood and Low Flow Events. Slope of change in the number of flood (A) and low flow (B) events each year for each gauge basin between 1983 and 2014. These patters are similar to the change in the magnitude of 90th and 10th percentile discharge. Most of the basin shows an increasing number of low flow events, with some decreases in the northern and eastern basin. Flood events are increasing in frequency over much of the central, western and northern basin, while decreasing the southern and far eastern basin. Areas in solid grey have no significant trend, while the patterned grey areas have no data.

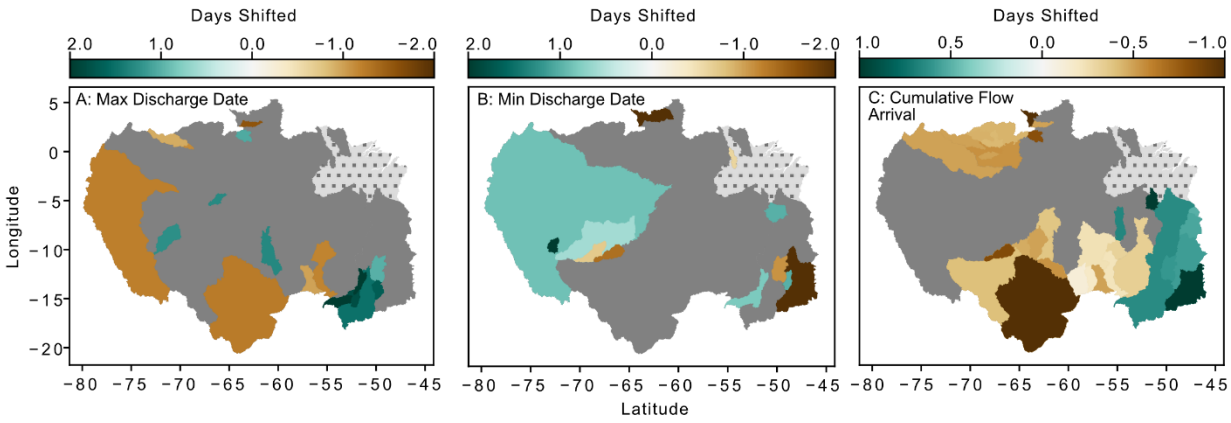

Figure A1.7 Change in Timing of Hydrograph Events. Changing in the date of annual maximum discharge (A) annual minimum discharge (B) and the arrival of half of the cumulative annual flow (C) between 1983 and 2014. Changes in the date of maximum flow are limited, while change in minimum flows are widespread, with both events shifting up to 2 days per year over the record. Cumulative flow arrival dates are shown to be sifting in the range of a day per year, with half of the years water arriving earlier in most areas of the southern, western and northwestern basin. Areas in solid grey have no significant trend, while the patterned grey areas have no data.

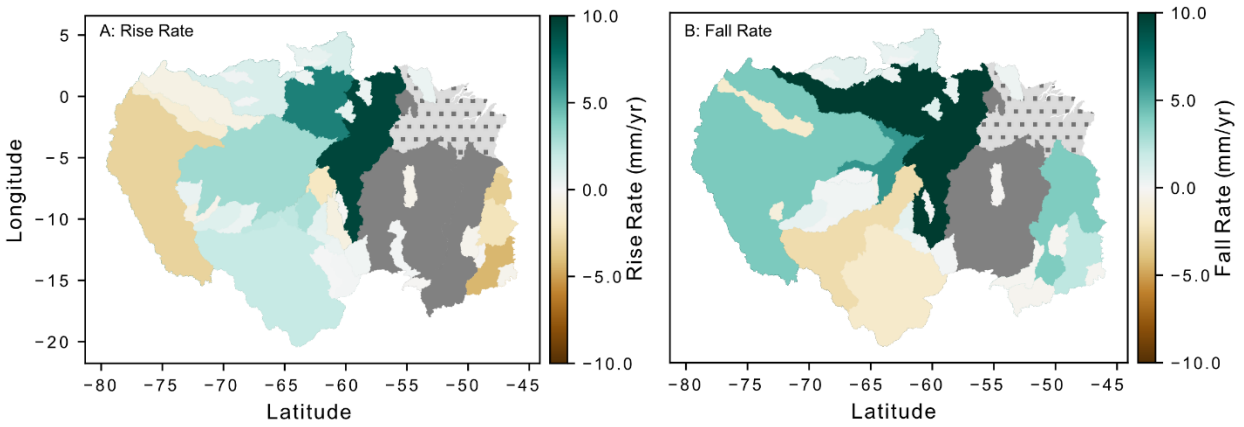

Figure A1.8 Change in the Hydrograph Rise and Fall Rate. Change in the rates of area normalized streamflow (basin yield) during the rising limb of the hydrograph (A) and falling limb of the hydrograph (B) in the gauge basins between 1983 and 2014. Together the change in these indices indicated that basins are becoming flashier, gaining and losing water at a faster rate. This is true over the majority of the central and northern portions of the basin. The western, southern and eastern basins show increases in one metric, but decreases in the other. This indicates imbalanced change in how fast water enters and leave the basin. Areas in solid grey have no significant trend, while the patterned grey areas have no data.

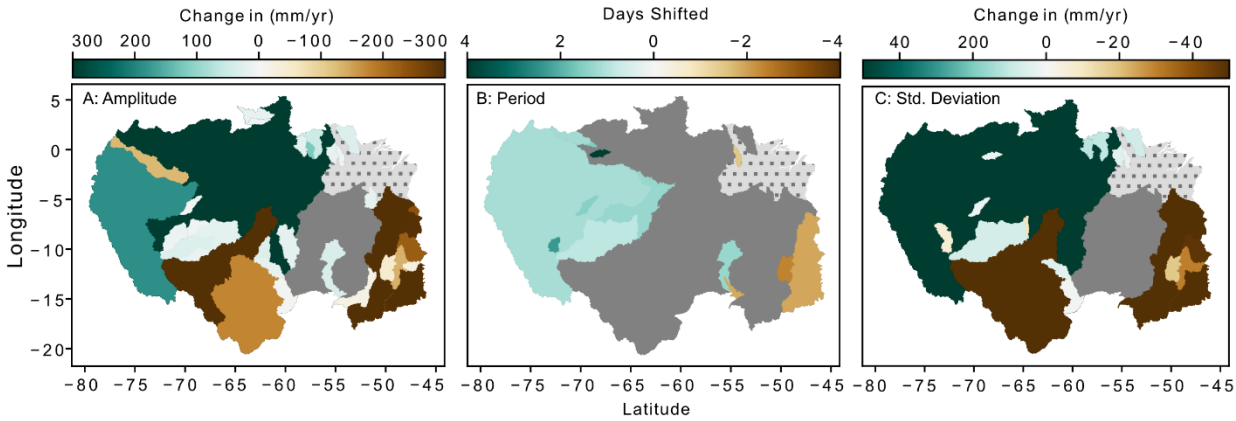

Figure A1.9 Change in the Hydrograph Amplitude, Period and Standard Deviation. Slope of change in hydrograph amplitude (A), hydrograph period (B) and the standard deviation of daily discharge values per year (C) between 1983 and 2014. In the areas of the basin experiencing increased (western and northern basins) the amplitude and standard deviation of the hydrograph have also increased. This indicates increased streamflow being correlated with intensification of the hydrograph. In areas of decreased discharge (South central and eastern portions of the basin) these two parameters have decreased. Areas in solid grey have no significant trend, while the patterned grey areas have no data.

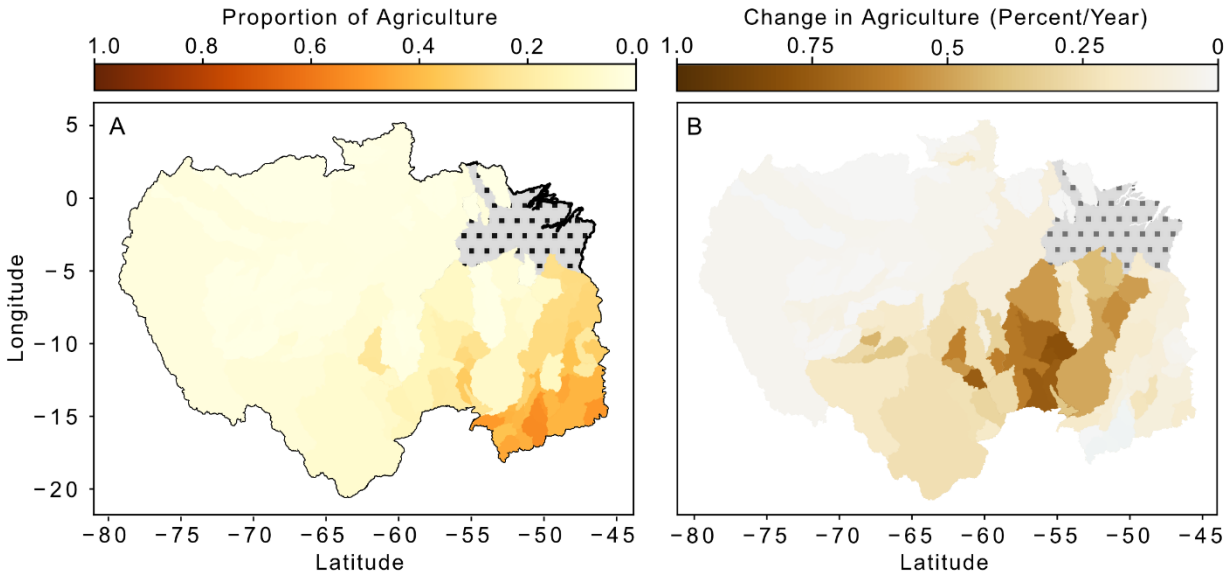

Figure A1.10 Change in Agriculture Land Cover. Percent of Agriculture (A) at the start of the ESA land cover records, showing significant agriculture in the Tocantins Region. Slope of change (B) in agriculture land cover between 1992-2015 showing significant increased in agriculture in the southern Amazon Basin, located primarily in the Xingu, Tocantins and Madeira basins. Areas in patterned grey lie outside of stream gauge catchments used in this study.

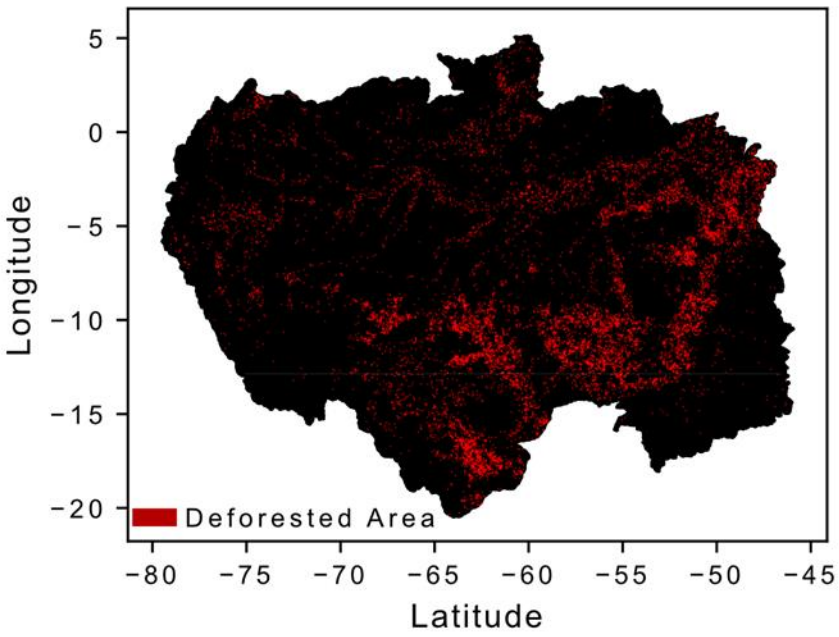

Figure A1.11 Deforested Area from 1992-2015. Map of deforested area from 1992-2015. Areas in red have lost forest cover, with a majority of the deforestation focused around access points (rivers and roads) and in the southern Arc-of-Deforestation

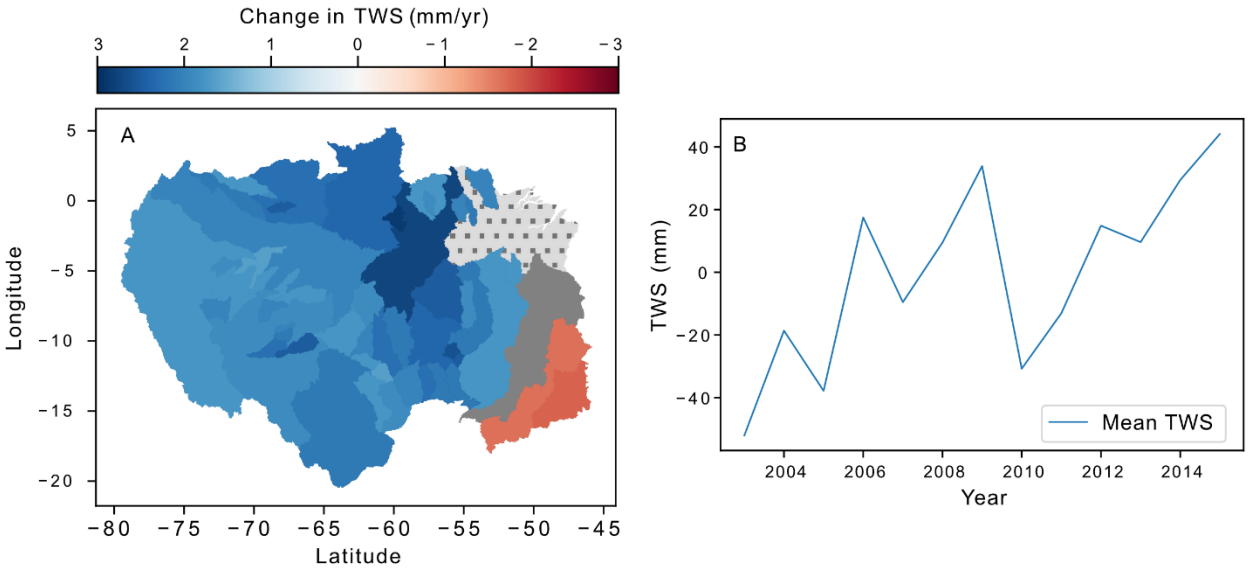

Figure A1.12 Change in Total Water Storage. Slope of change in Total water storage between 2002 and 2014 (A) showing significant increases in TWS over most of the basin, with decreasing TWS in most of the Tocantins. Areas in solid grey have no significant trend, while the patterned grey areas have no data. (B) Average annual total water storage of all basins shown in (A) though time have a clear trend of increasing annual TWS.

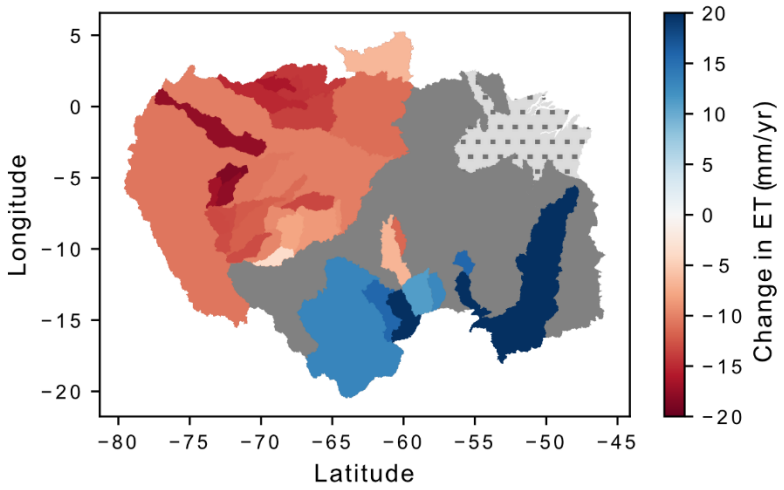

Figure A1.13 Change in MODIS Evapotranspiration. Slopes of significant change in MODIS ET estimates for 2006-2014 (A) show increasing evapotranspiration in the southern and southeastern Amazon, and decreasing in the central, western and northern portions of the basin. Areas in solid grey have no significant trend, while the patterned grey areas have no data.

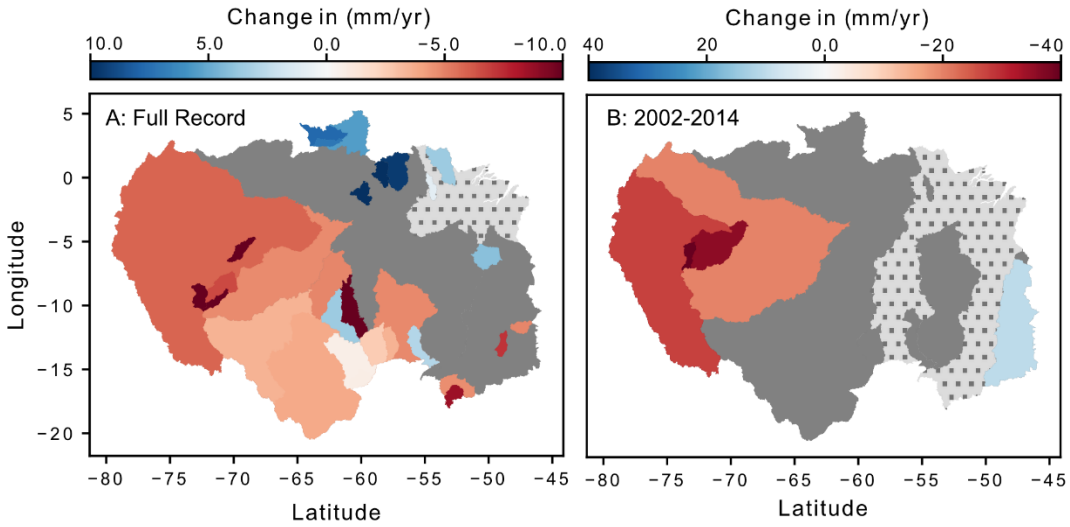

Figure A1.14 Change in End of Dry Season Streamflow. Slopes of significant change in December streamflow values for: A) the entire discharge record, and B) discharge data available between 2002-2014. December discharge values represent change in surface water at the end of the dry season. This constrains change in surface water storage at the end of the dry season, during which we estimate groundwater storage change from GRACE total water storage data. Areas in solid grey have no significant trend, while the patterned grey areas have no data.

REFERENCES

REFERENCES

Arantes, A.E., Ferreira, L.G., Coe, M.T., 2016. The seasonal carbon and water balances of the Cerrado environment of Brazil: Past, present, and future influences of land cover and land use. ISPRS J. Photogramm. Remote Sens. 117, 66–78. https://doi.org/10.1016/j.isprsjprs.2016.02.008

Arias, M.E., Farinosi, F., Lee, E., Livino, A., Briscoe, J., Moorcroft, P.R., 2020. Impacts of climate change and deforestation on hydropower planning in the Brazilian Amazon. Nat. Sustain. 3, 430–436. https://doi.org/10.1038/s41893-020-0492-y

Castello, L., Isaac, V.J., Thapa, R., 2015. Flood pulse effects on multispecies fishery yields in the Lower Amazon. R. Soc. Open Sci. 2, 150299. https://doi.org/10.1098/rsos.150299

Castello, L., Bayley, P.B., Fabré, N.N., Batista, V.S., 2019. Flooding effects on abundance of an exploited, long-lived fish population in river-floodplains of the Amazon. Rev. Fish Biol. Fish. 29, 487–500. https://doi.org/10.1007/s11160-019-09559-x

Coe, M.T., Costa, M.H., Soares-Filho, B.S., 2009. The influence of historical and potential future deforestation on the stream flow of the Amazon River - Land surface processes and atmospheric feedbacks. J. Hydrol. 369, 165–174. https://doi.org/10.1016/j.jhydrol.2009.02.043

Coe, M.T., Latrubesse, E.M., Ferreira, M.E., Amsler, M.L., 2011. The effects of deforestation and climate variability on the streamflow of the Araguaia River, Brazil. Biogeochemistry 105, 119–131. https://doi.org/10.1007/s10533-011-9582-2

Coe, M. T., Macedo, M. N., Brando, P. M., Lefebvre, P., Panday, P., & Silvério, D., 2016. The hydrology and energy balance of the Amazon basin. In *Interactions Between Biosphere, Atmosphere and Human Land Use in the Amazon Basin* (pp. 35-53). Springer, Berlin, Heidelberg. https://doi.org/10.1007/978-3-662-49902-3

Coe, M.T., Brando, P.M., Deegan, L.A., Macedo, M.N., Neill, C., Silvério, D. V., 2017. The Forests of the Amazon and Cerrado Moderate Regional Climate and Are the Key to the Future. Trop. Conserv. Sci. 10, 194008291772067. https://doi.org/10.1177/1940082917720671

Costa, M.H., Foley, J.A., 1999. Trends in the hydrologic cycle of the Amazon basin. J. Geophys. Res. Atmos. 104, 14189–14198. https://doi.org/10.1029/1998JD200126

Costa, M.H., Foley, J.A., 2000. Combined Effects of Deforestation and Doubled Atmospheric CO_2 Concentrations on the Climate of Amazonia. J. Clim. 18–34.

Costa, M.H., Botta, A., Cardille, J.A., 2003. Effects of large-scale changes in land cover on the discharge of the Tocantins River, Southeastern Amazonia. J. Hydrol. 283, 206–217. https://doi.org/10.1016/S0022-1694(03)00267-1

De Paiva, R.C.D., Buarque, D.C., Collischonn, W., Bonnet, M.P., Frappart, F., Calmant, S., Bulhões Mendes, C.A., 2013. Large-scale hydrologic and hydrodynamic modeling of the Amazon River basin. Water Resour. Res. 49, 1226–1243. https://doi.org/10.1002/wrcr.20067

Dias, L.C.P., Macedo, M.N., Costa, M.H., Coe, M.T., Neill, C., 2015. Effects of land cover change on evapotranspiration and streamflow of small catchments in the Upper Xingu River Basin, Central Brazil. J. Hydrol. Reg. Stud. 4, 108–122. https://doi.org/10.1016/j.ejrh.2015.05.010

Duffy, P.B., Brando, P., Asner, G.P., Field, C.B., 2015. Projections of future meteorological drought and wet periods in the Amazon. Proc. Natl. Acad. Sci. U. S. A. 112, 13172–13177. https://doi.org/10.1073/pnas.1421010112

Espinoza Villar, J.C., Guyot, J.L., Ronchail, J., Cochonneau, G., Filizola, N., Fraizy, P., Labat, D., de Oliveira, E., Ordoñez, J.J., Vauchel, P., 2009a. Contrasting regional discharge evolutions in the Amazon basin (1974-2004). J. Hydrol. 375, 297–311. https://doi.org/10.1016/j.jhydrol.2009.03.004

Espinoza Villar, J.C., Ronchail, J., Guyot, J.L., Cochonneau, G., Naziano, F., Lavado, W., de Oliveira, E., Pombosa, R., Vauchel, P., 2009b. Spatio-temporal rainfall variability in the Amazon basin countries (Brazil, Peru, Bolivia, Colombia, and Ecuador). Int. J. Climatol. 29, 1574–1594. https://doi.org/10.1002/joc.1791

European Space Agency. 2009. ESA Land Cover CCI Product User Guide Version 2. Technical Report. URL: http://maps.elie.ucl.ac.be/CCI/viewer/download/ESACCI-LC-Ph2-PUGv2_2.0.pdf Accessed June 25, 2018.

Funk, C.C., Peterson, P.J., Landsfeld, M.F., Pedreros, D.H., Verdin, J.P., Rowland, J.D., Romero, B.E., Husak, G.J., Michaelsen, J.C., Verdin, A.P., 2014. A Quasi-Global Precipitation Time Series for Drought Monitoring. U.S. Geol. Surv. Data Ser. 832, 4. https://doi.org/http://dx.doi.org/110.3133/ds832

Gleeson, T., Villhoth, K., Taylor, R., Perrone, D., Hyndman, D.W., 2019. Groundwater: a call to action. Nature 576. https://doi.org/10.1038/d41586-019-03711-0

Gloor, M., Brienen, R.J.W., Galbraith, D., Feldpausch, T.R., Schöngart, J., Guyot, J.L., Espinoza, J.C., Lloyd, J., Phillips, O.L., 2013. Intensification of the Amazon hydrological

cycle over the last two decades. Geophys. Res. Lett. 40, 1729–1733. https://doi.org/10.1002/grl.50377

Gorelick, N., Hancher, M., Dixon, M., Ilyushchenko, S., Thau, D., Moore, R., 2017. Google Earth Engine: Planetary-scale geospatial analysis for everyone. Remote Sens. Environ. 202, 18–27. https://doi.org/10.1016/j.rse.2017.06.031

Greenlee, D.D., 1987. Raster and vector processing for scanned linework. Photogramm. Eng. Remote Sens. 53, 1383–1387.

Guimberteau, M., Ciais, P., Pablo Boisier, J., Paula Dutra Aguiar, A., Biemans, H., De Deurwaerder, H., Galbraith, D., Kruijt, B., Langerwisch, F., Poveda, G., Rammig, A., Andres Rodriguez, D., Tejada, G., Thonicke, K., Von Randow, C., Randow, R., Zhang, K., Verbeeck, H., 2017. Impacts of future deforestation and climate change on the hydrology of the Amazon Basin: A multi-model analysis with a new set of land-cover change scenarios. Hydrol. Earth Syst. Sci. 21, 1455–1475. https://doi.org/10.5194/hess-21-1455-2017

Haghtalab, N., Moore, N., Heerspink, B.P., Hyndman, D.W., 2020. Evaluating spatial patterns in precipitation trends across the Amazon basin driven by land cover and global scale forcings. Theor. Appl. Climatol. https://doi.org/10.1007/s00704-019-03085-3

Hayhoe, S.J., Neill, C., Porder, S., Mchorney, R., Lefebvre, P., Coe, M.T., Elsenbeer, H., Krusche, A. V., 2011. Conversion to soy on the Amazonian agricultural frontier increases streamflow without affecting stormflow dynamics. Glob. Chang. Biol. 17, 1821–1833. https://doi.org/10.1111/j.1365-2486.2011.02392.x

Hyndman, D.W., 2014, Impacts of Projected Changes in Climate on Hydrology, Bill Freedman (ed.), Handbook of Global Environmental Change, Springer, Berlin, Heidelberg. https://doi.org/10.1007/978-94-007-5784-4_131

Hyndman, D.W., Xu, T., Deines, J.M., Cao, G., Nagelkirk, R., Viña, A., McConnell, W., Basso, B., Kendall, A.D., Li, S., Luo, L., Lupi, F., Ma, D., Winkler, J.A., Yang, W., Zheng, C., Liu, J., 2017. Quantifying changes in water use and groundwater availability in a megacity using novel integrated systems modeling. Geophys. Res. Lett. 44, 8359–8368. https://doi.org/10.1002/2017GL074429

Kendall, M.G. 1975. Rank Correlation Methods, 4th edition, Charles Griffin, London.

Landerer, F.W., Swenson, S.C., 2012. Accuracy of scaled GRACE terrestrial water storage estimates. Water Resour. Res. 48, 1–11. https://doi.org/10.1029/2011WR011453

Latrubesse, E.M., Arima, E., Ferreira, M.E., Nogueira, S.H., Wittmann, F., Dias, M.S., Dagosta, F.C.P., Bayer, M., 2019. Fostering water resource governance and conservation in the Brazilian Cerrado biome. Conserv. Sci. Pract. 1, 1–8. https://doi.org/10.1111/csp2.77

Lavagnini, I., Badocco, D., Pastore, P., Magno, F., 2011. Theil-Sen nonparametric regression technique on univariate calibration, inverse regression and detection limits. Talanta 87, 180–188. https://doi.org/10.1016/j.talanta.2011.09.059

Lehner, B., Verdin, K., Jarvis, A. 2006. HydroSHEDS Technical Documentation. World Wildlife Fund US, Washington, DC. Available at http://hydrosheds.cr.usgs.gov

Levy, M.C., Lopes, A. V., Cohn, A., Larsen, L.G., Thompson, S.E., 2018. Land Use Change Increases Streamflow Across the Arc of Deforestation in Brazil. Geophys. Res. Lett. 45, 3520–3530. https://doi.org/10.1002/2017GL076526

Lewinsohn, T.M., Prado, P.I., 1994. How many species are there? Conserv. Biol. 19, 619–624. https://doi.org/10.1007/BF02291892

Li, F., Zhang, G., Xu, Y.J., 2014. Spatiotemporal variability of climate and streamflow in the Songhua River Basin, northeast China. J. Hydrol. 514, 53–64. https://doi.org/10.1016/j.jhydrol.2014.04.010

Maeda, E.E., Ma, X., Wagner, F., Kim, H., Oki, T., Eamus, D., 2017. Evapotranspiration seasonality across the Amazon basin. Earth Syst. Dyn. 439–454. https://doi.org/10.5194/esd-2016-75

Melack, J.M., and Coe, M.T. Amazon floodplain hydrology and implications for aquatic conservation, Aquat. Conserv. *in review*.

Malhi, Y., Roberts, J.T., Betts, R.A., Killeen, T.J., Li, W., Nobre, C.A., 2008. Climate change, deforestation, and the fate of the Amazon. Science (80-.). 319, 169–172. https://doi.org/10.1126/science.1146961

Mann, H.B., 1945. Nonparametric Tests Against Trend Author. Econometrica 13, 245–259.

Miguez-Macho, G., Fan, Y., 2012. The role of groundwater in the Amazon water cycle: 1. Influence on seasonal streamflow, flooding and wetlands. J. Geophys. Res. Atmos. 117, 1–30. https://doi.org/10.1029/2012JD017539

Miguez-Macho, G., Fan, Y., 2012. The role of groundwater in the Amazon water cycle: 2. Influence on seasonal soil moisture and evapotranspiration. J. Geophys. Res. Atmos. 117. https://doi.org/10.1029/2012JD017540

Molina-Carpio, J., Espinoza, J.C., Vauchel, P., Ronchail, J., Gutierrez Caloir, B., Guyot, J.L., Noriega, L., 2017. Hydroclimatology of the Upper Madeira River basin: spatio-temporal variability and trends. Hydrol. Sci. J. 62, 911–927. https://doi.org/10.1080/02626667.2016.1267861

Mu, Q., Heinsch, F.A., Zhao, M., Running, S.W., 2007. Development of a global evapotranspiration algorithm based on MODIS and global meteorology data. Remote Sens. Environ. 111, 519–536. https://doi.org/10.1016/j.rse.2007.04.015Neill, C., Coe, M.T., Riskin, S.H., Krusche, A. V., Elsenbeer, H., Macedo, M.N., McHorney, R., Lefebvre, P., Davidson, E.A., Scheffler, R., Figueira, A.M. e. S., Porder, S., Deegan, L.A., 2013. Watershed responses to Amazon soya bean cropland expansion and intensification. Philos. Trans. R. Soc. B Biol. Sci. 368, 20120425–20120425. https://doi.org/10.1098/rstb.2012.0425

Niu, J., Shen, C., Chambers, J.Q., Melack, J.M., Riley, W.J., 2017. Interannual variation in hydrologic budgets in an amazonian watershed with a coupled subsurface-land surface process model. J. Hydrometeorol. 18, 2597–2617. https://doi.org/10.1175/JHM-D-17-0108.1

Panday, P.K., Coe, M.T., Macedo, M.N., Lefebvre, P., Castanho, A.D. de A., 2015. Deforestation offsets water balance changes due to climate variability in the Xingu River in eastern Amazonia. J. Hydrol. 523, 822–829. https://doi.org/10.1016/j.jhydrol.2015.02.018

Pekel, J.F., Cottam, A., Gorelick, N., Belward, A.S., 2016. High-resolution mapping of global surface water and its long-term changes. Nature 540, 418–422. https://doi.org/10.1038/nature20584

Penatti, N.C., Almeida, T.I.R. de, Ferreira, L.G., Arantes, A.E., Coe, M.T., 2015. Satellite-based hydrological dynamics of the world's largest continuous wetland. Remote Sens. Environ. 170, 1–13. https://doi.org/10.1016/j.rse.2015.08.031

Pokhrel, Y.N., Fan, Y., Miguez-Macho, G., Yeh, P.J.F., Han, S.C., 2013. The role of groundwater in the Amazon water cycle: 3. Influence on terrestrial water storage computations and comparison with GRACE. J. Geophys. Res. Atmos. 118, 3233–3244. https://doi.org/10.1002/jgrd.50335

Rattis. L., Brando, P.M, Macedo, M.N., Spera, S., Castanho, A., Marques, E., Queiroz, N., Silverio, D., Coe, M.T., When Brazil will reach the limit of rainfed agriculture? Nat. Clim. Change. *in review*.

Running S., Mu, Q. 2015. MOD16A2 MODIS/Terra Evapotranspiration 8-day L4 Global 500m SIN Grid. NASA LP DAAC. University of Montana and MODAPS SIPS - NASA. http://doi.org/10.5067/MODIS/MOD16A2.006

Schramm, M., 2016. Mann-Kendall-Trend. Gitlab repository, https://github.com/mps9506/Mann-Kendall-Trend. Accessed March 23, 2018.

Sen, P.K., 1968. Estimates of the Regression Coefficient Based on Kendall's Tau. J. Am. Stat. Assoc. 63, 1379–1389. https://doi.org/10.1080/01621459.1968.10480934

Seabold, S., Perktold, J., 2010. "statsmodels: Econometric and statistical modeling with python." Proceedings of the 9th Python in Science Conference.

Salati, E., Dall'Olio, A., Matsui, E., Gat, J.R., 1979. Recycling of water in the Amazon Basin: An isotopic study. Water Resour. Res. 15, 1250–1258. https://doi.org/10.1029/WR015i005p01250

Silvério, D. V., Brando, P.M., Macedo, M.N., Beck, P.S.A., Bustamante, M., Coe, M.T., 2015. Agricultural expansion dominates climate changes in southeastern Amazonia: The overlooked non-GHG forcing. Environ. Res. Lett. 10. https://doi.org/10.1088/1748-9326/10/10/104015

Sorribas, M.V., Paiva, R.C.D., Melack, J.M., Bravo, J.M., Jones, C., Carvalho, L., Beighley, E., Forsberg, B., Costa, M.H., 2016. Projections of climate change effects on discharge and inundation in the Amazon basin. Clim. Change 136, 555–570. https://doi.org/10.1007/s10584-016-1640-2

Spera, S.A., Galford, G.L., Coe, M.T., Macedo, M.N., Mustard, J.F., 2016. Land-use change affects water recycling in Brazil's last agricultural frontier. Glob. Chang. Biol. 22, 3405–3413. https://doi.org/10.1111/gcb.13298

Stickler, C.M., Coe, M.T., Costa, M.H., Nepstad, D.C., McGrath, D.G., Dias, L.C.P., Rodrigues, H.O., Soares-Filho, B.S., 2013. Dependence of hydropower energy generation on forests in the Amazon Basin at local and regional scales. Proc. Natl. Acad. Sci. U. S. A. 110, 9601–9606. https://doi.org/10.1073/pnas.1215331110

Swenson, S., Wahr, J., 2006. Post-processing removal of correlated errors in GRACE data. Geophys. Res. Lett. 33, 1–4. https://doi.org/10.1029/2005GL025285

Swenson, S.C. 2012. GRACE monthly land water mass grids NETCDF RELEASE 5.0. Ver. 5.0. PO.DAAC, CA, USA. http://dx.doi.org/10.5067/TELND-NC005.

Timpe, K., Kaplan, D., 2017. The changing hydrology of a dammed Amazon. Sci. Adv. 3, 1–14. https://doi.org/10.1126/sciadv.1700611

Theil,H. 1950. A rank-invariant method of linear and polynomial regression analysis, I, II, III. Proc. R. Neth. Acad. Sci, 53, Part I: 386-392, Part II: 521-525, Part III: 1397-1412.

Tomasella, J., Pinho, P.F., Borma, L.S., Marengo, J.A., Nobre, C.A., Bittencourt, O.R.F.O., Prado, M.C.R., Rodriguez, D.A., Cuartas, L.A., 2013. The droughts of 1997 and 2005 in Amazonia: Floodplain hydrology and its potential ecological and human impacts. Clim. Change 116, 723–746. https://doi.org/10.1007/s10584-012-0508-3

Travis E. Oliphant, 2006. A guide to NumPy. Trelgol Publishing, USA

Virtanen, P., Gommers, R., Oliphant, T.E., Haberland, M., Reddy, T., Cournapeau, D., Burovski, E., Peterson, P., Weckesser, W., Bright, J., van der Walt, S.J., Brett, M., Wilson, J., Millman, K.J., Mayorov, N., Nelson, A.R.J., Jones, E., Kern, R., Larson, E., Carey, C.J., Polat, İ., Feng, Y., Moore, E.W., VanderPlas, J., Laxalde, D., Perktold, J., Cimrman, R., Henriksen, I., Quintero, E.A., Harris, C.R., Archibald, A.M., Ribeiro, A.H., Pedregosa, F., van Mulbregt, P., SciPy 1.0 Contributors, 2020. SciPy 1.0: fundamental algorithms for scientific computing in Python. Nat. Methods. https://doi.org/10.1038/s41592-019-0686-2

von Randow, C., Manzi, A.O., Kruijt, B., de Oliveira, P.J., Zanchi, F.B., Silva, R.L., Hodnett, M.G., Gash, J.H.C., Elbers, J.A., Waterloo, M.J., Cardoso, F.L., Kabat, P., 2004. Comparative measurements and seasonal variations in energy and carbon exchange over forest and pasture in South West Amazonia. Theor. Appl. Climatol. 78, 5–26. https://doi.org/10.1007/s00704-004-0041-z

Vörösmarty, C.J., Green, P., Salisbury, J., Lammers, R.B., 2000. Global water resources: Vulnerability from climate change and population growth. Science (80-.). 289, 284–288. https://doi.org/10.1126/science.289.5477.284

Werth, D., Avissar, R., 2004. The regional evapotranspiration of the Amazon. J. Hydrometeorol. 5, 100–109. https://doi.org/10.1175/1525-7541(2004)005<0100:TREOTA>2.0.CO;2

CHAPTER 2: INVESTIGATING THE EFFECTS OF LAND COVER ON GROUNDWATER DYNAMICS AND STREAMFLOW IN THE SOUTHERN AMAZON BASIN HEADWATERS

Abstract:

Increased demand for arable land and infrastructure has driven mass deforestation and land cover change across the Amazon Basin, which is responsible for globally important water and energy fluxes. These changes are concentrated in the southern headwaters region of the Amazon Basin, which are susceptible to land cover driven changes in surface and groundwater resources. Previous research has demonstrated that deforestation in this region reduces ET and increases streamflow. Less well understood are how ground- and soil-water stores are changing, particularly given the relative lack of data on the dynamics of these subsurface systems. Here, we used process-based models to investigate the subsurface hydrologic dynamics of a research site in the headwaters of the Xingu River Basin, within Brazil's agricultural frontier. We model the surface, vadose zone, and saturated zone fluxes into and out of the system, focusing on the changes in depth to groundwater and streamflow discharge, for both current land cover and a historical ("no-deforestation") land cover scenario. Results of the vadose-zone and groundwater models demonstrate significant shifts in the water balance, with deforestation altering both surface and groundwater dynamics. In the current land use scenario, simulated water table elevations under soy agriculture are up to 10 m higher than in forested regions. To quantify the effect of deforestation, we calculated the difference in simulated streamflows and water table elevations between "current land use" and "no deforestation" scenarios. This comparison showed that deforestation increased annual average streamflows by 46% and water table elevations by 0.043m/yr between 2006 and 2018.

1. Introduction:

Globally, water resources are threatened by anthropogenic impacts including pollution (e.g. Kolpin et al., 1998), nutrient loading (e.g. Vitousek at al., 1997), over extraction (e.g. Haacker et al., 2016), damming (e.g. Timpe and Kaplan, 2017), climate change (e.g. Vörösmarty et al., 2000), and landscape alteration (e.g. Coe et al., 2009). These changes are especially evident in areas experiencing rapid development and landscape alteration, such as in the Amazon River Basin (Levy et al., 2018). The water balance has also been altered across the Amazon due to landscape changes, including alterations to streamflow, precipitation and ET (Dial et al., 2015, Espinoza et al., 2009, Haghtalab et al., 2020) and building of reservoirs (Moran et al., 2018). Of particular concern in the Amazon Basin is the extent to which widespread deforestation is altering the water balance partitioning between evaporation and runoff, and subsequent precipitation recycling of transpired water within the basin. The Amazon Basin receives up to 3000 mm of precipitation annually, approximately half of which is evapotranspired back into the atmosphere by dense rainforest vegetation (Madea et al., 2017). A significant percent of the annual rainfall in the Amazon is sourced from this recycled water, as demonstrated by a progressive inland gradient in 18O enrichment of precipitation (Salati et al., 1979).

Immense deforestation has already occurred in the southern Arc-of-Deforestation region, which lies within the headwaters of the Xingu, Tapajos and Madeira Rivers. This deforestation was historically driven by the need for cattle pasture land, but more recently, conversion to soy agriculture has become the dominant driver of deforestation (Fernside, 2005). Furthermore, the rate of deforestation recently has increased from a low of 4571 km/year in 2012 to 9762 km/year in 2019 (INPE, 2019). Recent research has suggested that if deforestation continues, the Amazon

may reach a “tipping point”, where the system will no longer be able to return enough water to the atmosphere to support the rainforest ecosystem (Lovejoy and Nobre, 2018).

Landcover change in the Upper Xingu Basin has been shown to significantly alter the surface water fluxes at local to regional scales (Coe et al., 2009, Dias et al., 2015, Hayhoe et al., 2011). Field and modeling investigations have demonstrated that deforestation increases river discharge and land surface temperature, while decreasing evapotranspiration (ET). Hayhoe et al. (2011) monitored river discharge in forested and soy agriculture dominated first order stream catchments in the Upper Xingu Basin and demonstrated a four-fold increase in river discharge in the soy watersheds when compared to forests systems. Dias et al. (2015) simulated precipitation, ET, and streamflow differences across land covers (rainforest, grassland, soy, and pasture) using land surface and crop models. Soy agricultural areas were shown to have significantly lower ET and higher streamflows. At the scale of the Xingu Basin, Panday et al. (2015) showed that observed deforestation from the 1970’s to 2000’s resulted in a 6% increase in streamflow and a 3% decrease in ET. Less well understood however, is the role of saturated groundwater systems in the hydrologic dynamics of the Amazon headwaters, or how groundwater responds to the observed landscape changes.

Across the Amazon Basin, groundwater is the least well understood component of the water balance, and its responses to climate and land cover change are poorly constrained. Previous modeling studies have investigated the importance of groundwater in the Amazon hydrologic cycle at the Amazon Basin scale. Work by Miguez-Macho et al. (2012) demonstrated that groundwater is an important component of streamflow across the Amazon Basin, especially in the upland or headwater regions. These large-scale models however don’t have the spatial resolution to accurately simulate groundwater dynamics in headwaters regions. Previous studies

of deforestation effects on the water balance of the Amazon headwaters do not explicitly characterize or model the saturated groundwater system. Instead, change in groundwater storage is generally inferred from statistical water balance calculations or using remote sensing data (Panday et al., 2015, Dias et al. 2015). Field studies have shown that groundwater is important for regulating river discharge and total water storage in this region. Heyhoe et al. (2011) estimated that up to 90% of river discharge in the Xingu headwater catchments are sourced from groundwater, using statistical hydrograph separation techniques. A more detailed study of the saturated system is needed to better understand the role of groundwater dynamics in Amazon headwaters hydrology and its response to changes in climate and land cover.

The overarching goal of this work is to quantify the groundwater dynamics of the upper Amazon Basin, and to simulate how changing land cover has affected these headwater systems. A better understanding of subsurface water dynamics in this region is critical to project how further changes to the landscape will affect water resources in the Amazon River Basin and associated Rainforest ecosystems.

Specifically, we seek to investigate the current distribution and dynamics of groundwater in the saturated zone, and assess the extent to which it controls river discharge. We predict that groundwater is the dominant source of streamflow in these headwaters, and that explicitly simulating saturated groundwater will improve our ability to model streamflow in the regions headwater reaches. We simulate fluxes for both the current land cover distribution and under a counterfactual “no-deforestation” scenario. Comparing the results of this scenario to current conditions will allow us to quantify the effects of deforestation on groundwater. We expect that conversion to soy agriculture has increased both groundwater storage, and groundwater-derived streamflow.

2. Methods

2.1 Study Location:

This study focuses on the Tanguro Ranch Research Station (Figure 2.1), located within the headwaters of the Xingu River Basin, on an 80,000 ha soybean ranch in the state of Mato Grosso, Brazil. Research at this site has focused on forest ecology, effects of fires, along with nutrient and surface water dynamics (Brando et al., 2014, Neill et al., 2013, Dias et al., 2015, Hayhoe et al, 2011). The Tanguro Region experienced deforestation and conversion from transitional rainforest to pasture lands in the 1980s, with further conversion to soy agriculture in the early 2000s (Neil et al., 2013). This land use history is similar to much of the Arc-of-Deforestation, which is the Amazon's epicenter of deforestation along the southern extent of the basin (Barona et al., 2010). This site hosts a set of river gauging stations in first- and second-order watersheds across a range of the land cover conditions from the mid-2000s to present (Figure A2.1). Each river gauging site has a transect of 5-7 shallow riparian groundwater monitoring wells, extending from the stream toward the uplands on both sides of the channel (Figure A2.1). Rainfall, other climate conditions, evapotranspiration, and soil moisture data are also available at this site. The mean annual precipitation at Tanguro Ranch from 2000 to 2018 was 1785 mm/year with a strongly seasonal pattern; mean wet season rainfall was 1735 mm/year while the dry season average was only 63 mm/year.

The shallow groundwater system at Tanguro Ranch is controlled by its Oxisol soils. Most of the region has 20 to 100 m of fluvial deposits with a sandy clay texture (55% sand, 2% silt, and 43% clay), overlying Precambrian gneiss (Hengl et al., 2017, Scheffler et al. 2011). Oxisols are highly weathered, resulting in clay aggregates that allow rapid water drainage while retaining significant soil moisture levels (Neil et al. 2013, Renck and Lehmann., 2004, Scheffler et al.

2011). These soils are widespread across the southern Amazon Basin headwaters region, which has experienced heavy deforestation and conversion to soy agriculture (Eswaran and Reich, 2005, Neil et al., 2013). Tanguro Ranch thus provides an excellent venue to study the effects of changing land use in the Amazon headwaters on saturated groundwater dynamics.

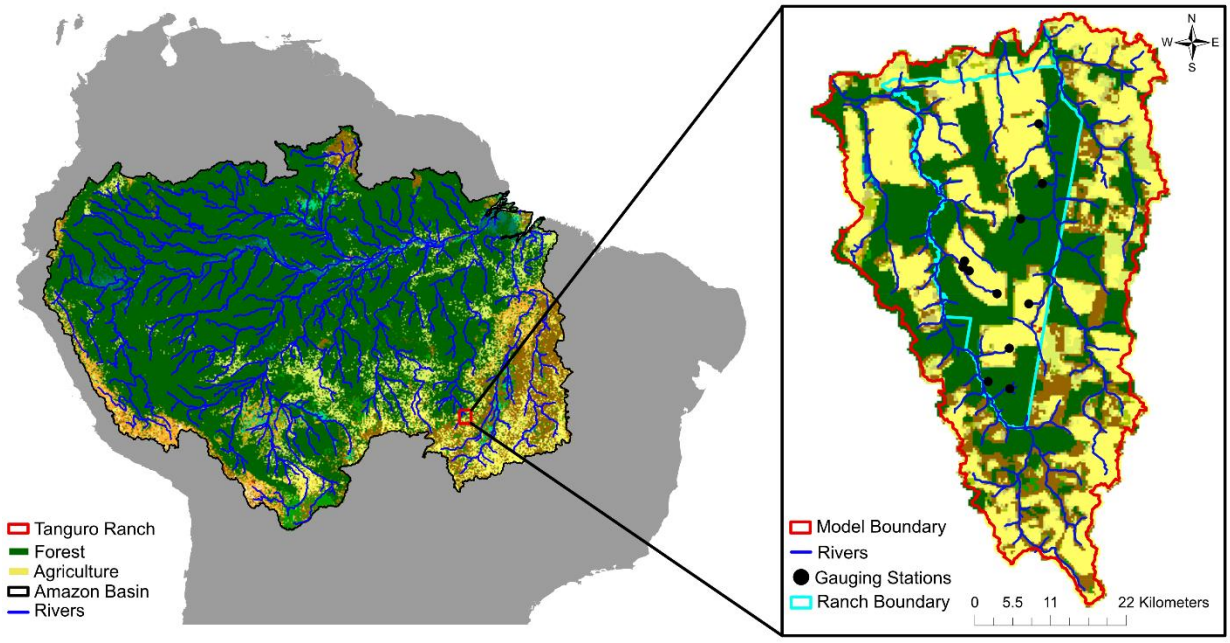

Figure 2.1 Groundwater Model Study Area. Location of Tanguro Ranch long term ecological research site and groundwater model domain (inset), with 2015 land cover from the European Space Agency (ESA, 2017) and Amazon Basin river network from HydroSHEDS (Lehner et al., 2006).

2.2 Data Sources and Analysis:

We synthesized field data from the Tanguro Ranch research station to parameterize the groundwater model. Since the mid-2000s, stream discharge and riparian groundwater levels across the site were regularly monitored in first- and second-order watersheds as described in Heyhoe et al. (2011). We used discharge data from the seven watersheds (Figure A2.1) with most reliable stage-discharge relationships and long-term streamflow records to calibrate our groundwater model. During a 2018 field campaign, we also characterized the shallow aquifer hydraulic conductivity and specific storage values using pump tests in each well of the riparian

transects for six of the watersheds (Figure A2.1). Water levels were monitored using a pressure transducer at 0.5 second intervals during both pumping and recovery phases of these tests. These water level data were processed in Python to remove data points outside of the pump test duration, and to convert data from elevation to drawdown relative to initial head. Using this processed data, hydraulic conductivity (K) values were estimated by curve fitting in AQTESOLV (Duffield, 2007) using the Theis method (Theis, 1935).

Soil moisture has been continuously monitored at six-hourly intervals from January of 2011 to present under both rainforest and soy agriculture land covers using Time Domain Reflectometry (TDR) probes deployed horizontally from soil pits. Each pit was outfitted with twelve probes at depths of 10, 30 and 50cm in the near surface, and at 100cm intervals between 100 and 900cm. These soil moisture data were used to validate our vadose zone unsaturated flow models for the forest and soy land cover types at Tanguro, as discussed below.

Precipitation data for the vadose zone model was downloaded from the Climate Hazards group InfraRed Precipitation with Stations (CHIRPS) 0.05 degree gridded daily precipitation product (Funk, 2014). These daily rainfall grids were extracted across the Tanguro Ranch site to create a time series estimates of average rainfall for our 2006-2018 model period. We chose to use the CHIRPS precipitation product because the Tanguro Ranch weather station's tipping bucked rain gauge is unreliable for recording large rainfall events, and there are significant gaps in the data record during our study period. The CHIRPS product is available at daily resolution throughout our study period, and agrees well with periodic measurements taken from a manual rain gauge at the site.

Estimates for aquifer bottom depth were extracted from the International Soil Reference Information Centre (ISRIC) *SoilGrids* 250 m gridded depth to bedrock layer (Hengl et al., 2017).

For this region, this product has a clear signature of land cover in the data, such that areas overlain by forest cover have artificially shallow bedrock. We removed this bias by masking out the depth to bedrock layer in the forested zone, and interpolated across the masked out areas using Empirical Bayesian Kriging in the Geospatial Analyst package of ArcGIS Pro Version2.2.0 (Krivoruchko, 2012). Finally, we enforced a 1m minimum thickness between the bedrock and surface elevations as there are no known outcrops of bedrock at the surface across this site.

Landcover data were extracted from the European Space Agency (ESA) Climate Change Initiative (CCI) Land Cover Climate Research Data with 300-m resolution, available annually from 1992 to 2015. Land cover was relatively constant in the Tanguro region during this period, with most of the deforestation occurring in the 1980's. As such, we assume no significant land cover change between 2015 and 2018. We used the extent of forest and soy agriculture in 2015 to extract remote seining inputs (LAI and ET) separately for the two dominant land cover types within our model domain.

We used the Moderate Resolution Imaging Spectroradiometer (MODIS) MOD16A2 gridded 8-day net evapotranspiration product (Running and Mu, 2015) to drive ET demand in our HYDRUS model (Šimůnek et al., 2005). Additionally, we used the MODIS MCD15A3H Leaf Area Index (LAI) 500m 4-day composite gridded product (Myneni et al. 2015). This LAI estimate was used to partition ET into daily potential surface evaporation and transpiration rates for the HYDRUS model (Šimůnek et al., 2008). These data products were processed by taking the spatial mean of each composite in the forest and soy agriculture zones defined above, and compiling land cover specific time series for each product.

The surface elevation data in the model was extracted from the HydroSHEDS 3-arc second conditioned DEM product (Lehner et al., 2006). This product is derived from Shuttle Radar Topography Michigan (SRTM) data, correcting for biases in SRTM due to land cover. Additionally, this product was used to create D8 flow direction (Greenlee, 1987) and flow accumulation rasters via ArcMap 10.2 Spatial Analyst Toolbox. The resulting flow accumulation raster was used to derive a river network, by selecting all cells in the raster with more than 200 cells of up upstream accumulation. This stream network was then used to condition the DEM, by uniformly down cutting streambeds 5m across the model domain, as well as to define drain cell elevations in the groundwater model. The downcutting depth was selected based on our survey data of the difference in elevation between river channels and the upland edge in the watersheds at Tanguro Ranch, which was approximately 5m.

2.3 Modeling:

To simulate the surface and vadose zone water fluxes, we used HYDRUS-1D to calculate evaporation, transpiration, infiltration, root water uptake, overland flow, and recharge to the saturated water table using a single layer model with uniform hydrologic properties (Šimůnek et al., 2005); this provided recharge fluxes to the saturated groundwater model discussed below. Unsaturated zone hydrologic dynamics were represented using the van Genuchten-Mualem model (van Genuchten, 1980). Initial parameters for saturated water content, residual water content, empirical parameters alpha and n as well as saturated hydrologic conductivity were taken from Rosetta estimates for Oxisols (Schaap et al., 2001). We also enabled hysteresis in the soil water retention function, allowing for independent relationships between soil moisture and pressure head for wetting and drying periods, with a separate alpha value for each. The HYDRUS model was parameterized by manually varying the Genuchten-Mualem model

parameters, primarily saturated hydrologic conductivity. Model performance was assessed as the root mean square error (RMSE) between the simulated and observed (TDR) soil moisture values. The unsaturated zone hydrology model was driven with MODIS ET and LAI data along with CHIRPS precipitation. In the model, the MODIS ET data were used to define the potential evaporative demand in the system, and LAI was used to partition potential evaporation and potential transpiration. Evaporative demand removes water from the surface, while transpiration demand is distributed along the root distribution and removes water from the subsurface. Two 1D models were created to represent these dynamics under forest and soy land covered areas. In the forest model, maximum rooting depth was set to 9m (Nepstad et al., 1994), and the persistent green canopy allowed transpiration throughout the year. The soy model had a maximum rooting depth of 2m, with a fallow period between harvest and planting (with a LAI value set to 0) in which no root water uptake or transpiration occurred. Aside from rooting depth and the presence of the soy fallow period, all other parameters were the same for the two models.

To simulate groundwater, streamflow, and riparian ET fluxes, we used the U.S. Geological Survey (USGS) modular groundwater modeling software MODFLOW-2000 (Harbaugh et al., 2000) implemented through the Groundwater Modeling System (GMS 10.2) (EMRL, 1999). A no flow boundary was defined around the domain by delineating watersheds based on the flow accumulation and flow direction products. This model boundary was created by merging the surface water drainage basins calculated for the Tanguro and Darro Rivers downstream of our area of interest (Figure A2.1). The model region contains the entire upper Darro, while the upper Tanguro River above our area of interest was excluded, where only a narrow domain adjacent to the river exists and extends to the south-east. The 2458 km^2 active portion of the model domain was discretized into 303,782 90-m square cells. The spatial

resolution of the model was determined by the resolution of the HydroSHEDS DEM. Due to the dissected nature of the landscape, rivers within the region were greater than 90m apart, so no cell contained more than one drain cell. The model had a single vertical layer, with top elevations defined by the conditioned DEM and bottom elevations defined by the interpolated depth to bedrock layer, and a minimum aquifer thickness of 1m enforced. Recharge was calculated as the flux of water below 18m depth from the HYDURS model, as independently simulated for forest and soy agriculture cells. We chose 18m as the output depth, as this was the depth to water in the only available upland region we could measure in the Tanguro region. This well is located at the south-central region of the ranch and is adjacent to one of the soy fields. We currently do not have enough data on depth to water in the upland region to vary recharge depth across the model domain, which would only alter the timing of the recharge pulse. These recharge rates were used to drive hydrologic fluxes in MODFLOW as defined based on extent of forest and soy areas within the model domain. Of the 2485 km^2 model region there are 1850 km^2 of forested land, and 760 km^2 were soy agricultural fields.

Riparian ET was simulated in the MODFLOW model using the EVT package. The maximum riparian evapotranspiration rate was calculated as the difference in HYDRUS modeled and MODIS remotely sensed ET over the forested areas. This assumes that any deficit between vadose zone ET and potential ET in the forested or near stream zones is filled by evapotranspiration from groundwater. Riparian ET was enabled in the forested areas, and in a 200m buffer around the stream network. Riparian ET occurs at the maximum rate when groundwater elevation is equal to the land surface, and decreases linearly to the extinction depth, set at 8m.

Most streams in the groundwater model were defined as drains, as the system is composed of gaining streams with sustained flow though the dry season, and minimal observed overland flow. Streambed conductance was set at 10m/day for the entire river network assuming that the riverbeds consist of re-worked Oxisols, with sandy beds visible and low turbidity observed across the river network. A short reach of the Tanguro River at the NW corner of the model was defined as a specified head boundary based on the DEM elevation to help constrain the model.

The groundwater flow model used three-month stress periods to represent the strong seasonal flux dynamics in this system. Stress periods in MODFLOW are defined as spans of time in a transient model with uniform forcing conditions. Stress periods for May-June-July and August-September-October represented the dry season, while November-December-January and February-March-April represented the wet season based on the clear shift in seasonal dynamics of recharge in this region as estimated from HYDRUS. Average seasonal dynamics of remotely sensed precipitation, evapotranspiration and leaf area index are shown in Figure A2.2. The model is initiated at the start of the dry season in May 2006, and terminates in April 2018 at the end of the wet season. The model spin-up procedure consisted of running: 1) a steady state model using average annual recharge conditions between 2006 and 2018, initialized with water levels at the DEM elevation, 2) a transient model for a twelve year period, initialized with output heads from the steady state model, and 3) a second transient model, initialized with the average end of wet season groundwater heads from the first transient model to minimize the effect of starting groundwater elevations. We chose these starting heads because average precipitation conditions for 1996 to 2006 closely matched that of our simulation period (Figure A2.3).

A uniform and isotropic value of hydraulic conductivity (K) was used for the entire model domain as there is insufficient information available to develop parameters zones across the site. The model K value was calibrated by manually adjusting the parameter, within the range of K values measured in the field from 4 to 8 m/day, to minimize the root mean square error (RMSE) between the average of quarterly modeled and observed streamflows across the stream sites (Figure A2.1). The calibrated model was then used to simulate groundwater heads and streamflow for the two model scenarios. To quantify the likely effects of deforestation on groundwater levels, we calculated the difference in average groundwater elevation between the current and "no deforestation" model scenarios at each time step. We then assessed the trend in this difference using the Theil-Sen estimator (Theil 1950, Sen 1968), to quantify the expected rate of change in groundwater storage due to deforestation.

3. Results and Discussion:

3.1 Field Investigations:

Analysis of pump test data showed high saturated-aquifer hydraulic conductivity (K) values across the 6 tested transects on Tanguro Ranch. K estimates for individual wells ranged from ~0.1 to 13 m/day, with average K values along transects ranging from 1.18 to 8.41 m/day (Table 2.1). Examples of the pump test data and curve fitting are shown in Figure A2.4. Generally, wells with the lowest K values were near the river channel in organic rich riverine sediment deposits. Results from shallow soil infiltrability tests under forest and soy plots yielded similar average saturated conductivity estimates of 1.9 to 13.5 m/day (Scheffler et al. 2011). We are not aware of any other K values derived from direct characterization of the saturated zone in the Xingu headwaters region.

Table 2.1 Summary of Hydraulic Conductivity Estimates. Average saturated hydraulic conductivity values derived from pump test data across six watersheds representing forest and soy agriculture dominated drainages at Tanguro Ranch.

Site	Dominant Land Cover	Average K (m/d)	Standard Deviation (m/d)
APP-2	Forest	8.41	2.10
APP-2A	Forest	1.60	0.70
APP-M	Forest	4.89	5.29
APP-5	Soy	1.18	1.06
APP-Cascavel	Soy	2.38	1.97
APP-Area3	Soy	3.72	1.01

3.2 Vadose Zone Modeling:

The minimum RMSE for soil moisture values under forest and soy regions for the HYDRUS simulations were found using the parameters summarized in Table A2.1, including a saturated conductivity value of 8.64 m/day. This value is at the high end of the range of parameters measured along the average well transects. Modeled soil moisture is in good agreement with that of the TDR data from both forest and soy zones, although there is an offset between the absolute measured and observed water content maximum and minimum values (Figure A2.5). Additionally, we validated model performance by comparing modeled MODIS remotely sensed evapotranspiration for both the forest and soy zones at Tanguro (Figure A2.6). The model reasonably matched both the timing and magnitude of both seasonal and annual variations in ET, however ET was not included in the objective function for parameter estimation.

Surface and vadose zone water balances are significantly altered by conversion from forest to soy agriculture. On an annual basis, the forested landscapes partition precipitation primarily into transpiration, while evaporation and recharge are low across the model period (Figure 2.2). Deep rooted forest vegetation is able to extract water from the soil at depths exceeding 8 m, resulting in high annual ET rates and low recharge rates relative to the other

components of the water balance (Nepstad et al., 1994). Under soy fields, annual transpiration and evaporation are roughly equivalent, while their sum is significantly reduced, leading to less water returned to the atmosphere and more recharge than forest areas. This shift in the water balance is a result of the shallow rooting depth of soy crops, their reduced LAI relative to forested land cover, and the approximately 6 month fallow period with no transpiration between harvest in March-April and planting in October-November (Liu and Kogan, 2002). This reduces the ability for the landscape to transpire water, increases soil moisture, and allows more water to ultimately reach the saturated zone.

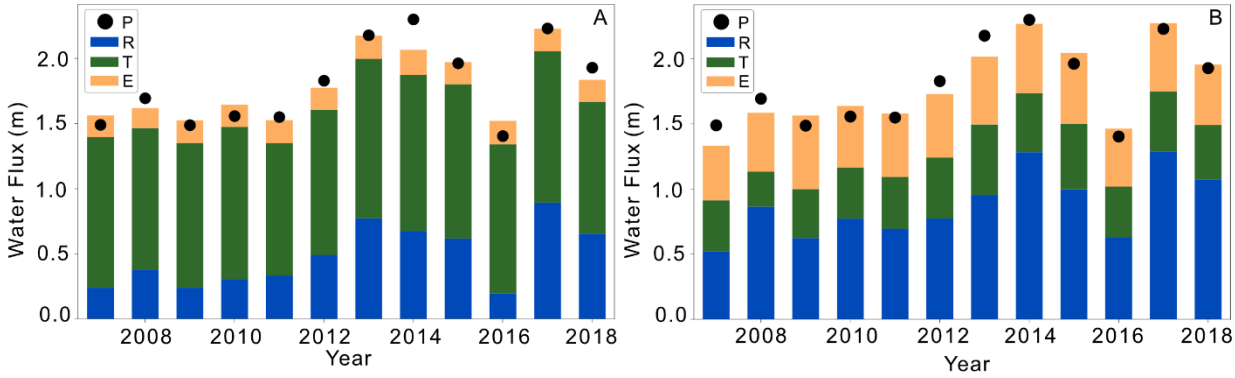

Figure 2.2 Forest and Soy Water Balance. Water balance breakdowns simulated in HYDRUS for (A) forest and (B) soy agriculture areas at Tanguro Ranch. The forest water balance is dominated by transpiration (T), while the soy water balance is dominated by recharge (R), with atmospheric return fluxes split evenly between evaporation (E) and transpiration.

These differences are especially apparent in a seasonal breakdown of the water balances for the two land covers (Figure A2.7). In the wet season, transpiration dominates the forest water balance, while the soy fluxes are split between evaporation, transpiration, and recharge. In the dry season, forest transpiration remains elevated and limits recharge, while in soy the fallow period allows for elevated recharge. This highlights the ability of rainforest vegetation to access water in the soil column and continue to transpire it year round, while soy allows significantly more water to reach the saturated zone as transpiration is absent during the fallow season.

Conversion to soy agriculture also alters the timing of recharge fluxes to the saturated zone (Figure 2.3). Under forested conditions the peak of recharge is approximately 3 months after peak precipitation. Under soy fields, peak recharge occurs approximately 1 month after peak precipitation. Additionally, soy recharge rates are higher than those under forested areas throughout the year.

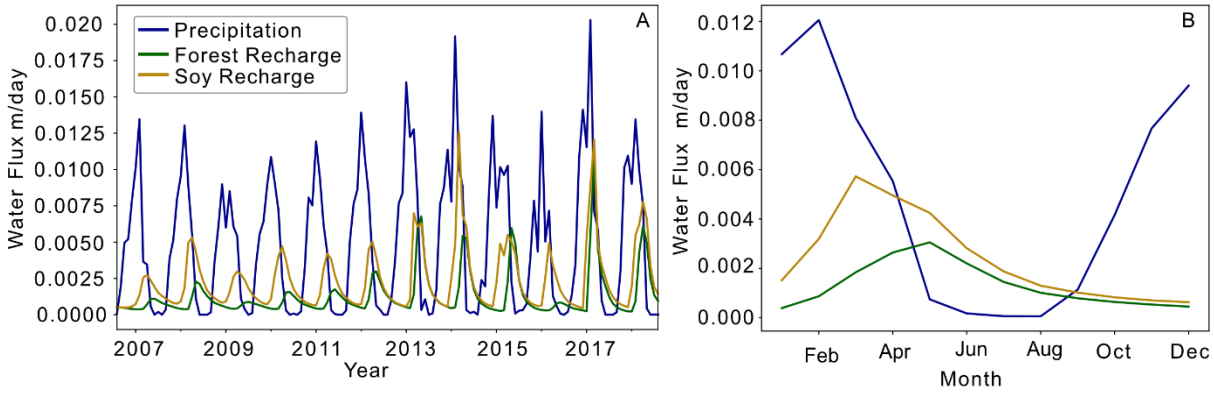

Figure 2.3 Timing of Rainfall and Recharge. Timing of annual modeled recharge for forest (green) and soy (yellow) relative to precipitation (blue) for (A) the entire model time period and (B) averaged across all model years. Deforestation and subsequent conversion to soy agriculture increases recharge throughout the year and shifts peak recharge two months earlier on average.

3.3 Groundwater Modeling:

Results of model calibration are shown in Figure A2.8, with the lowest residual between simulated and observed flows achieved using a saturated conductivity of 5.5 m/day; this value was used for the rest of the simulations. This value falls within both the measured saturated K values derived from pump tests (Figure A2.9) and the infiltrability derived Ksat values from Scheffler et al. (2011), but is lower than the optimal unsaturated K value used in the HYDRUS model. The specific storage value in the model was fixed at $1x10^{-5}$ m^{-1} across the entire aquifer.

Using these parameters, the model is able to capture the seasonal pattern of discharge, as well as the range of streamflow values across the simulation period (Figure 2.4). The model matches the seasonal and absolute minimum flows well, but fails to reach the seasonal and

absolute peak flows. The difference in timing of simulated and observed peak discharge is likely due to the absence of any overland flow or direct precipitation processes in the MODFLOW model. These runoff processes are important during heavy rainfall periods, and thus high discharge events are not well captured in this model. Streamflow in the Tanguro region, however is predominantly sourced from groundwater, thus there is a reasonable match between modeled and observed flows despite a relatively simple model. Hayhoe et al. (2011) demonstrated that in the Tanguro catchments, groundwater accounted for between 87% and 99% of streamflow, based on baseflow hydrograph separations of the measured streamflow data. Subsurface flows are also the dominant streamflow process in forest and soy catchments across the Upper Xingu Basin. Dias et al. (2015) were able to match streamflow records using a modeling scenario in which subsurface flow was the dominant runoff process. They concluded groundwater is critical in regulating stream flows within this region, but suggested net decreases in groundwater storage were needed to sustain stream flows. These predictions were made using land surface and crop models that lack explicit simulation of the groundwater system. Conversely, our model was able to reasonably match the magnitude of streamflows without an overall decrease in groundwater storage across the model period.

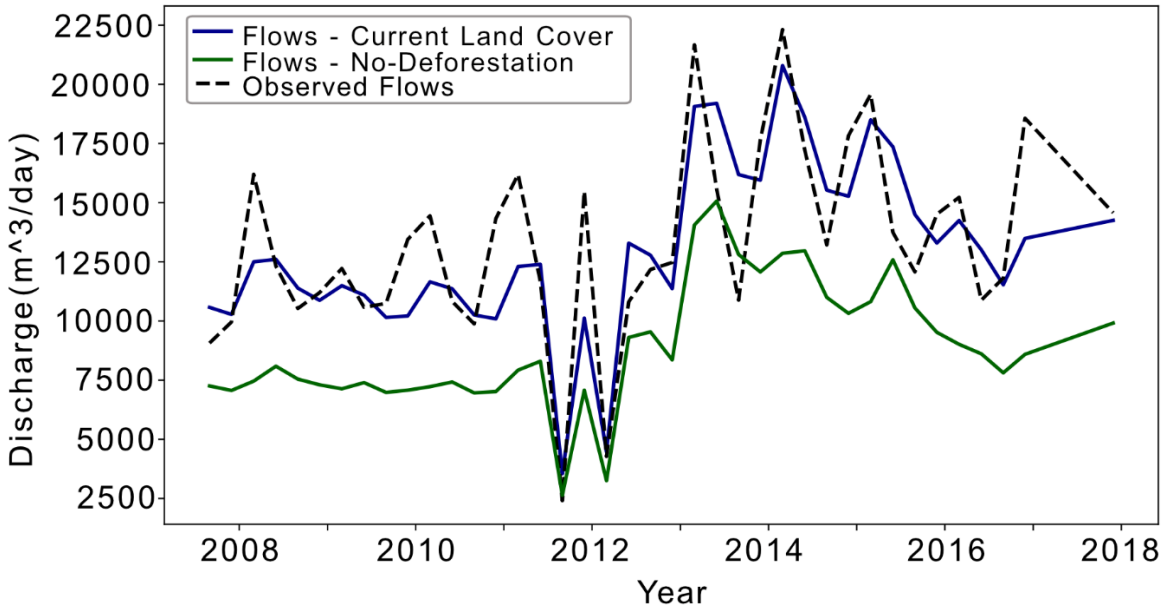

Figure 2.4 Modeled and Observed Streamflows. Average modeled and observed streamflow across all monitored watersheds at Tanguro Rach. Modeled streamflows capture the seasonal patterns and range of observed values, but does not capture the magnitude of seasonal changes. Streamflows for the "no-deforestation" scenario are consistently lower than those of the current land use model scenario and the observed flows under the current land use distribution.

Model performance varies considerably across individual sites, as shown in Figure A2.9. This variation in performance is attributed to the use of uniform river channel downcutting and streambed hydraulic conductivity parameters across the stream network. We do not currently have enough field data to vary these conditions across the entire length of the river network. Additionally, most of these monitored sites are in first and second order streams, which are the most numerous and variable component of a river network. While individual small streams are easy to instrument and model, their number and heterogeneity make accurate characterization difficult at regional scales, especially in data poor areas such as the upper Amazon Basin. Capturing small stream hydrologic dynamics in models such as the one presented here, allow us to better constrain hydrologic processes such as recharge and aquifer conductivity rates whose effects can be much harder to separate at regional models. In addition to assessing model performance by RMSE, we sought to match the overall water fluxes at our largest streamflow

site, APP6/7. Figure A2.13 shows we are reasonably representing the average discharge flux at this location.

We were able to reasonably simulate the river discharge dynamics described above using only one saturated conductivity parameter, which is higher than would be predicted using grain size analysis for Oxisol soils. The high degree of clay particle aggregation in the Oxisols allows for rapid drainage and saturated conductivity (Neil et al. 2013, Renck and Lehmann., 2004, Scheffler et al. 2011). Previous groundwater modeling efforts have assumed an exponential decay in saturated hydraulic conductivity with depth (Miguez-Macho and Fan, 2012) as is commonly assumed for modeling of temperate to tropical regions. The broad distribution and significant depth of the Oxisols suggest that this assumption may be invalid in our study region. The assumption of decreasing k with depth may lead to artificially elevated water table elevations and surface fluxes, or delayed hydrologic response times. A more robust set of model experiments would need to be evaluate the effects of K variation with depth in our study region.

The spatial distribution of groundwater elevations roughly follows the regional surface and bedrock topography gradients, with groundwater heads higher at the southern and eastern edges of the domain, and lower to the northern and western edges of the system (Figure A2.10A). Saturated aquifer thickness ranges from 1 to 80 m, with the thickest values in the central region, and thinnest in the southern end of the domain (Figure A2.10B). Saturated thickness follows a similar pattern as total aquifer thickness, which ranges from 10 to 100m across the model region (Figure A2.10C). Water table elevations across the model domain (Figure 2.5) decrease over the first six years of the simulation during a period of low precipitation, before increasing during the 2013-2018 period of elevated rainfall.

A clear seasonal pattern in heads is present throughout the model domain, with increasing seasonal variations during the wetter second half of the simulation period. Additionally, the elevation and seasonal variation of average heads are distinct for the two dominant land cover types Heads in agricultural regions of the model are consistently higher, and show a stronger seasonal signal (Figure A2.11). As is observed with recharge fluxes, peak groundwater elevations are also delayed from peak precipitation by approximately 3-4 months, resulting in elevated groundwater levels during the early dry season. A similar delay in peak rainfall and water table elevation was observed in the upland region of the Amazon by Miguez-Macho and Fan (2012). These results also indicate that the offset between peak precipitation and peak water table elevation is important for sustaining dry season streamflows across the Tanguro region.

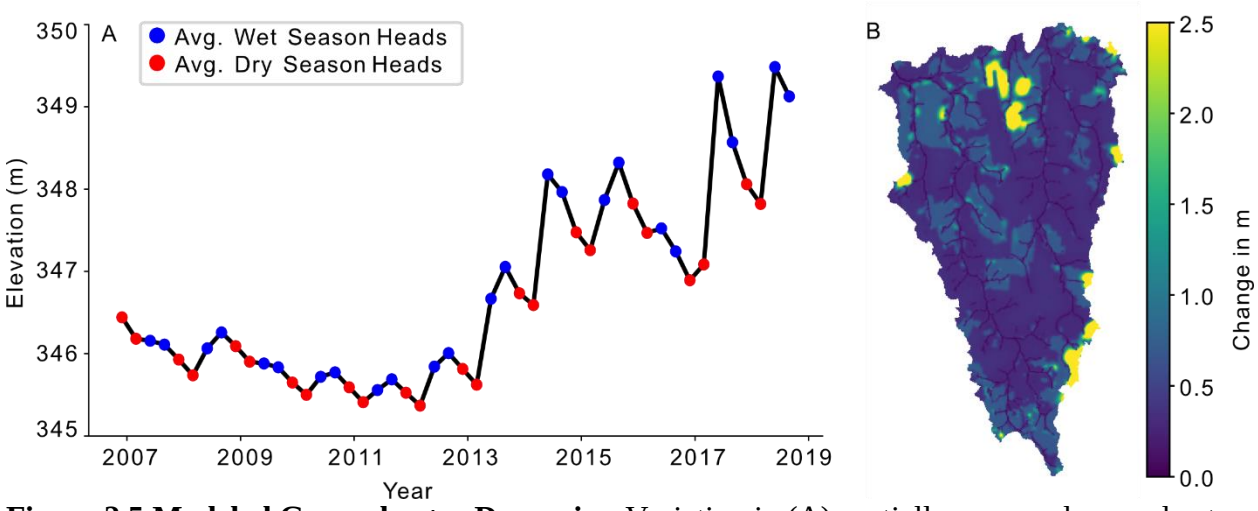

Figure 2.5 Modeled Groundwater Dynamics. Variation in (A) spatially averaged groundwater elevation over the simulation period and (B) difference between mean wet season and dry season elevations across the model domain for the current model scenario. Variations though time are dominated by a dry period from 2006-2012, and a wet period from 2013-2018. Seasonal variation in groundwater elevation is strongest in the agricultural regions of the domain.

The magnitude of seasonal changes in groundwater elevation are spatially distinct between the two landcovers (Figure 2.5). On average, differences between wet and dry season heads are approximately 1 m in agricultural areas, 0.5 m in forested areas, and uniformly low near the stream channels. Increased water table elevations and seasonality in soy fields are a

result of the altered surface water balance in agricultural plots. The increased recharge under soy fields is not evenly redistributed, but it alters the local water table and river discharge patterns in soy dominated areas. Localized increases in groundwater elevations may cause differences between surface watersheds and the potentiometric surface of the saturated zone. The resulting groundwater drainage areas, or groundwatersheds, are dynamic, distinct from surface topography, and may route water across surface watershed boundaries. Differences between a representative wet year (2017) and dry year (2010) show approximately a 4 m difference across all of the upland areas in the model region, and are low near the river channels (Figure A2.12). The stark difference in precipitation between wet and dry years dominates the effect across the entire model domain, and with similar responses in forest and soy regions.

The water table elevations for the "no deforestation" scenario showed a similar pattern of average head distribution, which is controlled by bedrock and land surface elevations along with the geometry of the river network (Figure A2.14). Water table elevations for the no deforestation model vary over a narrower range of values, but follow a similar pattern of drying in the first half of the simulation, and wetting in the second half (Figure A2.15A). Seasonal variation in the no-deforestation model is much more uniform, with 0.5 m difference between wet and dry seasons averaged across the entire model domain (Figure A2.15B). Small areas of greater seasonal variation, up to 1.5 m, are present in the near stream zones, likely due to riparian ET fluxes. All streams at this site, including those in soy fields, had a riparian buffer of rainforest vegetation around the stream channel. Roots from riparian vegetation are able to reach the shallow water table, leading to the potential for increased dry season ET. For the current land cover model, the variation in water table elevation due to land cover masks the signal of riparian ET rates in soy dominated streams.

Differences in the water table elevations between the two model scenarios are used to quantify the likely effects of deforestation on groundwater distribution and dynamics. Based on these scenario simulations, deforestation causes water table elevations to rise in agricultural zones across the model region (Figure 2.6B). Increases in soy zone water table elevations generally range between 5-8 m with maximum increase of up to 10 m. These impacts are localized, with areas that remain forested showing little difference between the two scenarios. Significant differences in saturated groundwater dynamics between the two model scenarios are driven by the same factors that cause differences in head across land cover conditions in the current model scenario. The increased rate and magnitude of recharge under soy crops leads to locally elevated groundwater elevations under soy fields.

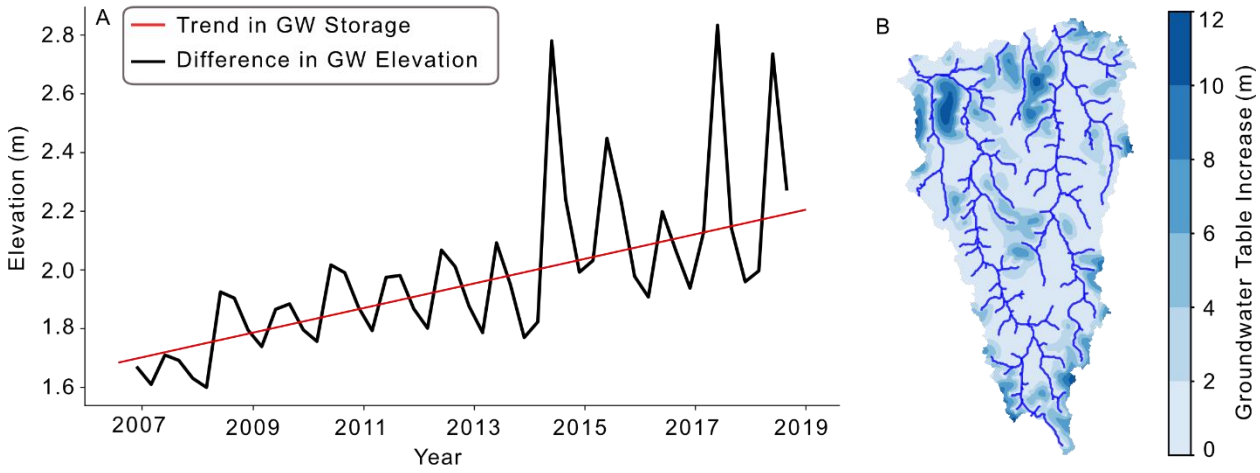

Figure 2.6 Effects of Deforestation on Groundwater. Differences in (A) spatially averaged heads though time and (B) temporally averaged groundwater table elevations for the current scenario minus the "no-deforestation" scenario, shown with the river network for hydrographic context. Differences in average head though time show an increase in groundwater table elevation and seasonality though time due to deforestation. The red line is the Sen's Slope trend, representing the rate of increase in groundwater storage. Spatial differences in average head show increased water table elevation of 5-8m in the soy fields due to deforestation.

Deforestation also results in consistently higher and more seasonally variable heads across the full simulation period, as shown in Figure 2.6A. Additionally, the magnitude of this difference increases across the simulation period at a rate of 4.3 cm/year. This indicates that

deforestation leads to increased storage within the groundwater system. This supports the finding of Chapter 1, which demonstrated increased groundwater storage in deforested areas of Southern Brazil with GRACE mass anomaly data.

In addition to altering the water table dynamics, deforestation also significantly increases streamflow. Compared to streamflow results from the no-deforestation simulation, stream discharge in current landscape conditions is significantly higher and more variable across the entire simulation period (Figure 2.4). On average, across the monitored watersheds, deforestation increases streamflow by ~46%. This difference is accentuated during high discharge periods in the wet season, leading to an average increase of ~105% in the magnitude of seasonal flow variation. Previous field studies at Tanguro have demonstrate that under the same rainfall conditions, mean annual streamflow in soy catchments is three to four times what is observed in forested catchments (Dias et al., 2015, Hayhoe et al., 2011). Furthermore, simulations by Dias et al. (2011) of the Upper Xingu Basin water balance using land surface and crop models suggest that across this region, stream discharge in soy catchments is approximately twice that of forested catchments.

Streamflows are also altered by changing climate patterns in the region. Levy et al. (2018) simulated stream discharge with and without observed climate change, and found that increases in streamflow across the Amazon-Cerrado transition zone were 58% of those predicted under stationary climate. Similarly, Panday et al. (2015) found climate change and deforestation to have opposing effects on streamflow, with climate changes reducing streamflows and deforestation increasing streamflows. Explicitly incorporating climate change into our model, through use of long term historical records or predictive scenarios, would allow us to quantify the combined effects of land cover and climate changes on groundwater dynamics in this region.

While local alterations to these small catchments result in both increased storage and streamflow, analysis from Chapter 1 suggest slightly decreasing flows at the scale of the full Xingu basin. While deforestation has been widespread in the Xingu headwaters, the existence of the Xingu Indigenous Park just north of Tanguro has limited land cover change in the central Xingu basin. Furthermore, other processes affecting regional scale hydrology such as changes in precipitation and evapotranspiration, as well as the construction of hydroelectric dams may be masking the effects of altered hydrology in the headwaters region. Quantifying how these complex factors affect the water balance across space and time in the Amazon Basin would require integrated, process-based simulations of the landscape hydrologic processes at the scale of the Xingu Basin.

3.4 Error Sources

Overall, our model can reasonably represent seasonal fluctuations of surface discharge across our study region with results supported by both field studies and previous modeling efforts. In the future, a number of sources of error in the model and input data that should be addressed. First, an elevation bias in forested regions is present in both the DEM and modeled bedrock elevation products. Although the HydroSHEDS data is corrected for land cover, there is a clear change in elevation at each boundary of forested and open or agricultural zones in our model region. This suggests that canopy reflectance of rainforest vegetation is not properly accounted for in this product. This artificially high elevation in forested areas was also present in the SoilGrids depth to bedrock layer. This product is the result of a global model of soil parameters, including land cover and topography. We attempted to remove this bias in our bedrock elevation map by selecting depth to bedrock values only in the open areas, and kriging these values across the model region. Due to significant variation in the surface elevations and

non-uniform bias across the region, we were not able to employ a robust improvement of the DEM. This may cause some discrepancy in the model properties based on the DEM, including aquifer thickness and river channel depth. Improved correction of the current DEM data, or higher resolution topographic imagery, such as from LIDAR, would greatly improve our land surface elevation estimates.

Second, areas of abnormal water table elevation change across seasons and scenarios are present at the southeastern boundary, as well as in the north central region of the model between the two major river systems (Figures 4B and 6B). For example, there is a lateral discontinuity in water table elevations (Figure A2.16) in the north central region of the model. The inability of water flow laterally in this zone likely causes increased variability over time. There is also water ponding at the southeastern boundary, which is likely a result of inclusion of a small zone of groundwater flow directed out of the model region to the southeast. The model boundary was derived by delineation of the surface water catchments in the Tanguro Ranch region using the HydroSHEDS DEM, so discrepancies between surface and bedrock topography may cause water to flow to the southwest and pond at the model's no-flow boundary.

A third source of error in the groundwater model is the use of uniform parameters across the model domain, including saturated hydraulic conductivity, stream channel downcutting and stream conductance. Additionally, the recharge fluxes from HYDRUS used for the entire model domain were output at a uniform depth, which may bias the timing and magnitude of recharge. Recharge depth estimates could be spatially varied in a future model run using estimates of depth to groundwater from our model results. Improving estimates of the spatial heterogeneity of these parameters would improve model results, and likely result in increased variation in water table and streamflow dynamics. Additionally, the use of automated parameter estimation will also

allow for a more robust and specific estimate of the optimal K value within the model region. However, we are able to predict averaged river discharge fluxes with the model. Overall our results are consistent with other studies that explore how deforestation alters the water balance in this region (Dias et al., 2015, Hayhoe et al., 2011)

Finally, the current temporal discretization of the model limits the extent to which we are able to capture hydrologic dynamics within seasons. Quarterly stress periods were used due to current technical constraints in the model code and computational resources. In the future, we plan to run this model at monthly or bi-weekly stress periods using cloud computing resources. Increasing the temporal resolution of the model will allow for a better assessment of changes in streamflow and groundwater dynamics associated with changes in land cover.

4. Conclusion:

Deforestation and associated conversion to soy agriculture greatly alters the surface, vadose zone, and saturated groundwater dynamics in the southern headwaters of the Xingu and Amazon Basins. Deforestation significantly reduces total evapotranspiration and increases recharge to the saturated zone, which results in a higher and more seasonally variable water table elevations and stream flows. This land cover transition increases water table elevations by up to 10 m, streamflow by an average of 46%, and groundwater storage by 0.043 m/year, while shifting peak recharge two months earlier in the year. All of these altered water balance dynamics are driven by the decreased rooting depth and six-month fallow season in soy fields.

These results also highlight the importance of deep-rooted forest ecosystems in maintaining the hydrologic connection from the atmosphere to the deep subsurface. The Tanguro Ranch site is representative of the soil, climatic, and vegetation conditions across which much of the deforestation and conversion to soy agriculture that are occurring across much of the

Southern Amazon Basin. At a landscape scale, reduced evapotranspiration, increased export though streamflow, and increased groundwater storage, limit the amount of water available to be recycled on a local and regional scale. As summarized by Lovejoy and Nombre (2018), this alteration of the landscape and water balance may push the Amazon to a tipping point where it can no longer retain and internally cycle enough water to sustain rainforest vegetation. A better understanding of how groundwater is affected by landscape alterations, and the extent to which it controls water storage and stream discharge, are critical to predicting the future hydrologic impacts of deforestation and the fate of Amazonian water resources.

Acknowledgments:

Primary funding for this work was though the following National Science Foundation grants: INFEWS/T3 Grant No. 1639115 “Rethinking Dams: Innovative hydropower solutions to achieve sustainable food and energy production, and sustainable communities” and INFEWS/T1 Grant No. 1739724 “Intensification in the world's largest agricultural frontier: Integrating food production, water use, energy demand, and environmental integrity in a changing climate”. Additional funding came from the Michigan State University: College of Natural Science, Graduate School and Department of Earth and Environmental Sciences. The field campaign at Tanguro Ranch would not be possible without the Amazon Environmental Research Institute (IPAM) who operates this field station. I thank Christopher Neill, David Hyndman, Anthony Cak, Divino Silvério and Leonardo Santos whom I worked with directly during the collection of field data. Additionally I thank Alex Kuhl and Mohammed Rahman who worked with me on the development of the HYDRUS models.

APPENDIX

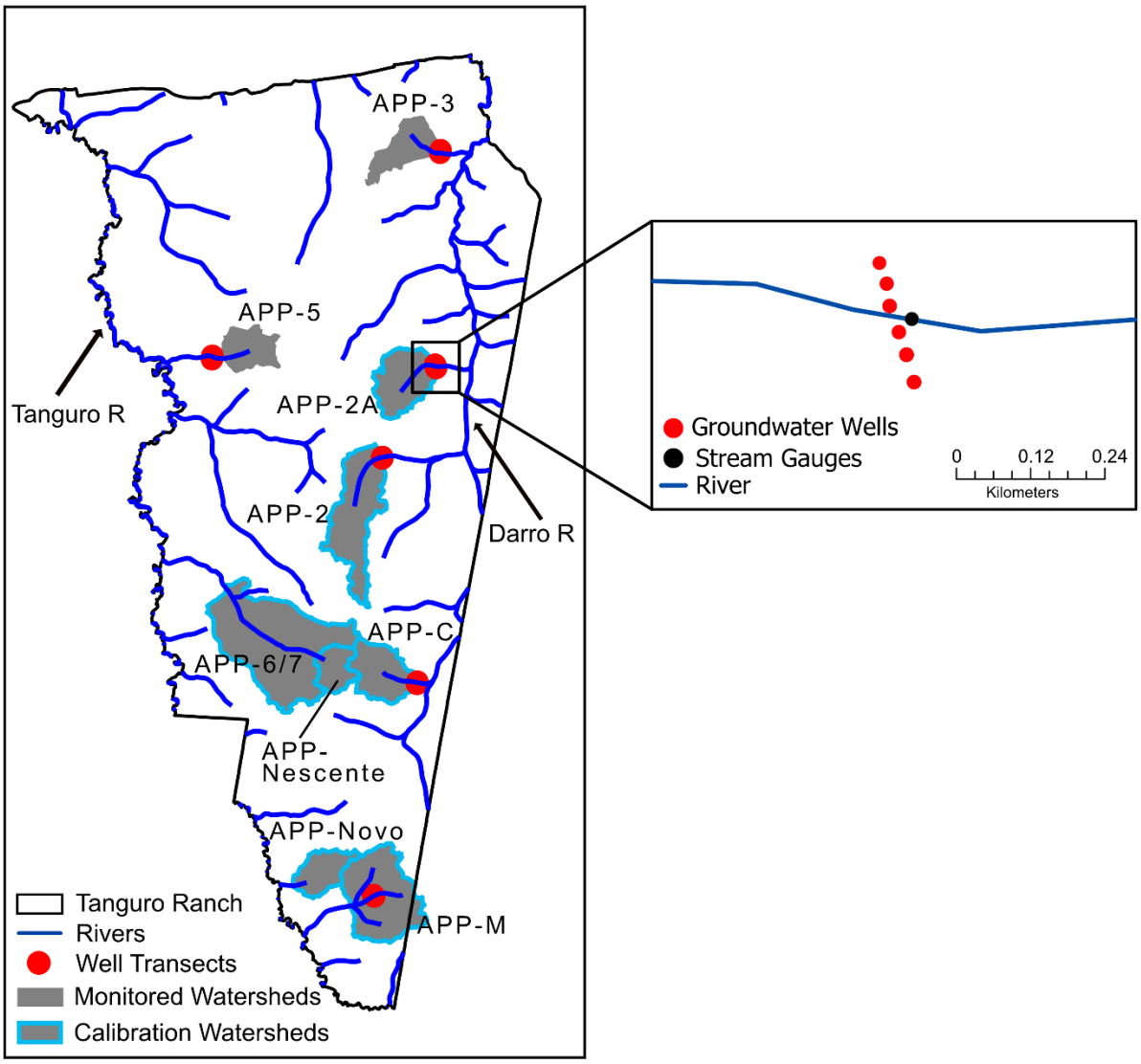

Figure A2.1 Tanguro Ranch Wells and Watersheds. Locations of the river network, monitored watersheds and riparian wells in which aquifer characterization tests were preformed at the Tanguro Ranch Research Site. Watersheds have been monitored since the early 2000's, and aquifer characterization tests were preformed in 2018. Watersheds with flow data used for model calibration are highlighted in light blue. The inset map shows an example of the riparian well transect location and spacing.

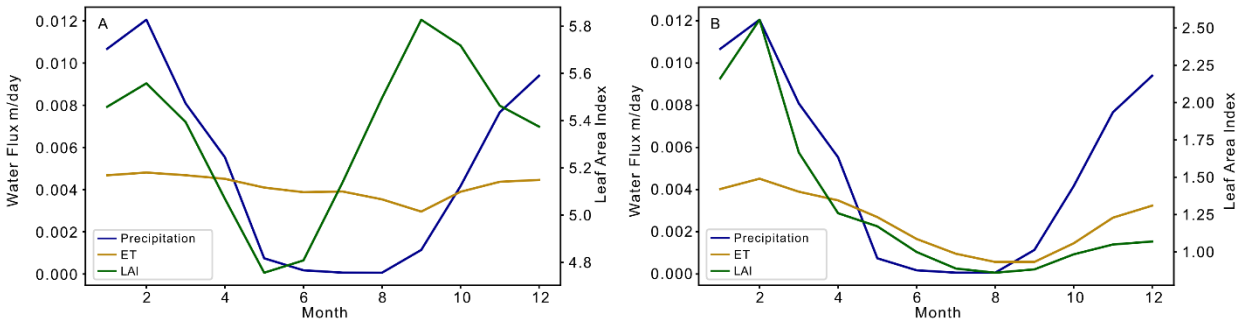

Figure A2.2 Average Precipitation, ET and LAI. Average remotely sensed precipitation, evapotranspiration and leaf area index for (A) forest and (B) soy plots at Tanguro Ranch. For both land covers, Precipitation and LAI peak in February, and reach a minimum in May or June. In the soy plots, minimum LAI corresponds to the fallow period between harvest and plating, and leads to reduced ET. In the forest plots, LAI values are much higher than in soy, and evapotranspiration remains high all year.

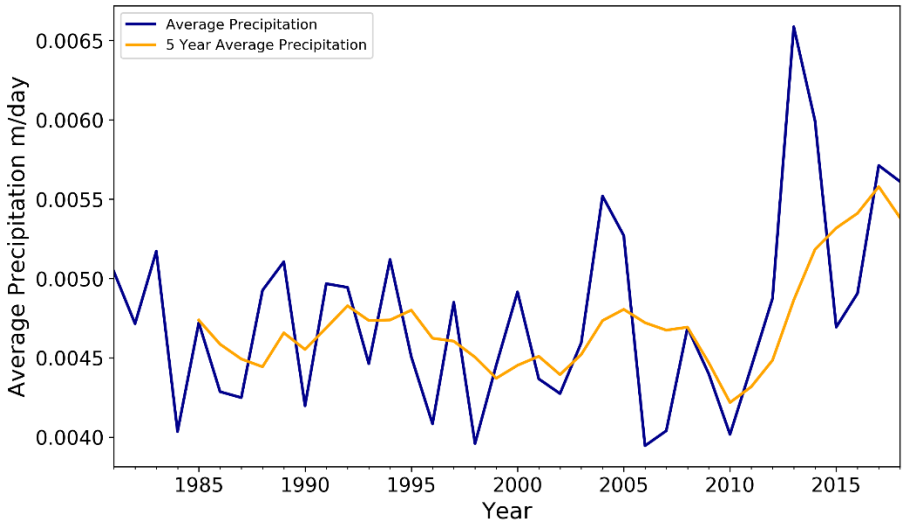

Figure A2.3 Tanguor Ranch Historical Precipitation 1985-2018. Annual average and 5-year rolling average precipitation at Tanguro Ranch from 1985-2018. Using these data we determined antecedent precipitation conditions in the 5 years before the model start date, and dictated the starting head conditions in the model. Based on the 5-year rolling average during 2000-2005 we started the model with average heads for the end of wet season as the model is initialized at the start of the 2006 dry season.

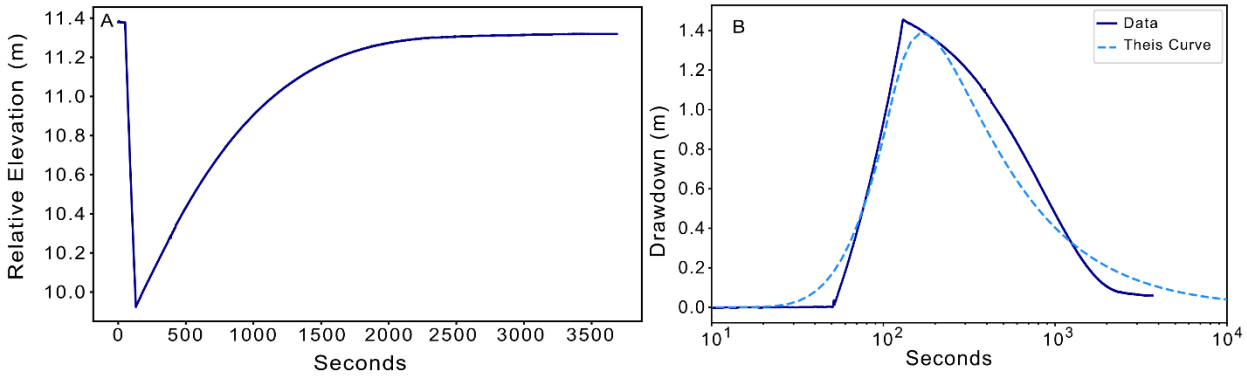

Figure A2.4 Pump Test Data Example. (A) Drawdown and recovery of riparian wells recorded using pressure transducers and (B) estimated saturated aquifer conductivity from curve fitting techniques. Pump tests were performed in riparian wells across six watersheds at Tanguro Ranch.

Table A2.1 Optimized HYDRUS Parameters. Optimized parameters for the soil water retention function used in HYDRUS simulations of forest and soy plots at Tanguro Ranch. Optimum parameters were selected by manually varying each value to minimize the root mean square error between simulated and observed (TDR) soil moisture. Hysteresis was enabled, so alpha values for wetting and drying periods are defined separately.

Parameter	Theta R (cm^3/cm^3)	Theta S (cm^3/cm^3)	Alpha Wetting (1/m)	Alpha Drying (1/m)	n	K (m/day)
Optimized Value	0.12	0.4	1.5	0.5	1.3	8.64

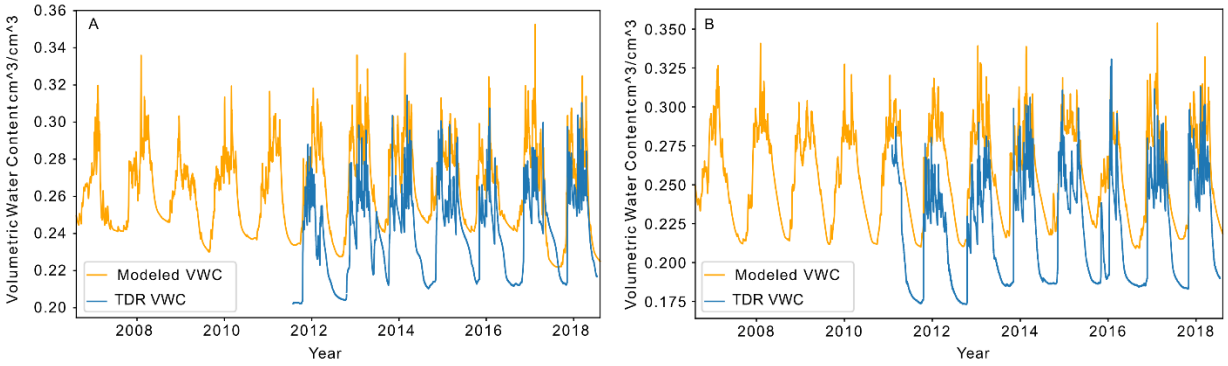

Figure A2.5 Soil Moisture Comparison. Comparison of soil moisture measured by time domain reflectometry and modeled in HYDRUS for (A) soy and (B) forest plots at Tanguro Ranch. For both land cover types, the modeled captures the timing and magnitude of seasonal soil moisture changes, however there is an offset between the absolute minimum and maximum values.

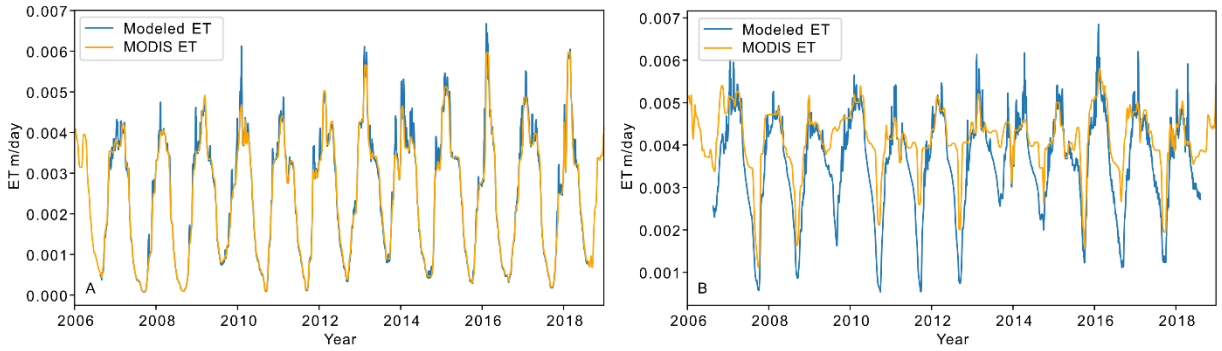

Figure A2.6 Evapotranspiration Comparison. Moving 8 day average of evapotranspiration from MODIS remotely sensed input data and HYDRUS model outputs for (A) soy and (B) forest plots at Tanguro Ranch. The HYDRUS model is able to capture the magnitude and timing of seasonal variations in both in ET of both land cover types, however seasonal minimums in the forest model are often overestimated.

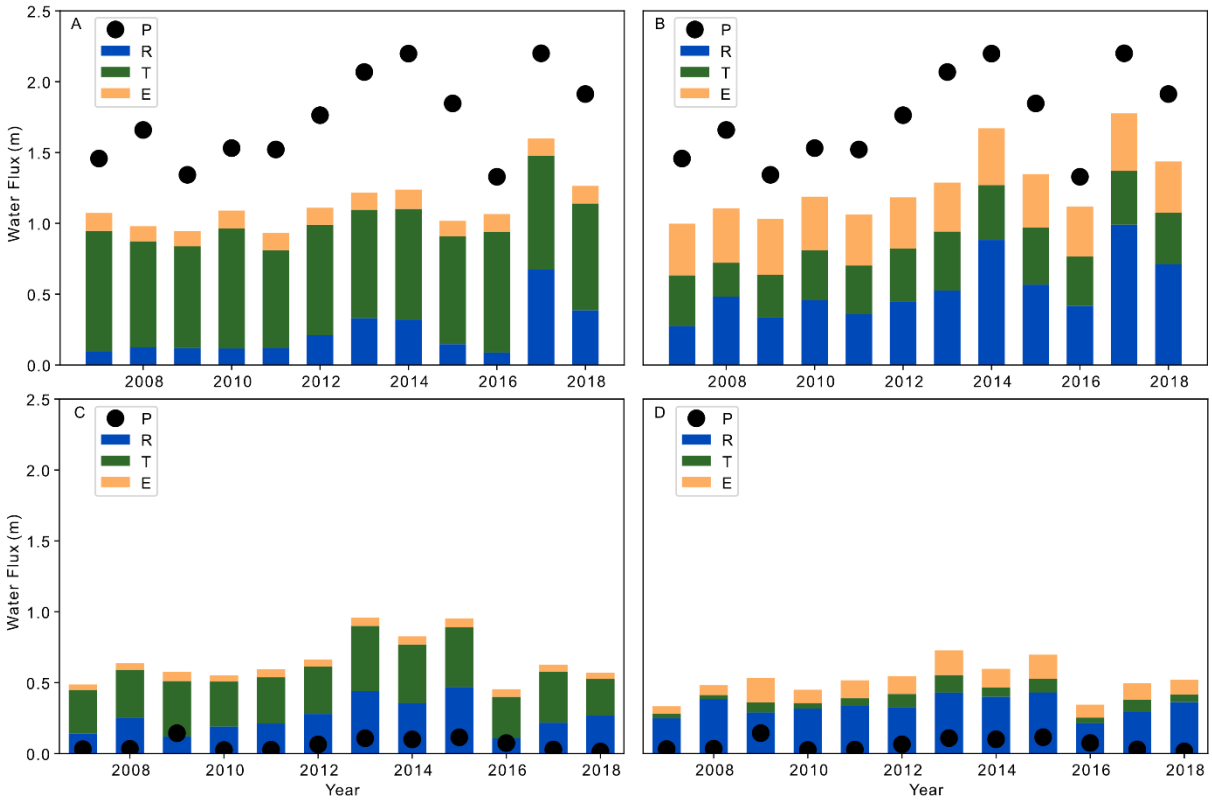

Figure A2.7 Seasonal Water Balances. Seasonal water balance partitioning for wet season forest (A), wet season soy agriculture (B), dry season forest (C) and dry season soy agriculture (D) areas at Tanguro Ranch. Wet season fluxes follow the patterns of the annual water balance. Seasonal breakdowns show increased wet season recharge in soy fields and persistent transpiration in the forested areas during the dry season.

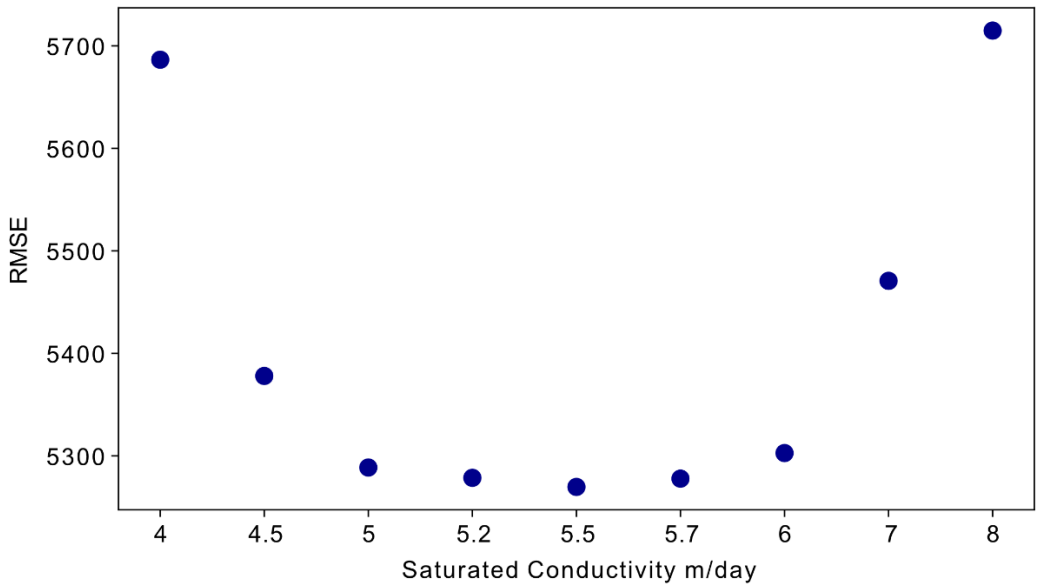

Figure A2.8 Groundwater Model Calibration. Results of model performance for variation of saturated conductivity across the range of values derived from in situ aquifer characterization data collected at Tanguro Ranch determined conductivity values. The average Root Mean Squared Error of the difference between modeled and observed flows across all sites was used to assess model performance. Optimum saturated conductivity was 5.5 m/day.

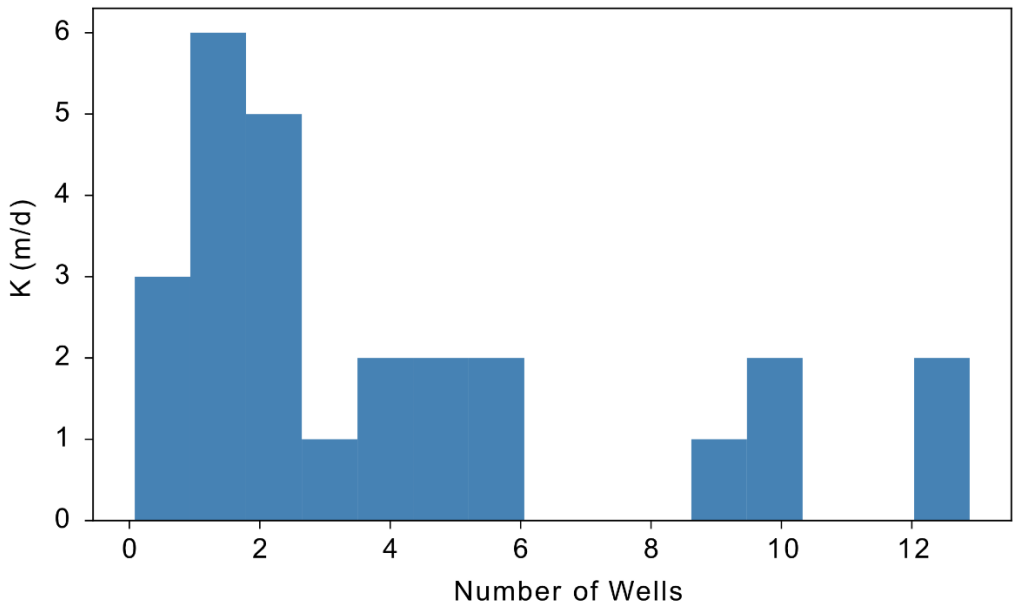

Figure A2.9 Hydraulic Conductivity Distribution. Distribution of hydraulic conductivity values across all 26 tested wells at Tanguro Ranch. Values range form 0.08 to 12.9m/day, with a mean of 4.1 m/day. The optimal K value used in the groundwater model was slightly higher than the average, at 5.5m/day.

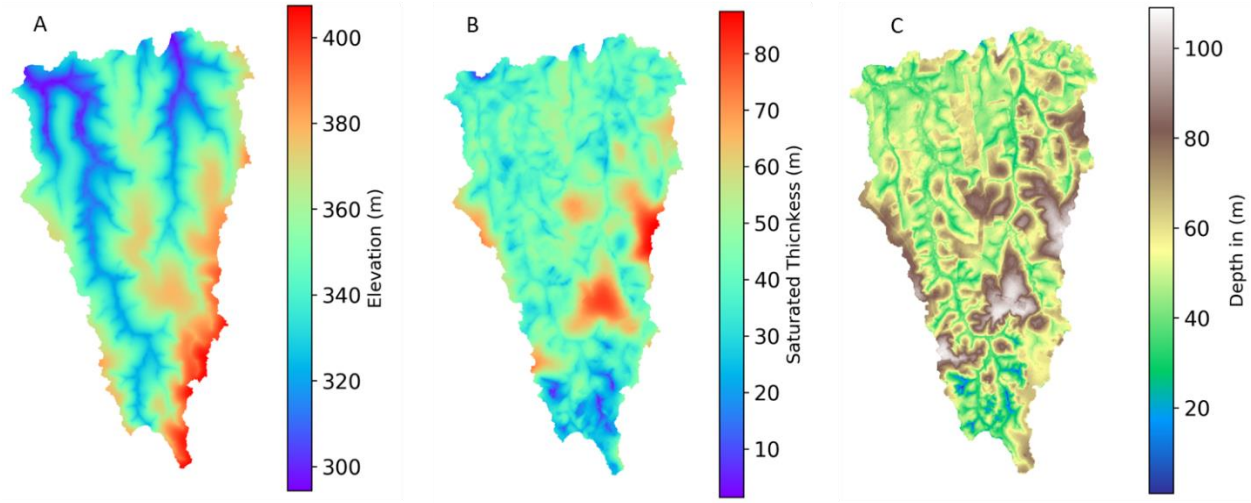

Figure A2.10 Groundwater Elevation and Thickness. Average simulated (A) groundwater table elevation, (B) saturated aquifer thickness, and (C) total aquifer thickness for the current model scenario. Groundwater table elevation high in the south and lower in the north and near stream channels. Saturated thickness ranged from 40-80 mover most of the domain, with sallower elevations at the southern end of the model region. Total aquifer thickness is deepest in the central region, and thickest at the northern end of the model.

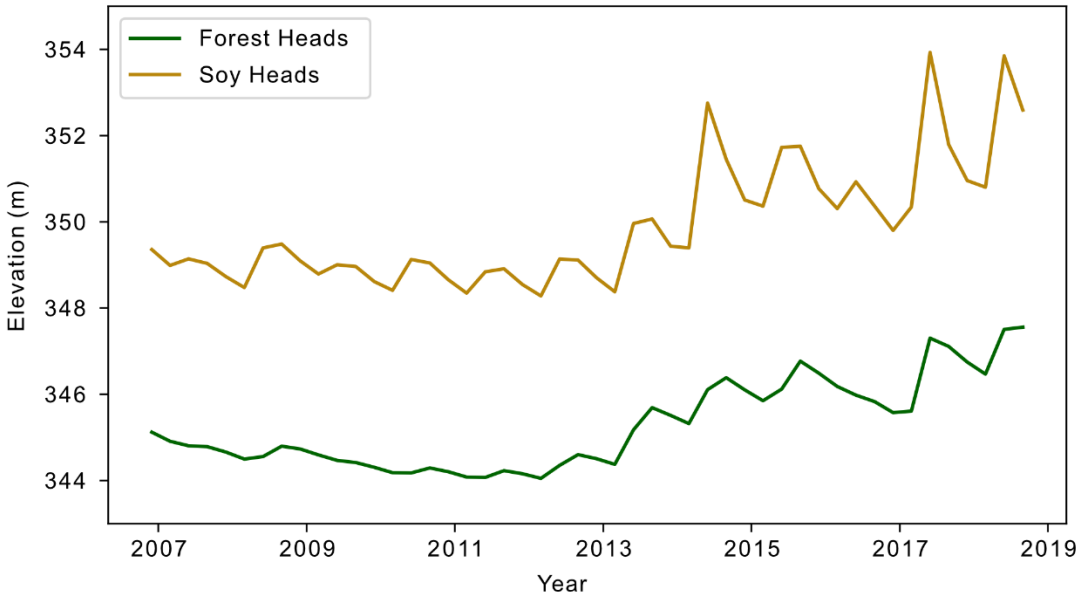

Figure A2.11 Average Groundwater Elevation by Land Cover. Average head across forest and soy areas for the current groundwater model simulation. Heads in the forested regions are consistently lower and show decreased seasonal variability compared to those in the agricultural regions.

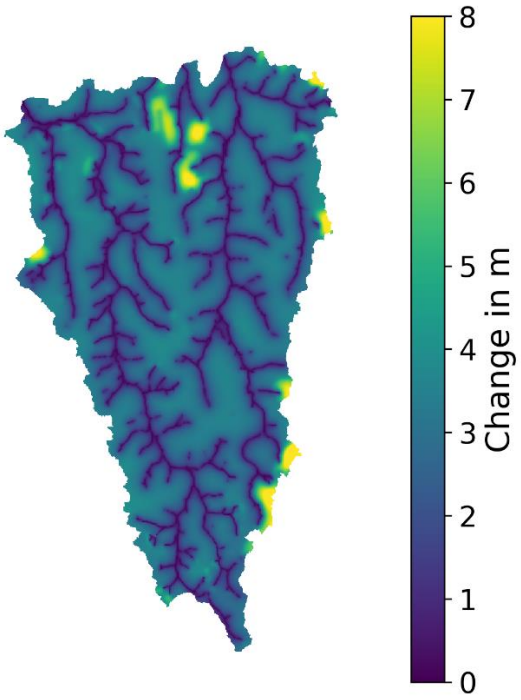

Figure A2.12 Wet and Dry Year Difference in Groundwater Elevation. Difference between a representative wet year (2017) and dry year (2010) water table elevation. Differences between wet and dry years are on average 4 m across the entire model domain with little difference in riparian zones.

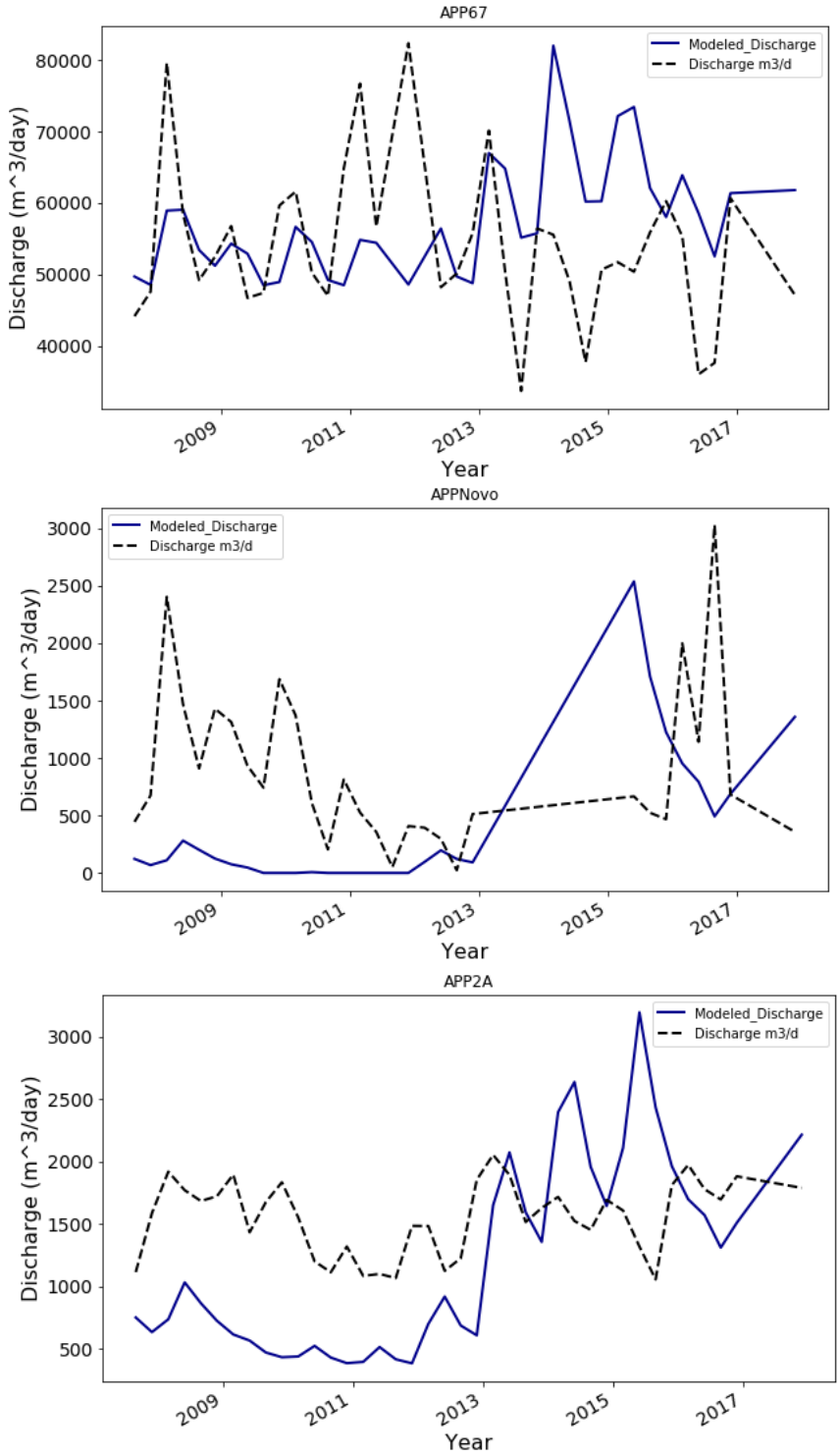

Figure A2.13 Selected Watershed Streamflow Comparison. Modeled and observed streamflow for selected watersheds at Tanguro Ranch. Model performance varies significantly though time and across sites. River conductance and channel morphology (downcutting) parameters are uniform within the model leading to the inability to capture detailed site dynamics across all locations.

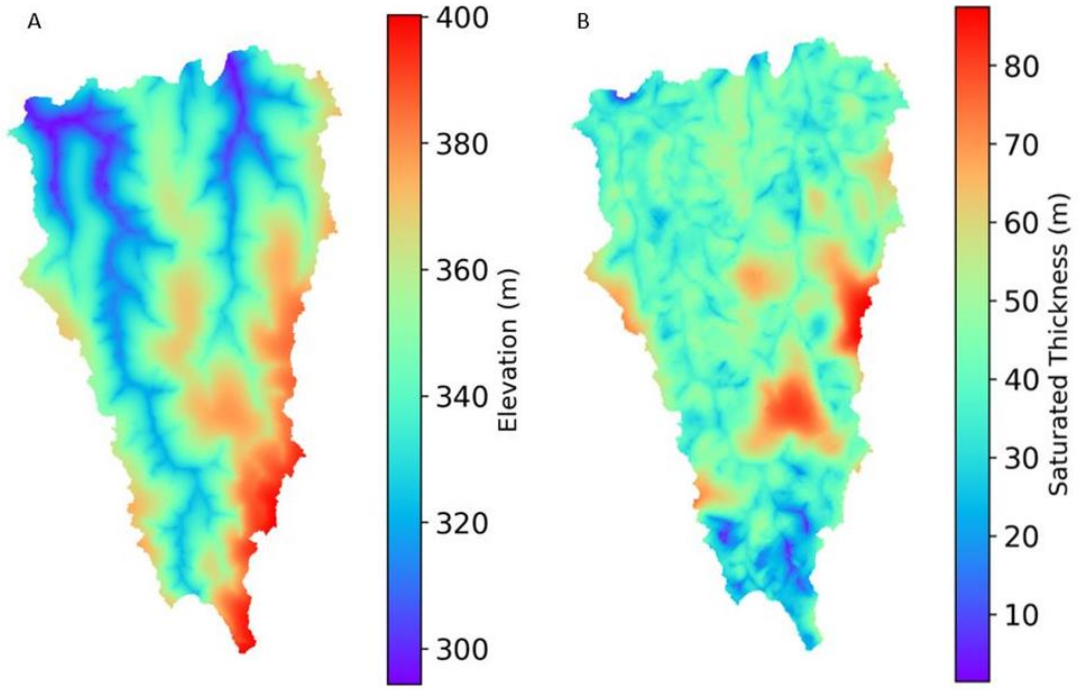

Figure A2.14 Groundwater Characteristics for No-Deforestation Scenario. Average simulated (A) groundwater table elevation and (B) saturated aquifer thickness for the no-deforestation model scenario. Groundwater head distribution and saturated aquifer thickness are very similar to those in the current model scenario and are controlled by surface and bedrock topography.

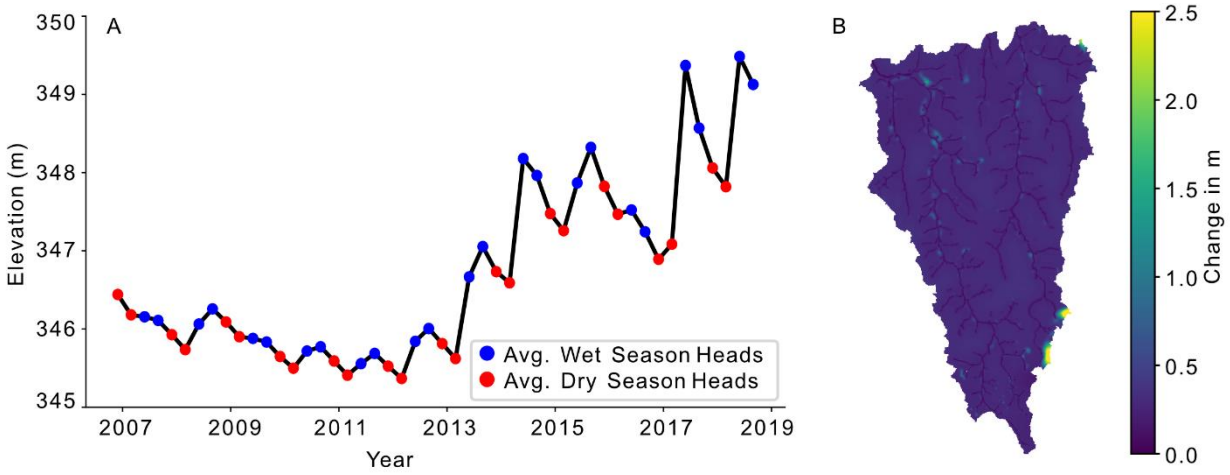

Figure A2.15 Groundwater Elevation Variation for No-Deforestation Scenario. Variation in (A) spatially averaged groundwater table elevation though time and (B) differences in mean seasonal heads across the model domain for the no-deforestation scenario. Average heads fluctuate across a narrower range of values but follow a similar temporal pattern as the simulation of current conditions. Seasonal differences are uniformly low at 0.5 m, with isolated areas of change up to 1.5 m in near-stream channel zones attributed to riparian ET.

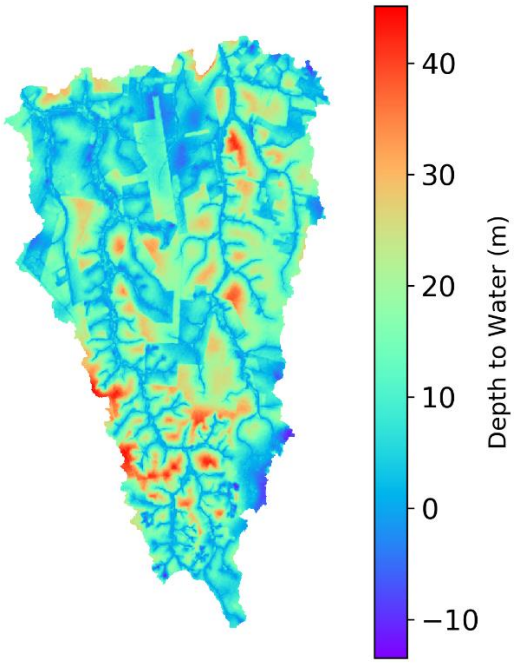

Figure A2.16 Mean Depth to Water in Current Model Scenario. Mean depth to water table across the model region for the current scenario. Depth to water table is low in the soy fields and near stream channel zones, while much deeper in forested areas. The subsurface discontinuities resulting from the forest canopy removal in the DEM are visible in the north-central region of the model.

REFERENCES

REFERENCES

Barona, E., Ramankutty, N., Hyman, G., Coomes, O.T., 2010. The role of pasture and soybean in deforestation of the Brazilian Amazon. Environ. Res. Lett. 5. https://doi.org/10.1088/1748-9326/5/2/024002

Brando, P.M., Balch, J.K., Nepstad, D.C., Morton, D.C., Putz, F.E., Coe, M.T., Silvério, D., Macedo, M.N., Davidson, E.A., Nóbrega, C.C., Alencar, A., Soares-Filho, B.S., 2014. Abrupt increases in Amazonian tree mortality due to drought-fire interactions. Proc. Natl. Acad. Sci. U. S. A. 111, 6347–6352. https://doi.org/10.1073/pnas.1305499111

Coe, M.T., Costa, M.H., Soares-Filho, B.S., 2009. The influence of historical and potential future deforestation on the stream flow of the Amazon River - Land surface processes and atmospheric feedbacks. J. Hydrol. 369, 165–174. https://doi.org/10.1016/j.jhydrol.2009.02.043

Dias, L.C.P., Macedo, M.N., Costa, M.H., Coe, M.T., Neill, C., 2015. Effects of land cover change on evapotranspiration and streamflow of small catchments in the Upper Xingu River Basin, Central Brazil. J. Hydrol. Reg. Stud. 4, 108–122. https://doi.org/10.1016/j.ejrh.2015.05.010

Duffield, G.M., 2007. *AQTESOLV for Windows Version 4.5 User's Guide*, HydroSOLVE, Inc., Reston, VA.

Espinoza Villar, J.C., Guyot, J.L., Ronchail, J., Cochonneau, G., Filizola, N., Fraizy, P., Labat, D., de Oliveira, E., Ordoñez, J.J., Vauchel, P., 2009. Contrasting regional discharge evolutions in the Amazon basin (1974-2004). J. Hydrol. 375, 297–311. https://doi.org/10.1016/j.jhydrol.2009.03.004

Eswaran, H., Reich, P.F., 2004. World Soil Map, in: Hillel, D., Hatfield, J.L. (Eds.), Encyclopedia of Soils in the Environment. Elsevier, pp. 352–365. https://doi.org/10.1016/B0-12-348530-4/00019-9

EMRL (1999) Groundwater Modeling System. Environmental Modeling Research Laboratory, Brigham Young University, Utah

Fearnside, P.M., 2005. Deforestation in Brazilian Amazonia: History, rates, and consequences. Conserv. Biol. 19, 680–688. https://doi.org/10.1111/j.1523-1739.2005.00697.x

Funk, C.C., Peterson, P.J., Landsfeld, M.F., Pedreros, D.H., Verdin, J.P., Rowland, J.D., Romero, B.E., Husak, G.J., Michaelsen, J.C., Verdin, A.P., 2014. A Quasi-Global

Precipitation Time Series for Drought Monitoring. U.S. Geol. Surv. Data Ser. 832, 4. https://doi.org/http://dx.doi.org/110.3133/ds832

Haacker, E.M.K., Kendall, A.D., Hyndman, D.W., 2016. Water Level Declines in the High Plains Aquifer: Predevelopment to Resource Senescence. Groundwater 54, 231–242. https://doi.org/10.1111/gwat.12350

Haghtalab, N., Moore, N., Heerspink, B.P., Hyndman, D.W., 2020. Evaluating spatial patterns in precipitation trends across the Amazon basin driven by land cover and global scale forcings. Theor. Appl. Climatol. https://doi.org/10.1007/s00704-019-03085-3

Harbaugh, B.A.W., Banta, E.R., Hill, M.C., Mcdonald, M.G., 2000. MODFLOW-2000 , The U .S . Geological Survey modular graound-water model — User guide to modularization concepts and the ground-water flow process. U.S. Geol. Surv. 130.

Hayhoe, S.J., Neill, C., Porder, S., Mchorney, R., Lefebvre, P., Coe, M.T., Elsenbeer, H., Krusche, A. V., 2011. Conversion to soy on the Amazonian agricultural frontier increases streamflow without affecting stormflow dynamics. Glob. Chang. Biol. 17, 1821–1833. https://doi.org/10.1111/j.1365-2486.2011.02392.x

Hengl, T., De Jesus, J.M., Heuvelink, G.B.M., Gonzalez, M.R., Kilibarda, M., Blagotić, A., Shangguan, W., Wright, M.N., Geng, X., Bauer-Marschallinger, B., Guevara, M.A., Vargas, R., MacMillan, R.A., Batjes, N.H., Leenaars, J.G.B., Ribeiro, E., Wheeler, I., Mantel, S., Kempen, B., 2017. SoilGrids250m: Global gridded soil information based on machine learning, PLoS ONE. https://doi.org/10.1371/journal.pone.0169748

Kelleher, C., Wagener, T., McGlynn, B., 2015. Model-based analysis of the influence of catchment properties on hydrologic partitioning across five mountain headwater subcatchments. Water Resour. Res. 2498–2514. https://doi.org/10.1002/2015WR017200.A

Krivoruchko, K. (2012). Empirical, Bayesian Kriging: Implemented in ArcGIS Geostatistical Analyst ArcUser Magazine, Fall 2012, pp. 6-10, Redlands, CA: Environmental Systems Research Institute, http://www.esri.com/news/arcuser/index.html

Kolpin, D.W., Barbash, J.E., Gilliom, R.J., 1998. Occurrence of pesticides in shallow groundwater of the United States: Initial results from the National Water-Quality Assessment program. Environ. Sci. Technol. 32, 558–566. https://doi.org/10.1021/es970412g

Lehner, B., Verdin, K., Jarvis, A. 2006. HydroSHEDS Technical Documentation. World Wildlife Fund US, Washington, DC. Available at http://hydrosheds.cr.usgs.gov

Levy, M.C., Lopes, A. V., Cohn, A., Larsen, L.G., Thompson, S.E., 2018. Land Use Change Increases Streamflow Across the Arc of Deforestation in Brazil. Geophys. Res. Lett. 45, 3520–3530. https://doi.org/10.1002/2017GL076526

Liu, W.T., Kogan, F., 2002. Monitoring Brazilian soybean production using NOAA/AVHRR based vegetation condition indices. Int. J. Remote Sens. 23, 1161–1179. https://doi.org/10.1080/01431160110076126

Lovejoy, T.E., Nobre, C., 2018. Amazon tipping point. Sci. Adv. 4, 1–2. https://doi.org/10.1126/sciadv.aat2340

Maeda, E.E., Ma, X., Wagner, F., Kim, H., Oki, T., Eamus, D., 2017. Evapotranspiration seasonality across the Amazon basin. Earth Syst. Dyn. 439–454. https://doi.org/10.5194/esd-2016-75

Miguez-Macho, G., Fan, Y., 2012. The role of groundwater in the Amazon water cycle: 1. Influence on seasonal streamflow, flooding and wetlands. J. Geophys. Res. Atmos. 117, 1–30. https://doi.org/10.1029/2012JD017539

Miguez-Macho, G., Fan, Y., 2012. The role of groundwater in the Amazon water cycle: 2. Influence on seasonal soil moisture and evapotranspiration. J. Geophys. Res. Atmos. 117. https://doi.org/10.1029/2012JD017540

Moran, E, M. C. Lopez, N. Moore, N. Mueller, and D. W. Hyndman, 2018, *Sustainable hydropower in the 21st century*, Proceedings of the National Academy of Sciences (PNAS), DOI:10.1073/pnas.1809426115

National Institute of Space Research (INPE). “PRODES deforestation." Accessed through Global Forest Watch on [4/25/2020]. www.globalforestwatch.org

Neill, C., Coe, M.T., Riskin, S.H., Krusche, A. V., Elsenbeer, H., Macedo, M.N., McHorney, R., Lefebvre, P., Davidson, E.A., Scheffler, R., Figueira, A.M. e. S., Porder, S., Deegan, L.A., 2013. Watershed responses to Amazon soya bean cropland expansion and intensification. Philos. Trans. R. Soc. B Biol. Sci. 368, 20120425–20120425. https://doi.org/10.1098/rstb.2012.0425

Nepstad, D.C., de Carvalho, C.R., Davidson, E.A., Jipp, P.H., Lefebvre, P.A., Negreiros, G.H., da Silva, E.D., Stone, T. a., Trumbore, S.E., Vieira, S., 1994. The role of deep roots in the hydrological and carbon cycles of Amazonian forests and pastures. Nature 372, 666–669. https://doi.org/10.1038/372666a0

Panday, P.K., Coe, M.T., Macedo, M.N., Lefebvre, P., Castanho, A.D. de A., 2015. Deforestation offsets water balance changes due to climate variability in the Xingu River in eastern Amazonia. J. Hydrol. 523, 822–829. https://doi.org/10.1016/j.jhydrol.2015.02.018

Renck, A., Lehmann, J. 2004. Rapid water flow and transport of inorganic and organic nitrogen in a highly aggregated tropical soil, Soil Science. 169-5, 330-341 https://doi.org/10.1097/01.ss.0000128016.00021.3d

Running S., Mu, Q. 2015. MOD16A2 MODIS/Terra Evapotranspiration 8-day L4 Global 500m SIN Grid. NASA LP DAAC. University of Montana and MODAPS SIPS - NASA. http://doi.org/10.5067/MODIS/MOD16A2.006

Myneni, R., Y. Knyazikhin, T. Park. *MCD15A3H MODIS/Terra+Aqua Leaf Area Index/FPAR 4-day L4 Global 500m SIN Grid V006*. 2015, distributed by NASA EOSDIS Land Processes DAAC. https://doi.org/10.5067/MODIS/MCD15A3H.006.

Salati, E., Dall'Olio, A., Matsui, E., Gat, J.R., 1979. Recycling of water in the Amazon Basin: An isotopic study. Water Resour. Res. 15, 1250–1258. https://doi.org/10.1029/WR015i005p01250

Scheffler, R., Neill, C., Krusche, A. V., Elsenbeer, H., 2011. Soil hydraulic response to land-use change associated with the recent soybean expansion at the Amazon agricultural frontier. Agric. Ecosyst. Environ. 144, 281–289. https://doi.org/10.1016/j.agee.2011.08.016

Sen, P.K., 1968. Estimates of the Regression Coefficient Based on Kendall's Tau. J. Am. Stat. Assoc. 63, 1379–1389. https://doi.org/10.1080/01621459.1968.10480934

Schaap, M.G., Leij, F.J., Van Genuchten, M.T., 2001. Rosetta: A computer program for estimating soil hydraulic parameters with hierarchical pedotransfer functions. J. Hydrol. 251, 163–176. https://doi.org/10.1016/S0022-1694(01)00466-8

Simunek, J., Sejna, M., Saito, H., Sakai, M., and van Genuchten, M. T. 2008. The HYDRUS 1D software package for simulating the one-dimensional movement of water, heat, and multiple solutes in variability-saturated media, Dep. of Environ. Sci., Univ. of Calif., Riverside, Calif.

Šimůnek, J., van Genuchten, M.Th., and Šejna, M. 2005. The HYDRUS-1D software package for simulating the movement of water, heat, and multiple solutes in variably saturated media. Version 3.0. HYDRUS Softw. Ser. 1. Dep. of Environ. Sci., Univ. of Calif., Riverside, Calif.

Theil,H. 1950. A rank-invariant method of linear and polynomial regression analysis, I, II, III. Proc. R. Neth. Acad. Sci, 53, Part I: 386-392, Part II: 521-525, Part III: 1397-1412.

Theis, C.V., 1935. The relation between the lowering of the piezometric surface and the rate and duration of discharge of a well using groundwater storage, Am. Geophys. Union Trans., vol. 16, pp. 519-524

Timpe, K., Kaplan, D., 2017. The changing hydrology of a dammed Amazon. Sci. Adv. 3, 1–14. https://doi.org/10.1126/sciadv.1700611

van Genuchten, M.T., 1980. A Closed-form Equation for Predicting the Hydraulic Conductivity of Unsaturated Soils. Soil Sci. Soc. Am. J. 44, 892–898. https://doi.org/10.2136/sssaj1980.03615995004400050002x

Vitousek, P.M., Aber, J.D., Howarth, R.W., Likens, G.E., Matson, P.A., Schindler, D.W., Schlesinger, W.H., Tilman, D.G., 1997. Human alteration of the global nitrogen cycle: Sources and consequences. Ecol. Appl. 7, 737–750. https://doi.org/10.1890/1051-0761(1997)007[0737:HAOTGN]2.0.CO;2

Vörösmarty, C.J., Green, P., Salisbury, J., Lammers, R.B., 2000. Global water resources: Vulnerability from climate change and population growth. Science (80). 289, 284–288. https://doi.org/10.1126/science.289.5477.284